2014

Crack Self-Healing in SiC/Spinel Nanocomposite

Fariborz Tavangarian
Louisiana State University and Agricultural and Mechanical College, f_tavangarian@yahoo.com

CRACK SELF-HEALING IN SIC/SPINEL NANOCOMPOSITE

A Dissertation

Submitted to the Graduate Faculty of the
Louisiana State University and
Agricultural and Mechanical College
in partial fulfillment of the
requirements for the degree of
Doctor of Philosophy

in

The Department of Mechanical Engineering

by
Fariborz Tavangarian
B.S., Isfahan University of Technology, 2007
M.S., Isfahan University of Technology, 2010
December 2014

ACKNOWLEDGEMENTS

I would like to express my deep appreciation to Dr. Guoiqang Li, the major professor and committee chairman, for his help, encouragement, unwavering support and invaluable guidance throughout the research. I would also like to acknowledge the precious help and assistance from Dr. Shengmin Guo and Dr. Ying Wang as members of my committee and Dr. Kevin S. McCarter, as the Dean's representative for his time and kind help.

This investigation was partially supported by Cooperative Agreement NNX11AM17A between NASA and the Louisiana Board of Regents under contract NASA/LEQSF (2011-14)-Phase3-05.

TABLE OF CONTENTS

ABSTRACT

Spinel is one of the best known and widely used ceramic materials. It has good thermal shock resistance, high chemical inertness in both acidic and basic environments, excellent optical and dielectric properties, high strength at both elevated and normal temperatures, and has no phase transition up to the melting temperature (2135°C). Spinel is used in the metallurgical, electrochemical, and chemical industrial fields. It has also found some applications in dentistry, catalyst supports, humidity sensors, reinforcing fibers, photoluminescent materials, etc. One of the limitations of spinel ceramic is its brittleness. Furthermore, at high temperature applications, a rapid heating or cooling can cause a high thermal gradient. Building up of such thermal stresses can lead to surface microcracking and crack growth, which finally can lead to a catastrophic failure of the component. In order to overcome this problem, it is highly desirable that the self-healing capability of spinel and spinel composites are investigated. In this research for the first time we studied the crack self-healing capability of nanostructure spinel. The results showed that grain growth and sintering phenomena are the two factors controlling the healing procedures. In the case of spinel ceramic, cracks can be completely healed after annealing the specimens at 1600°C for 100h with the strength recovery of 91%. On the other hand, it has been found that SiC can be used as a healing agent in many ceramics even in those ceramics without any crack healing ability. Therefore, first SiC/spinel nanocomposite was synthesized using talc, aluminum and graphite powders. The sintering behavior of the SiC/spinel nanocomposite was investigated and the best pellets from physical and mechanical properties point of views were selected to study the self-healing behavior of SiC/spinel nanocomposite. The results showed that SiC/spinel nanocomposite has an exceptional crack-healing ability as the surface cracks can be healed after sintering the specimens at 1550°C for 1 min in air with the strength recovery of 99%. Reaction of SiC with air and formation of SiO_2 and subsequently formation of mullite and dissociation of enstatite are the possible mechanisms responsible for crack healing in SiC/spinel nanocomposite.

CHAPTER 1 OVERVIEW

1.1 Introduction

Ceramic components are very sensitive to thermal and mechanical stresses. Due to the intrinsic brittleness of ceramics, their applications might be limited in some cases. In high temperature applications, rapid increase and decrease of temperature such as thermal shock may produce many microcracks, which, if not taking care of immediately and properly, cause structural failure of the component. Therefore, there is a crucial need to engineer the initiated cracks to prevent from catastrophic structural failure and maintain the integrity and service life of the structure.

In order to overcome this limitation, scientists have applied three methods: (1) increase the fracture toughness of ceramics by utilizing fibers, whiskers, secondary particles, phase transformation, microstructure control, etc. (2) apply nondestructive tests to inspect and externally repair cracks and (3) produce advanced ceramics with the crack self-healing ability.

Although increasing fracture toughness can enhance thermal shock tolerance, it cannot fully avoid micro or macro cracking under extreme loading conditions. Although it is possible to externally repair the cracks after non-destructive inspection, it is not ideal because most of the time, repair needs to be done during service. Therefore, crack self-healing is more desired.

In this research we studied the crack self-healing behavior of spinel ceramic and SiC/spinel nanocomposites. The results showed that these ceramics have crack self-healing ability and can heal the crack surfaces at high temperatures.

1.2 Report outline

This report deals with six sub-topics: A comprehensive overview on the self-healing properties of ceramic materials, synthesis and characterization of nanostructure spinel powder, crack self-healing capability of spinel ceramic, synthesis and characterization of SiC/spinel nanocomposites, and sintering and crack-healing behavior of SiC/spinel nanocomposite. The chapters are written in the form of a journal paper.

Chapter 2 presents a comprehensive overview on the self-healing properties of ceramic materials that almost covers all the studies in this field performed on different kinds of monolithic ceramics and ceramic composites. In this chapter the most recent achievements in the field of crack self-healing ceramics will be discussed and the mechanisms involved within the healing process will be addressed as well. Potential future development in this topical area is also discussed. To facilitate discussion, various ceramics and composites were classified into different categories and each section will discuss one type of these ceramics.

In chapter 3, the synthesis procedure of spinel ($MgAl_2O_4$) powder will be discussed. Ball milling method was used to synthesis spinel powder. Gibbsite ($Al(OH)_3$) and lansfordite ($MgCO_3.5H_2O$) were used as initial powders. The ball milled and annealed powders were characterized and the best procedure was determined to obtain nanocrystalline spinel powder.

In chapter 4, the crack self-healing capability of nanostructure spinel was evaluated. For this purpose, the obtained spinel nanopowder was uniaxially pressed into pellets in a hardened steel mold and sintered at 1200 °C for 1h. Then the obtained pellets were indented by Vickers indenter to produce surface cracks in the middle of the green samples. The pre-cracked specimens were annealed at various temperatures for different times to investigate the crack-healing behavior. The healing mechanism was investigated as well. Furthermore, the healing efficiency of the healed specimens was investigated in the form of strength recovery by diametral tensile strength (DTS) test or indirect tensile test (ITT) or split tensile test (STT).

In chapter 5, the synthesis procedure and characterization of SiC/spinel nanocomposites from talc which is one of the softest materials in nature was investigated. In order to obtain SiC/spinel nanocomposites, talc, aluminum and graphite powders were used as raw materials. Initial powders with appropriate molar ratio were mixed to yield SiC/spinel composite containing 27.26 wt.% SiC. The prepare powder mixture was mechanically activated in a planetary ball mill in an argon atmosphere and then the obtained powders were annealed at different temperatures in a vacuum. Also, the SiC/spinel formation mechanism was studied as well.

In chapter 6, the sintering behavior of SiC/spinel nanocomposite was studied. For this purpose, the obtained SiC/spinel nanocomposite was uniaxially pressed into pellets in a hardened steel mold and sintered at various temperatures for different holding times in a vacuum. The physical and chemical properties of the sintered specimens were evaluated and the best specimen from chemical and physical point of views was chosen to investigate its crack-healing behavior.

In chapter 7 the crack healing behavior and the healing efficiency of the synthesized SiC/spinel nanocomposite was investigated. Surface cracks were produced on the prepared SiC/spinel nanocomposite specimens and the indented samples were then annealed at various temperatures for different holding times. The optimal conditions to heal the cracks and to recover the strength as well as the healing mechanisms were investigated.

Chapter 8 summarizes the main results presented in this dissertation and gives recommendations for future works.

.

CHAPTER 2 CRACK SELF-HEALING IN CERAMIC MATERIALS[1]

2.1 Introduction

In recent years, enormous studies have been conducted on self-healing ceramics materials. Design of ceramic structures with the ability of crack self-healing in service is one of the most important objectives of many scientists. Development of such structures in fuel cells, aerospace, automotive, refractory, and military can save millions of dollars from maintenance cost viewpoint.

While crack self-healing has been a research topic of intensive research for years, there is a lack of a comprehensive study and overview on the self-healing capability of ceramics. To the best of our knowledge, there is no specific review paper, book or book chapter on overviewing the crack self-healing of ceramics materials. In one work, Madhan and Prabhakaran [1] reviewed a limited number of papers (33 papers), which mainly discussed on alumina, mullite, silicon carbide and silicon nitride ceramics. In another work, in a small section, Zwaag [2] explained the crack self-healing behavior of titanium-containing ceramic composites which takes place through the oxidation of titanium and the formation of TiO_2.

Considering the rapid development and the importance of crack-healing in ceramics, we feel that it is time to summarize the past advancement and provide perspectives for future research. This chapter is a comprehensive overview on the self-healing properties of ceramic materials that almost covers all the studies in this field performed on different kinds of monolithic ceramics and ceramic composites. In this chapter the most recent achievements in the field of crack self-healing ceramics will be discussed and the mechanisms involved within the healing process will be addressed as well. Potential future development in this topical area is also discussed. To facilitate discussion, we classify various ceramics and composites into different categories and each section will discuss one type of these ceramics.

2.2 $MgTi_2O_5$

The first report of crack self-healing in ceramic materials dated back to 1958 when Bush and Hummel were studying the mechanical properties of magnesium dititanate at high temperatures [3]. They observed that the strength and elastic modulus of specimens increased from room temperature to about 1000 °C. Further investigations showed that the extensive healing of ruptures and fractures is responsible for the strength and elastic modulus increase. This study was the onset of further investigations on the crack self-healing capability of ceramic materials to be utilized in structural applications.

[1] This chapter has been submitted as Fariborz Tavangarian, Guoiqang Li, Self-crack-healing in ceramic materials, to ELSEVIER, *Progress in Materials Science*, in April 2014 for peer reviewing process and currently is under review.

2.3 UO_2

Bain studied the crack healing behavior of uranium oxide fuel elements [4]. UO_2 fuel element will crack in power reactors when it is operated under thermal shocks. In some research it is shown that when the thermal gradient of the inner and outer surfaces of the annular UO_2 is more than 90 °C some cracks initiate and propagate both radially and circumferentially [4,5]. Bain showed that cracks can be healed due to the grain growth occurred after irradiation of the UO_2 structures at 1400 °C for 600 h [4]. In another work, Roberts and Wrona [6] investigated the crack healing behavior of UO_2 through the recovery of fracture strength at room temperature. Results showed that the strength of the samples can be recovered after annealing the specimens at 1800 and 2000 °C for 11 and 3 h, respectively. Metallographic observation of annealed specimens revealed that at the first stage cracks reduced to lines of cylindrical or spherical pores (figure 2.1, see a) and then the cylindrical pores changed to smaller spherical pores and remained as grain boundary porosity (figure 2.1, see b). Also they suggested that the healing process is not controlled by the grain growth rather by mass-transportation processes such as grain-boundary diffusion, bulk diffusion, surface diffusion, or evaporation and condensation [6].

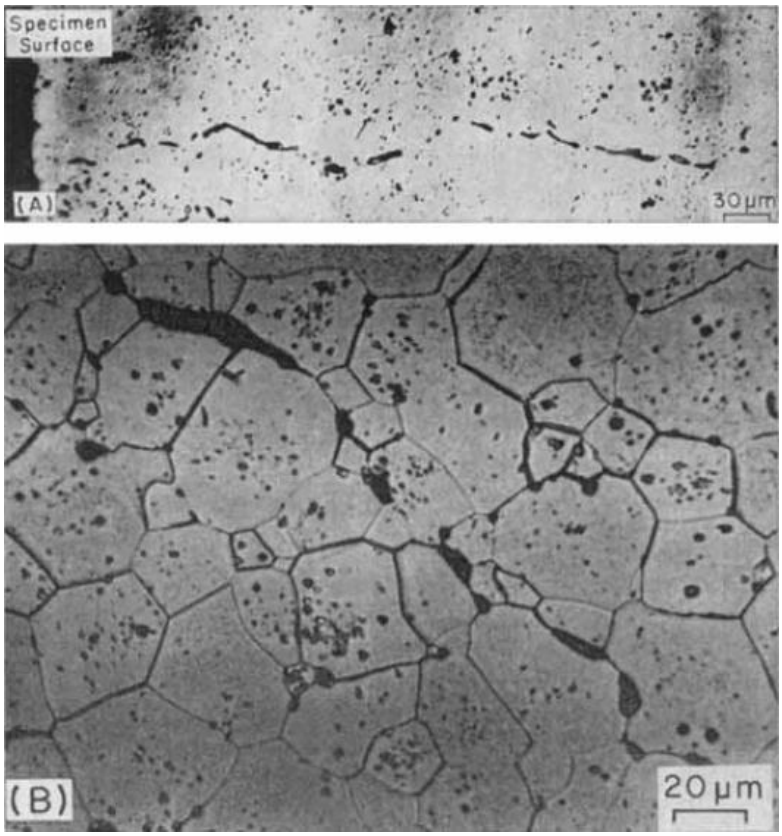

Figure 2.1. Crack healing in UO_2. (a) Thermal-shock crack annealed at 2000 °C for 1 h and (b) part of thermal-shock crack annealed at 2000 °C for 2 h. Reprinted with the permission from [6].

On the other hand, Dutton [7, 8] concluded that the healing process is not due to the sintering of small pores but from continual pinching off of the remaining pores which can be controlled by surface diffusion and increases the strength of the samples [6]. Bandyopadhyay and Roberts [9] reported that quench temperature strongly influences the density and width of cracks and therefore affects the healing behavior. For instance, to achieve a complete strength recovery of specimens quenched at 200 °C, sintering for 2 h is required at 1740 °C while those samples quenched at 700 °C only showed 11% of strength recovery after sintering at 1740 °C for 6 h [9]. In another work [10] they illustrated that the healing process consists of two stages: first pinching off of the crack lines (stage 1) and second sintering of the crack-like pores through the diffusional process (stage 2). Based on the experimental data in [6-9], they proposed a crack-healing diagram (figure 2.2) in which the stage of healing and the time required for complete strength recovery can be predicted. As can be seen in figure 2.2, with increasing the sintering temperature, the two straight lines meet which means that the occurrence of stage 1 and 2 is simultaneous and therefore pinching off and sintering occurs at the same time to the end of the healing process [10-12].

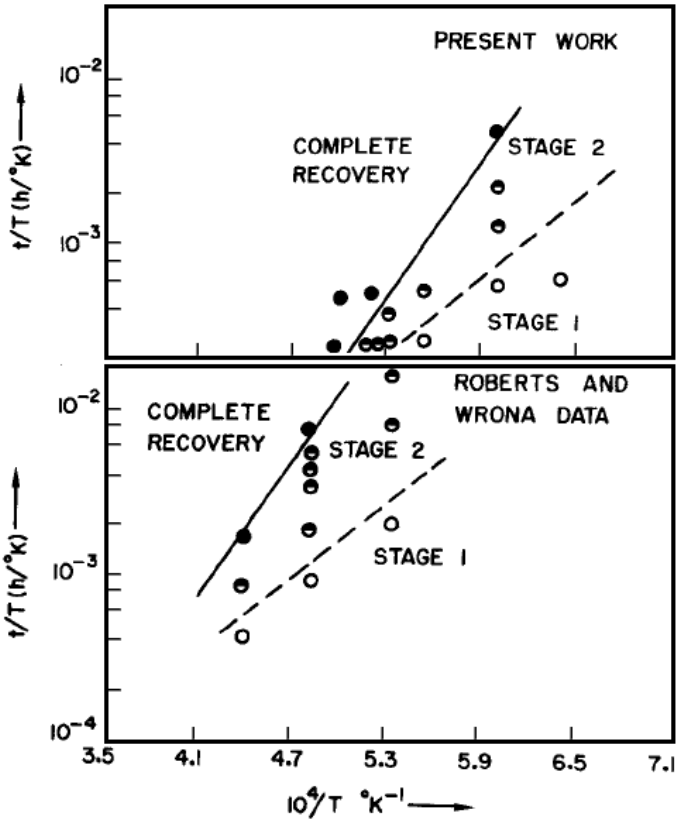

Figure 2.2. Plot of Ln (t/T) for different times and temperatures vs 1/T, subsequently termed the "crack-healing diagram.". Reprinted with the permission from [10].

2.4 Al_2O_3

The crack healing behavior of monolithic Alumina (Al_2O_3) was studied by many researchers [13-41]. In monolithic alumina the sintering mechanism is responsible for the healing process. Heuer and Roberts [13] found that the bending strength of single-crystal Al_2O_3 bars improved after sintering the specimens at above 1000 °C due to the modification of surface damage. Kim et al. [14] found that a surface crack of 100 µm can be healed by sintering the specimens above 1400 ºC for 1h. Gupta [15] demonstrated that crack healing in alumina is related to pore evolution in the microstructure during annealing. Figure 2.3 shows the surface of alumina samples after sintering at 1600 ºC for various times. As can be seen, it seems that cracks are healed via the disappearance of void space between adjacent grains. After 1.5 h of sintering most of the cracks are healed and 95% of the initial strength of the samples have been recovered (figure 2.3, see d).

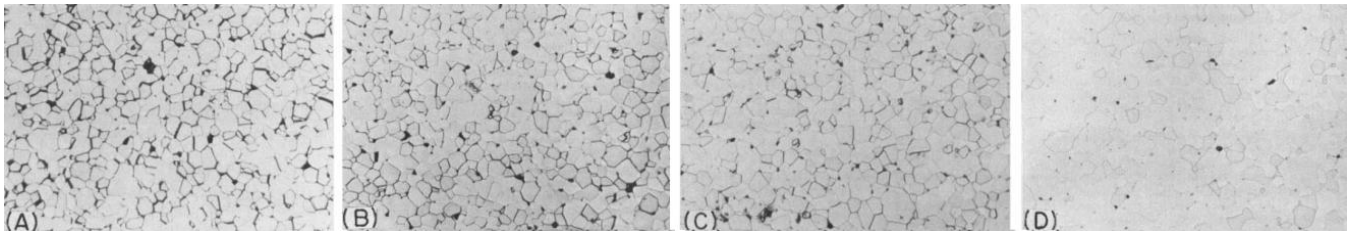

Figure 2.3. Crack-healing characteristics of Al_2O_3, as indicated by disappearance of grain-boundary cracks *(heavy lines).* (a) Thermally shocked blank and samples annealed at 1600°C for (b) 10 min, (c) 30 min, and (d) 90 min (× 100). Reprinted with the permission from [15].

Also it is shown that cylindrical voids which are initially formed by the pinching of cracks break up into spherical pores and then disappeared with increasing the holding times at elevated temperature (figure 2.4) [15]. Lange and Radford [16] also reported that a complete healing of alumina can be occurred after sintering of the samples at 1700 °C for 1h. They suggested that the healing process is as a result of the grain growth occurred from one side of the crack surface to the opposite side, which filled and eliminated the crack. Choi and Tikare [17] investigated the crack healing of alumina in both air and inert environments. They found that crack healing occurred at temperatures higher than 800 ºC in both air and inert (argon) atmospheres, showing that the healing mechanism is due to the transport of existing materials to the crack surfaces.

Wilson et al. [18] studied the influence of microwave heating in comparison with heating in a conventional furnace on the crack self-healing behavior of alumina. Their finding showed that the crack healing rate is almost similar at 1237 °C for both conventional and microwave heating procedures. However with increasing the annealing temperature to about 1469 °C, the healing rate of specimens in microwave heating almost doubles that of conventional heating. They found that microwave heating

increases the mass transportation via diffusion (through enhancing the lattice diffusion) and hence increase the crack healing rate [18,19].

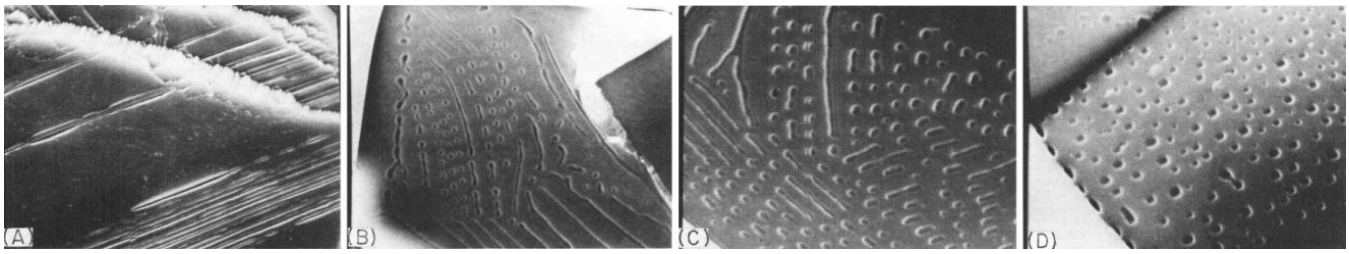

Figure 2.4. Pore evolution sequence during crack healing. (a) Typical pinching of thermally shocked cracks (×2910); (b) and (c) formation of cylindrical voids and their breakup into spherical pores (×3860); and (d) spherical pores (× 3860). Reprinted with the permission from [15].

2.5 ZrO_2

Zirconia (ZrO_2) shows a unique crack self-healing behavior [42-45]. Wang and Stevens [42] studied the crack healing behavior of partially stabilized zirconia. A powder mixture of zirconia containing 3 mol% Y_2O_3 was hot pressed at 1650 °C for 2h under the pressure of 20 MPa. Cracks were produced on the surface of the specimens using Vickers indenter under the load of 190 N. the pre-cracked samples were annealed at 1250 °C for 20 min. it was found that the bending strength of the annealed samples showed a 60% increase in comparison with pre-cracked specimens. Studies showed that heat treatment of the specimens at above ZrO_2(m) →ZrO_2(t) transformation temperature (1170 °C), leads to the crack healing and the crack tip rounding of tetragonal zirconia polycrystal (TZP) which results in the fracture strength recovery. The grain rearrangement due to the ZrO_2(m) →ZrO_2(t) transformation, the structural deformation and diffusion mechanisms in the crack opening process zone are responsible parameters for crack healing and crack tip rounding during the heat treatment [42,43].

2.6 ZnO

The crack self-healing behavior of ZnO ceramics was studied by Lange and Gupta [46]. For this purpose, deep surface cracks were produced by thermal shocks from 400 to 22 °C in water and then the specimens were reheated and tested for flexural strength. Generally speaking, sintering phenomenon is accompanied with grain growth which has a detrimental influence on strength; however in this experiment, as the holding time at high temperature increased the strength recovery increased as a result of healing process. It was shown that the healing process has a dominant influence on strength recovery while the grain growth has a secondary effect. In this research, the healing process is completed after sintering the samples at 1100 °C for 35 h.

2.7 MgO

Gupta [47] studied the crack healing behavior of thermally shocked MgO. The samples were quenched in water from 300 to 22 °C to produce cracks. 4-point flexural strength was used to determine the strength recovery of the healed samples. It was found that crack healing can be completely reached after sintering the MgO specimens at 1500 °C for 7h as a result of a mass transportation phenomenon. The mechanism of healing is similar to what is explained in Al_2O_3 ceramic above. In polycrystalline MgO, during the healing process cylindrical voids are first formed and then breakdown into several spherical pores (figure 2.5). With continuing the healing process, the produced spherical pores shrink and the strength of the structure increases [47].

Sangwal et al. [48] evaluated the surface morphology around nanoindentations (for loads up to 10μN) made on the (110) cleavage face of MgO crystals at room temperature by *in situ* atomic force microscopy. They found that an indented surface can be healed with time however the time of healing increased as the load of indentation increased or in other words with increasing the penetration depth of the indenter. Kinetics studies suggested that the recovery of indented surfaces of MgO structure takes place by local reorganization, and volume and surface diffusion processes [48].

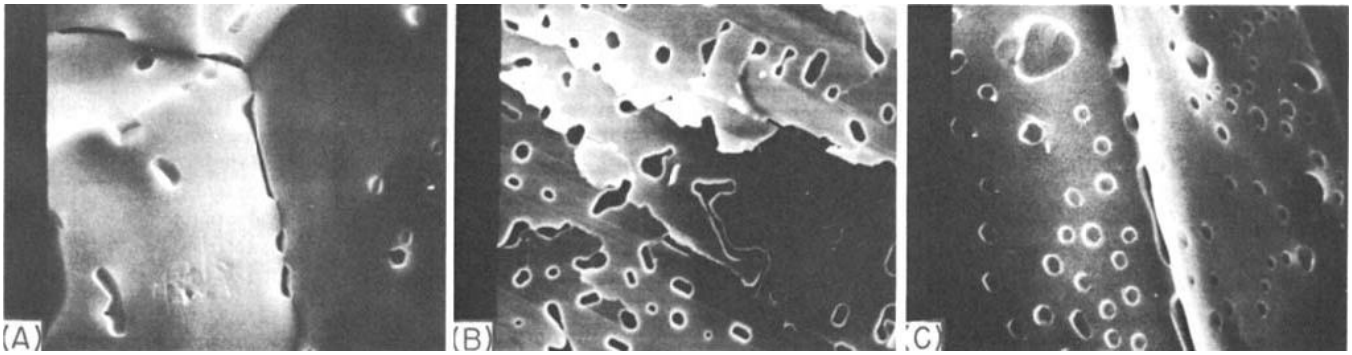

Figure 2.5. Crack morphology during annealing of thermally shocked MgO showing (a) crack pinching, (b) cylindrical and tubular pore formation, and (c) spherical pore formation (× 800). Reprinted with the permission from [47].

2.8 ThO_2

Bronisz and Douglass [49] investigated the relation between crack healing and grain growth in ThO_2 ceramic structure by transmission electron microscope. They observed that cracks in ThO_2 substrates heal directly by the growth of grains from one surface of the crack to the other. Also they reported that the effective temperature for grain growth is around 1500 ºC. These investigations suggest that under conditions during which grains grow, crack and healing might proceed by the same mass-transport mechanism [49].

2.9 Si_3N_4

Several researchers studied the crack self-healing behavior of monolithic Si_3N_4 and its composite doped with other components [18,19,50-65]. Petrovic et al. [50] found that, at room temperature, the crack growth rate under bending strength test for high temperature annealed samples decreased. These specimens also showed higher strength in comparison with those samples without high temperature annealing procedures. Later studies showed that this ceramic has the self-healing ability at high temperatures. In fact one of the possible reasons for slow crack growth at high temperature could be due to the crack healing of the Si_3N_4 ceramic due to the oxidation. The crack healing behavior of hot pressed Si_3N_4 in air and N_2 atmospheres was studied [51,52]. The strength of the annealed samples increased (30%) at above 1200 ºC in N_2 atmosphere as a result of the release of residual contact stresses without the contribution of crack healing phenomenon. On the other hand, those samples annealed in air showed a completely different trend. With increasing the annealing temperature from 800 to 1200 ºC the strength of the sample increased enormously (160%) which can be attributed to the crack healing occurred as a result of the oxidation of silicon nitride. A decrease in the strength was observed for those samples annealed at 1300 ºC which is ascribed to the formation of new defects in the structure due to the release of N_2 gas [53]. Similar observation was reported by Easler et al. [54]. They found that the strength of Si_3N_4 specimens increased after sintering at 1370 °C for 30 min and then decreased for longer sintering times. They suggested that the primary increase in the strength could be due to the rounding or blunting of the crack tips while the decrease in the strength may be ascribed to the development of newly formed defects and flaws in the structure.

Zhang et al. [55] studied the crack healing behavior of silicon nitride containing 7.5 wt% yttrium oxide (Y_2O_3) and 2.5 wt% silica (SiO_2) as additives to investigate the dominant crack healing mechanism in silicon nitride. They found that with increasing the annealing time the fracture toughness increased as a result of the development of bonds between the crack walls and subsequently healing of existing cracks. They found that the crack healing in Si_3N_4 occurs through several possibilities including: the oxidation of silicon nitride grains, oxidation of intergranular phases (formation of $Y_2Si_2O_7$), crystallization of intergranular glass phases, relaxation of creep at the crack tip, and the dominant mechanism of flow of yttria containing glass to multigrain junctions from adjacent areas with subsequent crystallization [55].

Wiederhorn and Tighe [56] also studied the crack healing behavior of yttria-doped hot-pressed silicon nitride. Specific cracks were created on prepared bars from yttria-doped silicon nitride and subjected to four-point bending test at 1200 ºC under static stress of 350 MPa. They found that annealing at 1200 ºC for 100 h increased the strength of the samples in comparison with those annealed just for 30 min. The strength of annealed samples for 100 h was almost similar to the non-indented samples. Detailed investigation of the fractured specimens also revealed that in the healed samples at 1200 ºC for 100 h the fracture occurred from other flaws in the surface rather than from the indentation location. Complete crack healing of the samples also reported under the applied stress of 450 MPa at 1200 ºC [56].

2.10 $CaCO_3$

The crack-healing behavior of calcite ($CaCO_3$) was studied by Hickman and Evans [66]. The heat treatment was performed in a dry CO_2 atmosphere at 780-850 °C from 0.5 to 1320 h. They observed that healing procedures starts with the formation of tubes around the perimeter of the cracks followed by pinching off of bubbles from these tubes. The formation of pillars and peninsular structures at surface irregularities accelerated the healing rate of the cracks. They also found that the healing progress is strongly depends on the crack width; as the crack width increases the healing degree decreases. For example, those samples with crack apertures of less than 60 nm were completely healed after heat treatment at 850 °C for 25h; however, those with crack apertures of 700 nm showed a partial healing after healing at 850 °C for 1320h [66].

2.11 Er_2O_3

Chikada et al. [67] investigated the in situ self-healing capability of erbium oxide (Er_2O_3) coating on the oxidized V–4Cr–4Ti substrate. Cracks were produced by heat treatment of the samples at 500 °C for 100h or by mechanical bending process. In order to heal the produced cracks, specimens were immersed in liquid Li doped with 5 wt.% Er at 600 °C for 100 h and then at 700 °C for 100 h. The presence of Er in the liquid Li and also the presence of oxygen in the substrate heal the cracks in situ and fill the crack with newly formed Er_2O_3 and hence eliminate the need to disassemble the component in complex structures to heal the cracks. Figure 2.6 shows the *in situ* self-healing process occurred on the oxidized V–4Cr–4Ti substrate at the presence of liquid Li doped with Er.

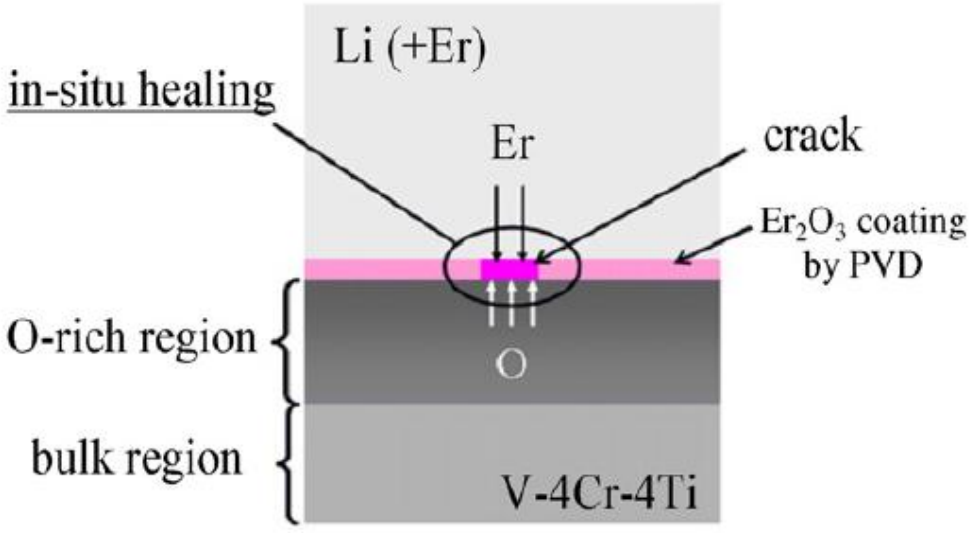

Figure 2.6. Scheme of self-healing Er_2O_3 coating. Reprinted with the permission from [67].

2.12 TiO_2

Lamaka et al. [68,69] developed a self-healing anticorrosion TiO_2 porous layer as a nanostructured reservoir for benzotriazole covered with hybrid sol-gel film to protect AA2024 aluminum alloy. Utilizing electrochemical impedance spectroscopy (EIS) they found that the samples including the TiO_2 interlayer immersed in 0.05 M NaCl showed a decrease and increase in impedance while those samples which were only coated with hybrid sol-gel film just showed a gradual decrease (figure 2.7, see a and b, respectively). The decrease and increase of the impedance can be referred to the initiation of the crack and self-healing process, respectively.

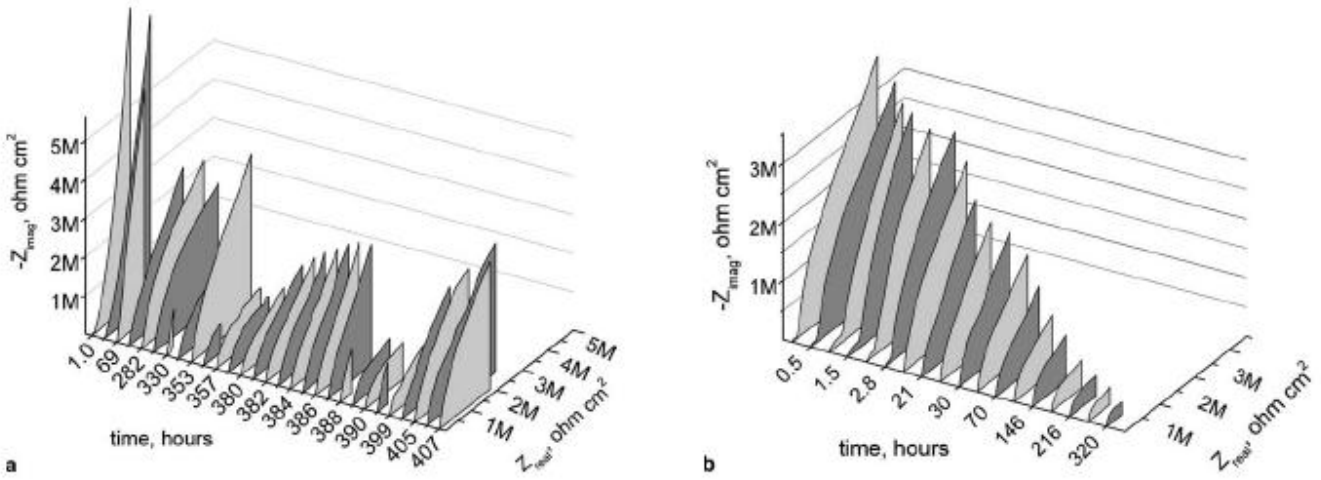

Figure 2.7. Impedance variation of AA2024-T3 treated with (a) benzotriazole-doped TiO_2 covered with sol–gel film and (b) undoped sol–gel coating immersion in 0.05 M NaCl. Reprinted with the permission from [68].

In fact, with initiation of a crack, the existing benzotriazole in TiO_2 nanostructured reservoir is released, promoted by water access, reacts with the initial products of corrosion, produces a deposition at the location of the crack, acts as an inhibitor, heals the crack, and increases the impedance (figure 2.8). While on the other sample, a continuous decrease of the impedance can be explained by the high concentration of corrosion induced defects on the alloy surface [68-70].

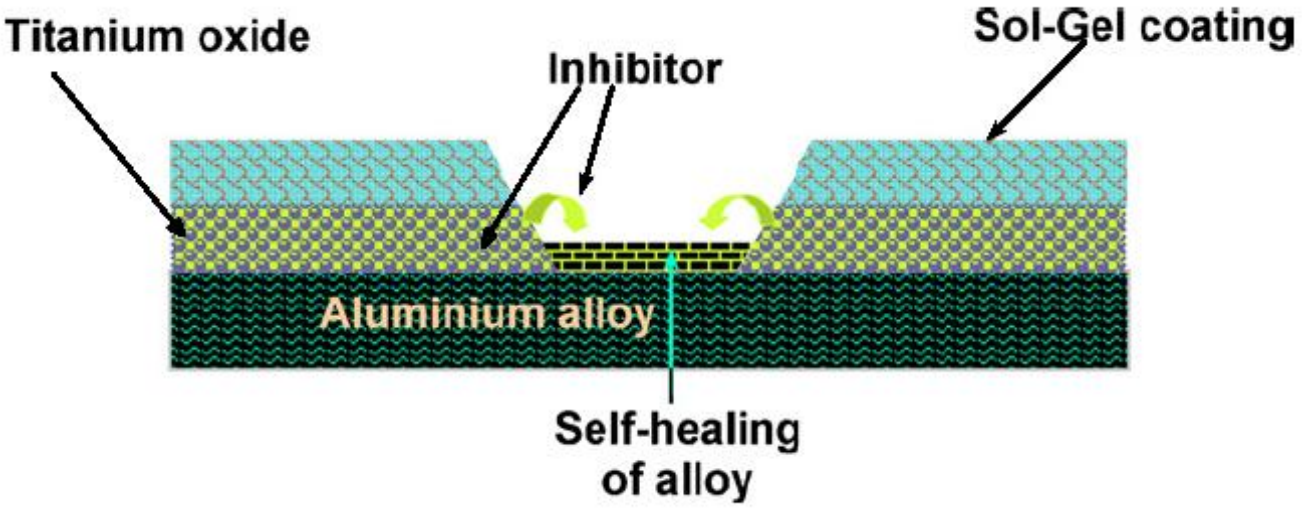

Figure 2.8. Schematic representation of the TiO_2 nanostructure reservoir doped with inhibitors and self-healing mechanism after damage initiation. Reprinted with the permission from [69].

2.13 Ti_3AlC_2

Song et al. [71,72] investigated the self-healing behavior of Ti_3AlC_2 ceramic in a high-temperature oxidizing environment. Figure 2.9 shows the crack location after complete healing procedure at 1100 °C for 2 h in air. As can be seen in this figure, Al_2O_3 is formed near the walls of the crack while TiO_2 formed in the middle of the crack. Besides they found that cracks with smaller width (less than 1 μm) do not show the TiO_2 layer and they are mainly filled with Al_2O_3 structure. To find the healing mechanism of Ti_3AlC_2, they investigated the fracture surface of the pre-cracked sample after various holding times at high temperature as shown in figure 2.10. They found that an oxide layer starts to grow on the fracture surface with passing time. Using XRD, it was found that after 360s sintering at 1100 °C, Al_2O_3 is formed on the fracture surface. With increasing the holding time to 900s, TiO_2 is also detected in the XRD patterns in addition to Al_2O_3. These findings showed that Al_2O_3 is the first oxide layer formed on the crack wall followed by the formation of the TiO_2 for longer sintering time. This can be ascribed to the weaker Ti-Al metallic bonding in comparison to Ti-C covalent bonding [73,74]. Furthermore, from thermodynamic point of view, the Gibbs free energy for the formation of Al_2O_3 is more negative than that of TiO_2 and CO_2 [74,75].

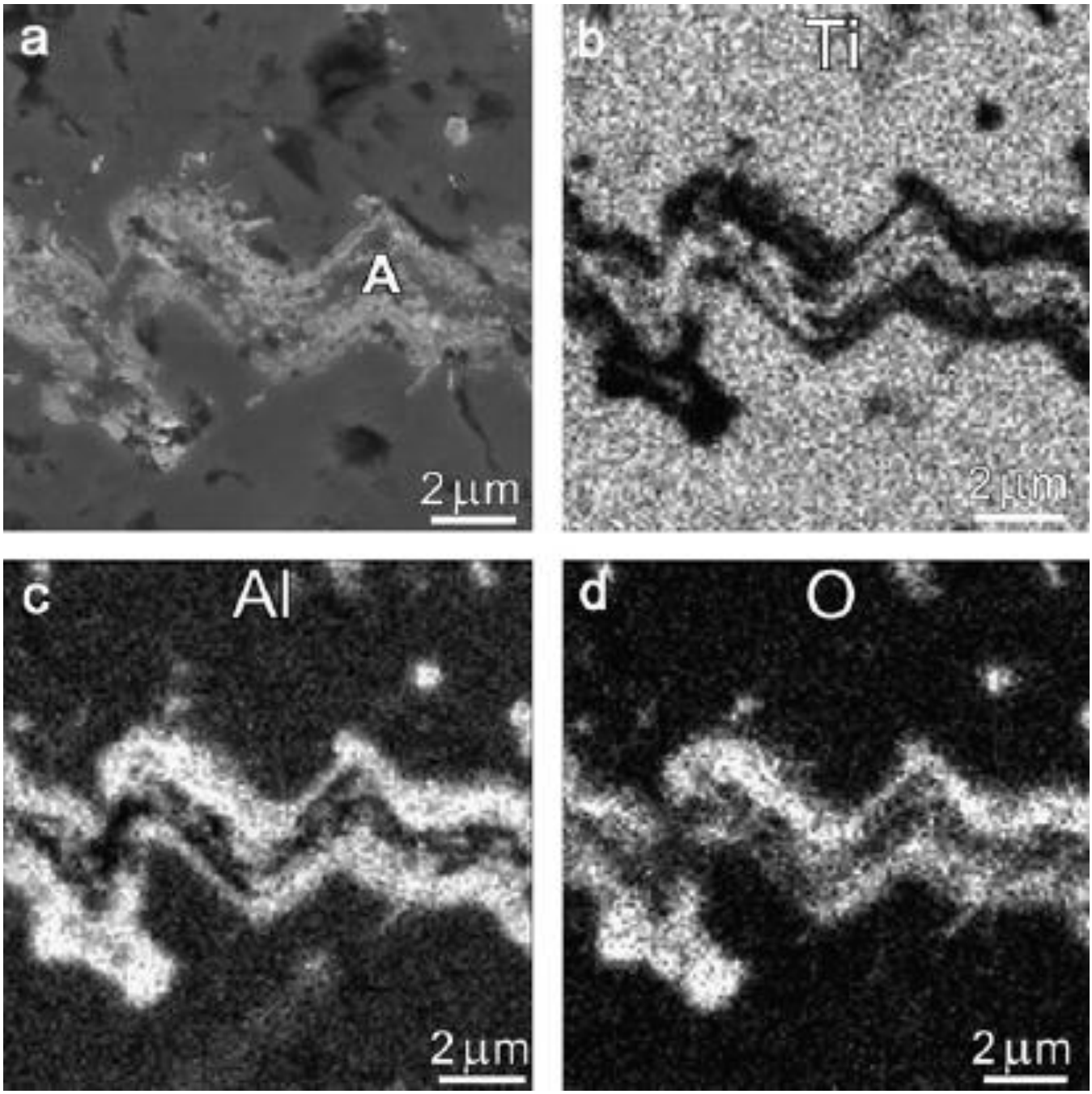

Figure 2.9. Cross-section of the healed Ti_3AlC_2 sample. (a) SEM micrograph, (b) Ti, (c) Al, and (d) O maps. Reprinted with the permission from [71].

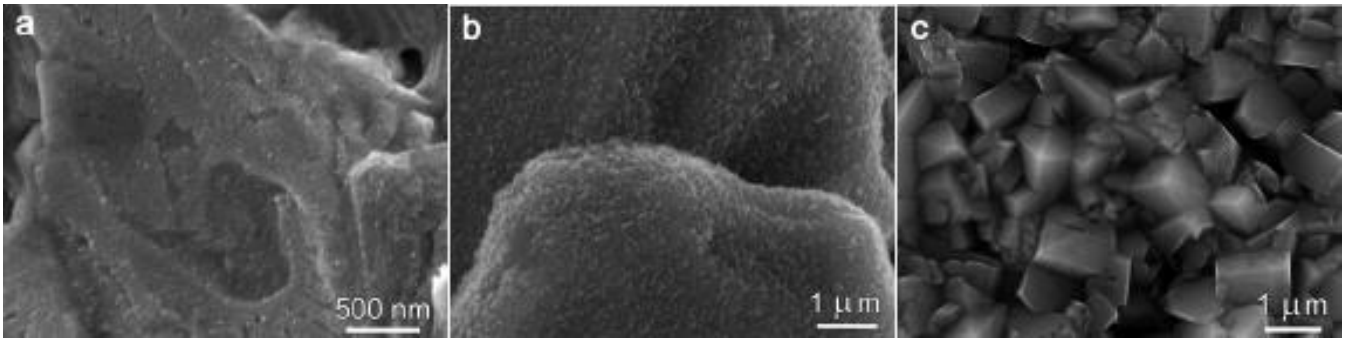

Figure 2.10. SEM micrograph of the fracture surface of Ti_3AlC_2 ceramic after oxidation for (a) 180, (b) 360 and (c) 900 s. Reprinted with the permission from [71].

More investigation [72] revealed that the oxidation process occurred according to figure 2.11. At the initial stage, Al_2O_3 starts to nucleate at the ledges of the fracture surface and grow to cover the surface of Ti_3AlC_2 and as a result an outward growth of the oxide layer occurs. Then TiO_2 starts to nucleate in the middle and at the formed Al_2O_3 grain boundaries (figure 2.11, see b and c). Subsequently, oxygen diffuses through the Al_2O_3 and TiO_2 layers to react with Ti_3AlC_2 and formed more oxides. With the consumption of Ti_3AlC_2 substrate, the interface between Ti_3AlC_2 and Al_2O_3 moves inward while the formation of oxides, diffusion of Ti to the oxide free surface and formation of more rutile cause an outward growth of oxide front [72,76]. With thickening the oxide layer, the volume loss occurred due to the oxidation of Ti_3AlC_2 cannot be filled with the formed alumina and subsequently some pores form underneath the alumina layer [72].

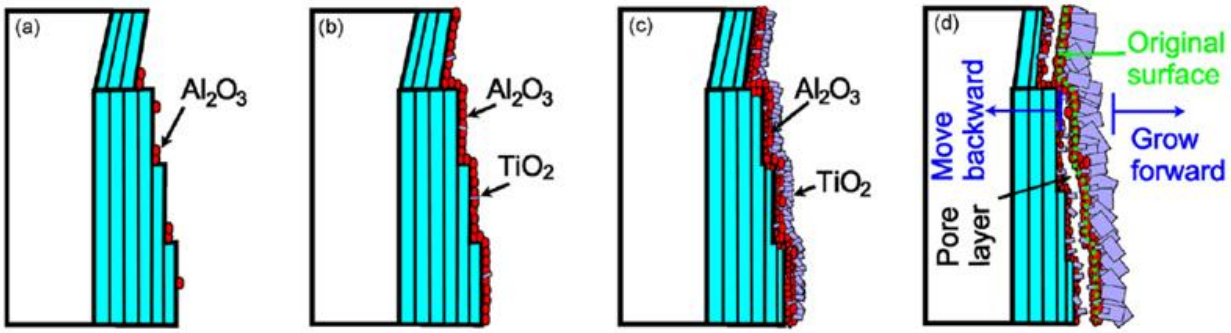

Figure 2.11. Schematic representation of the nucleation, growth and pore formation of oxide scale on Ti_3AlC_2. (a) nucleation of Al_2O_3 on the ledges of the fractured lamellar Ti_3AlC_2 grains; (b) formation of Al_2O_3 layer and nucleation of TiO_2 at Al_2O_3 grain boundaries; (c) thickening of Al_2O_3 layer and outward growth of TiO_2 layer on alumina layer; and (d) formation of porous layer once the inward grown Al_2O_3 cannot effectively compensate the volume loss of Ti_3AlC_2 caused by oxidation. Reprinted with the permission from [72].

2.14 Ti_2AlC

The relation between self-healing and surface structure of Ti_2AlC was investigated by Yang et al. [77]. Their findings showed that a well protective columnar Al_2O_3 structure formed on the flat surfaces of the base matrix; however, in the presence of large surface cavities, an equiaxed layer formed which is finer and looser in comparison with columnar Al_2O_3 structure. Figure 2.12 shows a schematic of the formed grains based on the substrate morphology. As can be seen, on a relatively flat surface, compact columnar grains formed at the interface of Ti_2AlC and Al_2O_3 layer and hence provided a very strong protective layer (figure 2.12, see a). In contrast, on the location of a cavity, small equiaxed grains of Al_2O_3 formed accompanied with micro-voids and hence provide faster diffusion paths for Al and Ti atoms to the free surface (figure 2.12, see b). Therefore on the top of a cavity, large rutile grain can form (Figure 2.12, see b and c). A schematic representation of the above procedures is shown in figure 2.12 part c.

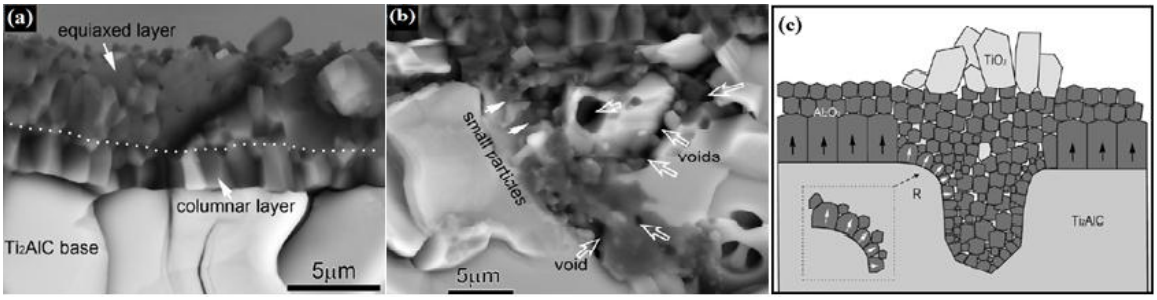

Figure 2.12. SEM micrographs of fracture cross sections of Ti_2AlC oxidized for 100 h show the microstructure of Al_2O_3 layer formed (a) at a flat surface and (b) in a cavity. (c) Schematic drawing shows the influence of surface cavity on the formation of oxides scale during high temperature oxidation in air. The arrows indicate the fastest growth directions of α-Al_2O_3 grains in the first layer. Reprinted with the permission from [77].

Li et al. [78] investigated the repeated crack self-healing ability in the same place of Ti_2AlC. For this purpose, they introduced a crack in the initial sample with the length of 1000 μm by 3-point bending test. The healing procedure is performed at 1200 °C for 2h in air. Fracture was then induced in the same location again and similar healing cycles were performed to heal the cracks (figure 2.13). They found that up to the fourth fracture and healing cycle, the cracks can be completely healed and filled with the oxide materials, although with increasing the number of fracture cycles, the crack became wider after healing process. For more fracture cycles it is not possible to heal the crack with the same healing process. For example, for a complete healing of a sample with 8 fracture cycles, they reported that the holding time at 1200 °C should be increased to 100 h (figure 2.14). The healing mechanism is similar to what explained in Ti_3AlC_2. Al_2O_3 formed adjacent to the crack walls and TiO_2 formed in the middle of the crack. Again in cracks with small width, no rutile was observed in healed crack.

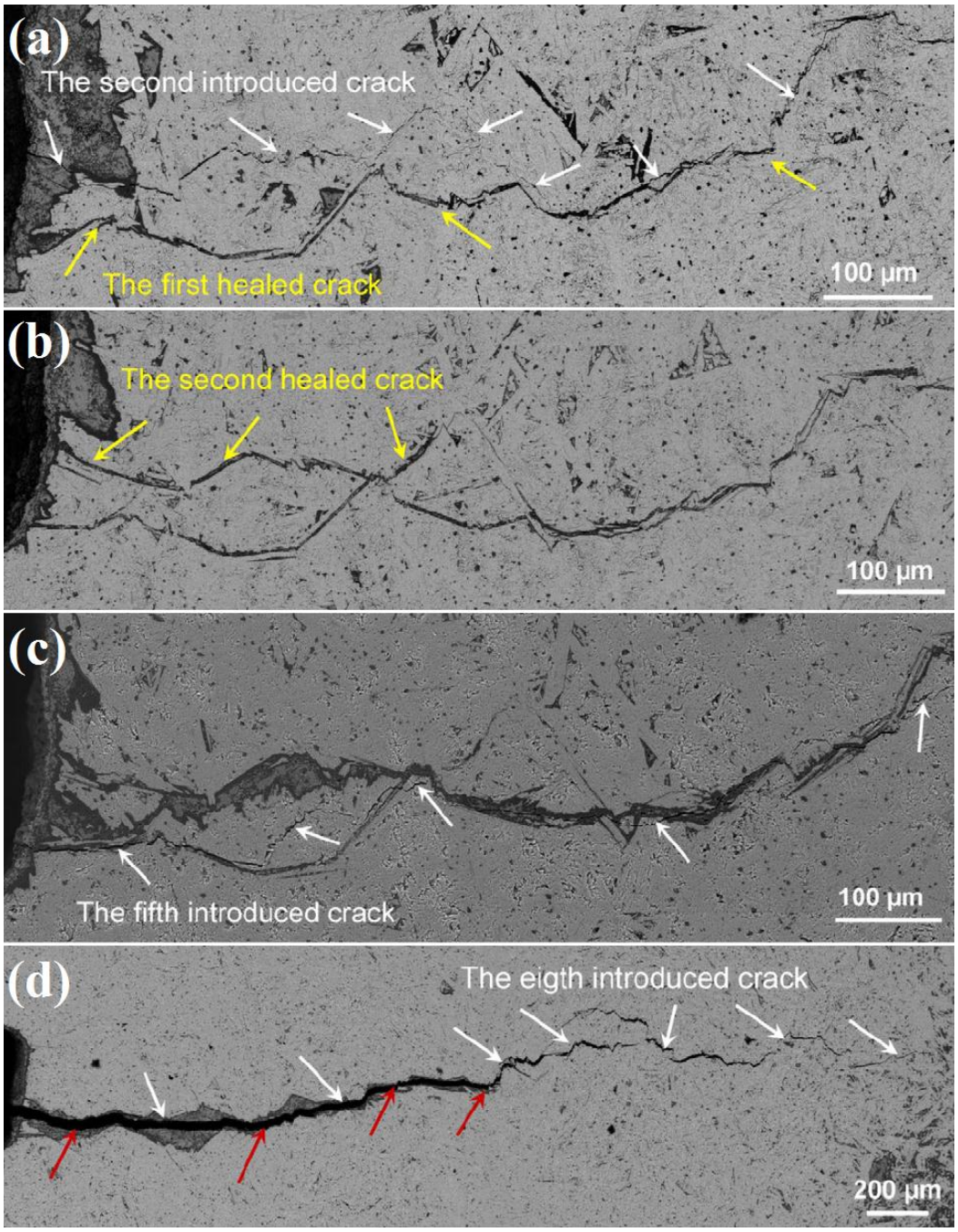

Figure 2.13. Back-scattered scanning electron micrographs of fracture and crack healing of Ti_2AlC samples. (a) Crack path after one cycle of healing and subsequent fracture. The yellow arrows indicate the crack completely filled, the white arrows indicate the newly introduced crack. Note that the subsequent crack almost deflects around the healed zone of the first crack. (b) After two cycles of healing, the second crack was completely filled again. (c) Crack path after four cycles of healing, and subsequent fracture. (d) Crack path after seven cycles of healing, and subsequent fracture. The red arrows indicate the location of remnant crack parts. Reprinted with the permission from [78].

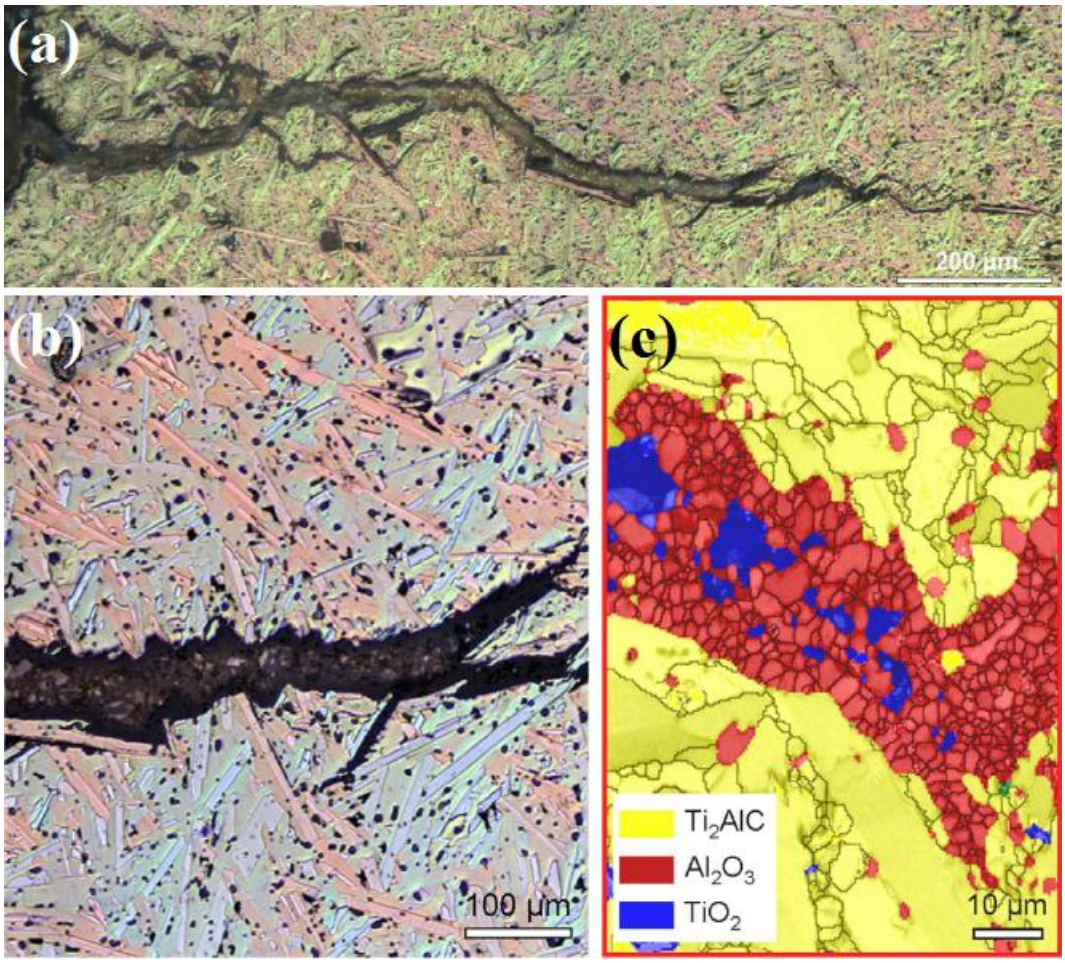

Figure 2.14. Low- and high-magnification images showing the completely filled crack in the sample after 8th fracture and then annealing at 1200 °C for 100 h. (a) Optical overview image of the healed crack. (b) An enlarged optical image taken from (a). Two opposite fracture surfaces were covered by the same Al_2O_3 layer (black) and the gap between two surfaces was fully filled by a mixture of Al_2O_3 (black) and TiO_2 (large white particles). (c) Detailed micrograph of the healed damage zone obtained with scanning electron microscopy using electron backscatter diffraction. Reprinted with the permission from [78].

2.15 Cr_2AlC

Li et al. [79] studied the oxidation and crack self-healing behavior of Cr_2AlC ceramic. Prepared Cr_2AlC bulk specimens were annealed at 1100 °C for various times and then the thickness of the produced Al_2O_3 oxide was measured in each sample (figure 2.15). According to the obtained diagram, they calculated the healing time theoretically. For instance, to heal a crack with the width of 2 µm, each crack wall should develop 1 µm oxide scale. Using the obtained diagram in figure 2.15, they found that the Cr_2AlC ceramic can form an oxide scale with the thickness of 1.03 µm after annealing at 1100 °C for 4h.

Hence the specimens were annealed at 1100 °C for 4h (desired healing time) and 100h (over complete healing time) to investigate the healing behavior. After annealing for 4h the crack is filled completely with Al_2O_3 and Al-containing Cr_2O_3 solid solution. However with increasing the holding time up to 100h, only Al_2O_3 was detected in the obtained samples detected by energy-dispersive X-ray spectrometer (EDS) and electron probe microanalysis (EPMA). It seems that with increasing the holding time up to 100h all the Cr_2O_3 was evaporated from the system. Although with increasing the holding time a more porous structure was obtained (due to the evaporation of Cr_2O_3) the strength of the specimens increased. This can be ascribed to the formation of uniform Al_2O_3 which might bond the crack walls firmly [79].

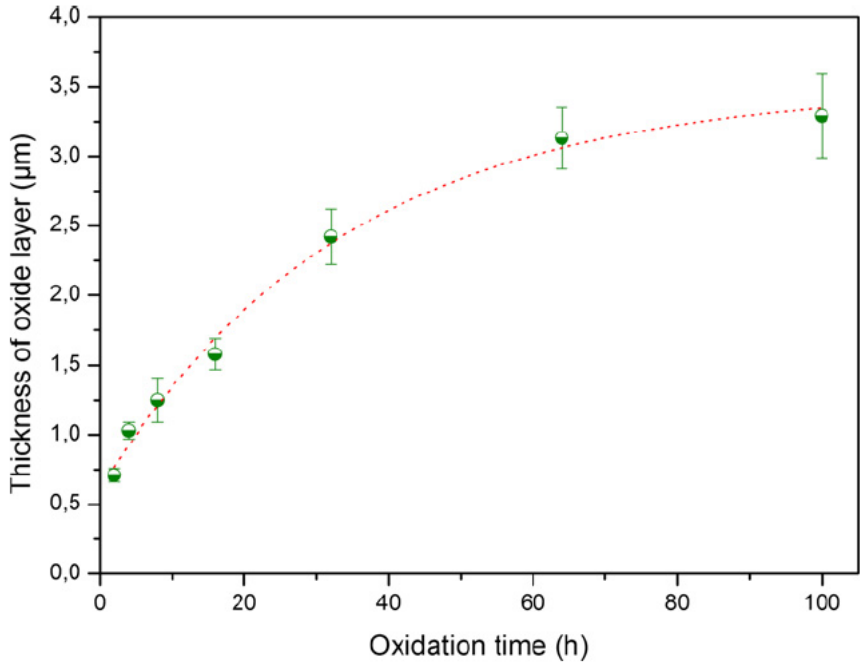

Figure 2.15. Thickness of oxide scale formed on the surface of Cr_2AlC ceramic substrate as a function of isothermal oxidation time at 1100 °C. Reprinted with the permission from [79].

2.16 Al_4SiC_4

The mechanical properties of Al_4SiC_4 ceramic were investigated by Huang and Wen [80]. They observed that the bending strength of the specimens at 1300 °C (449.7 MPa) is 1.5 times of that at room temperature (297.1 MPa), which can be attributed to the release of residual stress and crack-healing of the surface of the ceramic due to the oxidation. Parts a and b in figure 2.16 show the surface of the Al_4SiC_4 specimens after the bending test at 1000 and 1300 °C, respectively. As can be seen, pores and cracks can be clearly detected on the surface of the sample sintered at 1000 °C, while for the specimen sintered at 1300 °C a viscous flow of a glassy phase filled the pores and hence healed the structure and

consequently increased the high temperature bending strength of the ceramic. XRD and EDS analysis confirmed the formation of Al_2O_3 and amorphous oxide of aluminosilicate glass on the surface of healed sample at 1300 °C. In order to prove that the crack healing is responsible for bending strength increase, similar experiment was performed at 1300 °C in a vacuum. The results showed that the bending strength of the specimen sintered in a vacuum (269.8 MPa) was almost the same as that at room temperature. The SEM micrograph of the surface of the sintered specimen at 1300 °C in a vacuum showed similar pores and crack to specimen sintered at 1000 °C (figure 2.16, see c). Subsequently, it can be concluded that the crack self-healing occurred at the sample sintered at 1300 °C in air is responsible for the increase in the bending strength.

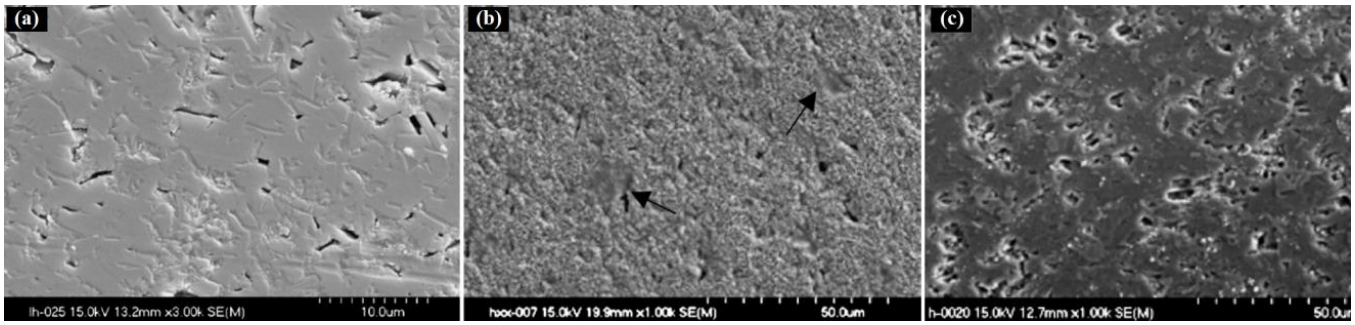

Figure 2.16. SEM micrograph of the surface morphologies of the specimens after the high temperature bending testing at (a) 1000 °C in air, (b) 1300 °C in air and (c) 1300 °C in a vacuum. Reprinted with the permission from [80].

2.17 $Zr_2Al_4C_5$

Chen et al. [81] reported the crack-healing capability of $Zr_2Al_4C_5$ ceramic. They found that $Zr_2Al_4C_5$ specimens can heal the crack from 800 to 1200 °C. The maximum flexural strength (283 MPa) obtained for the samples healed at 1000 °C for 1h which is lower than that of the initial specimens before introducing any crack (420 MPa). XRD and Raman spectroscopy confirmed the formation of t-ZrO_2 and α-Al_2O_3 oxides in the healed specimens. Unlike what is reported in Ti_3AlC_2 and Ti_2AlC systems, in $Zr_2Al_4C_5$ ternary system a continuous α-Al_2O_3 oxide layer is not formed on the substrate surface. Instead a homogenous oxide scale of ZrO_2 and Al_2O_3 were formed due to the close affinity of Al and Zr with oxygen. The reason of this behavior is the similar Gibbs free energy for the formation of Al_2O_3 and ZrO_2 [82]. Consequently, Al and Zr oxidized simultaneously and formed a continuous oxide layer on the surface of $Zr_2Al_4C_5$.

2.18 TiC + mixture(TiC/Al_2O_3) + Al_2O_3

Gao et al. [83,84] developed a self-healing composite coating for the tritium permeation barriers (TPBs) in fusion reactors. They investigated different coatings such as TiC + mixture (TiC/Al_2O_3)+Al_2O_3, NiAl +Al_2O_3, mixture (TiC/Al_2O_3)+Al_2O_3 and NiAl + TiC + mixture (TiC/Al_2O_3)+Al_2O_3. The results showed that coating with the composition of TiC + mixture (TiC/Al_2O_3)+Al_2O_3 can withstand thermal shocks due to the good adherence between different layers of the coating. They found that self-healing ability of TiC is responsible for such a behavior. TiC reacts with oxygen and forms TiO_2 which filled the produced crack in thermal shock cycles. On the other hand, TiC may decrease the grain size and the melting point of Al_2O_3 which in turn help the formation of more compact coating [83,85]. It was observed that in this coating, the porosity decreased by 90% after heat treatment due to the self-healing phenomenon. A schematic self-healing behavior of TiC + mixture (TiC/Al_2O_3) + Al_2O_3 coating is shown in figure 2.17 [84]. Also figure 2.18 shows the surface of a pre-cracked sample before and after heat treatment at 600 °C for 30h. As can be seen after annealing, the crack is completely healed. EDS observation confirmed that after the healing procedure the content of carbon decreased in the structure from 20 at.% to less than 10 at.%, suggesting the slow oxidation of TiC and formation of TiO_2 [84].

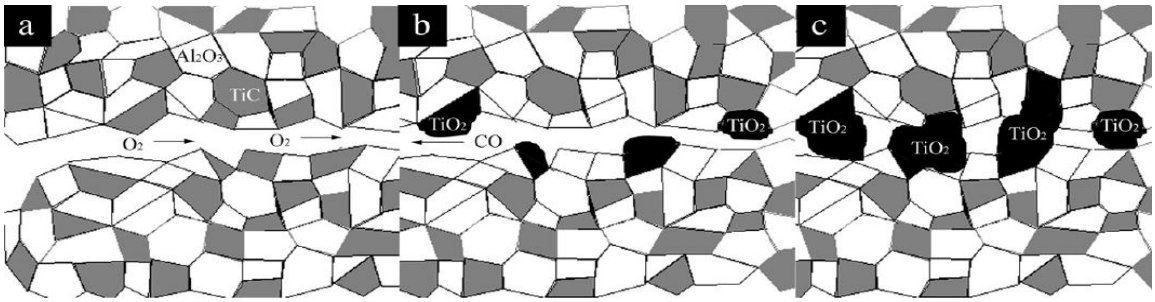

Figure 2.17. Schematic diagram of the self-healing process of TiC + mixture (TiC/Al_2O_3) + Al_2O_3 coating. Reprinted with the permission from [84].

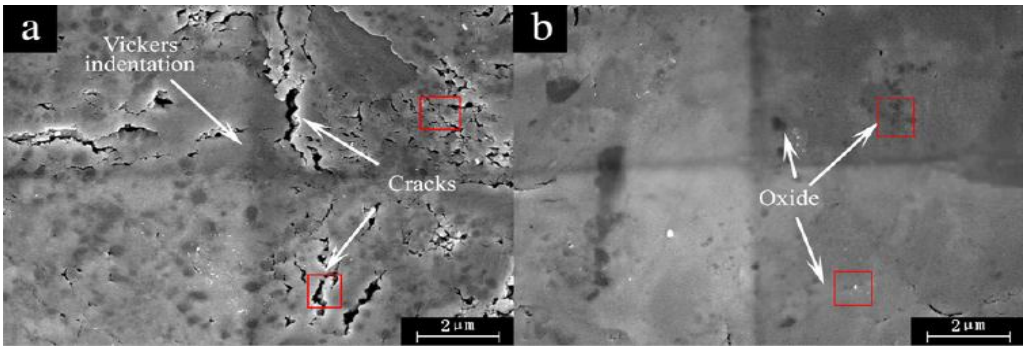

Figure 2.18. SEM micrographs of a pre-cracked sample (a) before and (b) after annealing at 600 °C for 30 h in air. Reprinted with the permission from [84].

2.19 Al_2TiO_5

Ohya et al. [86] investigated the bending strength and Young's modulus of aluminum titanate ceramics from room temperature to 1300 °C. They found that both bending strength and Young's modulus increased with increasing the annealing temperature. The bending strength increased from 62 MPa to 280 MPa and the Young's modulus increased from 29 GPa to 99 GPa after sintering the specimens at 1100°C. They found that the healing mechanism at high temperature is crack-cylinderization and crack-tip blunting. The results showed that at 1200 °C the spherical voids disappeared and the healing process was accomplished completely.

2.20 SiC

SiC is the most and extensively used material as a healing agent. Various researchers studied the self-healing behavior of SiC alone and as a healing agent in different composites [87-110]. With initiating a crack, SiC reacts with oxygen to form SiO_2 at high temperature and fills the crack. Lange [87] found that the flexural strength of pre-cracked SiC specimens were increased after annealing at 1400 °C for up to 100h while those samples annealed in a vacuum did not show a noticeable strength increase in comparison to pre-cracked samples. Further investigation showed that a film of SiO_2 is formed on the surface of the specimens and subsequently fills and heals the cracks. In another work [88], Petrovic and Jacobson examined the room-temperature fracture stress of SiC specimens annealed in air and in a vacuum. The results showed that the strength of those samples annealed in air was noticeably higher than that annealed in a vacuum. In the case of SiC, two kinds of oxidation may happen depend on the partial pressure of the oxygen; passive oxidation and active one [89,90]. In passive oxidation, a layer of SiO_2 forms on the surface which is accompanied by a measurable weight gain. While in active oxidation volatile SiO gas forms which leaves the SiC substrate and hence the material is accompanied with a weight loss. Petrovic and Jacobson found that the oxidation occurred in their experiment is passive at all temperatures. Korouš et al. [91] investigated the crack self-healing behavior of three commercially available SiC ceramics. They found that the optimum healing temperature of pre-cracked specimens for material A (Ividen Co., Ltd., SC-850) and material B (Hitachi Chemical Co., Ltd., Hekisaroi) was 1400°C and for material C (Kyocera Co., Ltd., SC-221) was 1500°C. A complete strength recovery at room temperature was observed for cracks with the length of 100 μm. Kim et al. [92] studied the strength change and oxidation behavior of four different types of reaction-bonded SiC (RBSC) ceramics after annealing at 1300 °C for up to 100h. RBSCs are composed of a combination of large SiC particles, a fine carbon source and liquid silicon and they are used to synthesize large bodies with complex shapes. The silicon and carbon react in situ to produce fine SiC particles. The results showed that the weight gain after oxidation increased by increasing the amount of free silicon. Also the flexural strength of the samples increased with increasing the oxidation time up to 50 h and then decreased. They ascribed the increase in the strength to the healing process of the cracks and they suggest that the decrease in the strength could be due to the formation of new cracks as a result of the thermal mismatch between the substrate and the produced SiO_2 oxide layer. However in another study, Chu et al. [93] demonstrated

that the strength increase in the healed samples is due to the residual stress produced by the thermal expansion mismatch between SiO_2 and SiC substrate. The results showed that lower thermal expansion coefficient of amorphous SiO_2 in comparison with SiC produces a compressive stress in cracks during cooling of the healed specimens at high temperature which is counteracted by the tensile stress in the matrix and hence increase the strength of the healed specimens (figure 2.19). Nam studied the crack-healing ability of pre-cracked SiC specimens after coating with SiO_2 nanocolloid [94]. The crack healing was performed for 1h at 900 °C in air. It was found that there are a critical number of coatings that may lead to crack healing. Figure 2.20 shows the obtained micrographs by scanning probe microscope (SPM) for 1.0, 1.8 and 4.05 µm crack widths after coating and heat treatment for one and three times. As can be seen in figure 2.20 part a, the crack is completely healed after one time. However for three times treatment (figure 2.20, see b and c) a partial healing was observed. The crack healing behavior of SiC/AlN composite is studied by Magnani et al. [95]. The strength of the pre-cracked specimens (with surface cracks ≤300µm) was completely recovered after heat treatment at 1100 °C for 1h in air. Investigations revealed that the main mechanism for crack healing is crack closure and rebonding of crack surfaces as a result of the oxidation of cracked walls and the production of mullite ($3Al_2O_3 \cdot 2SiO_2$) and SiO_2 [95].

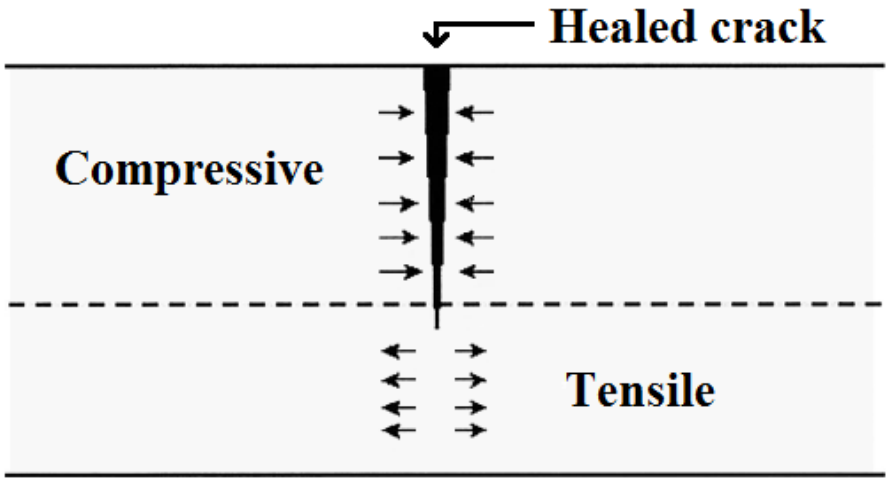

Figure 2.19. Schematic illustration of the residual stress produced by thermal expansion mismatch between amorphous silica within a healed crack and the surrounding silicon carbide. Note that the stress is compressive within the crack and tensile in the uncracked region. Reprinted with the permission from [93].

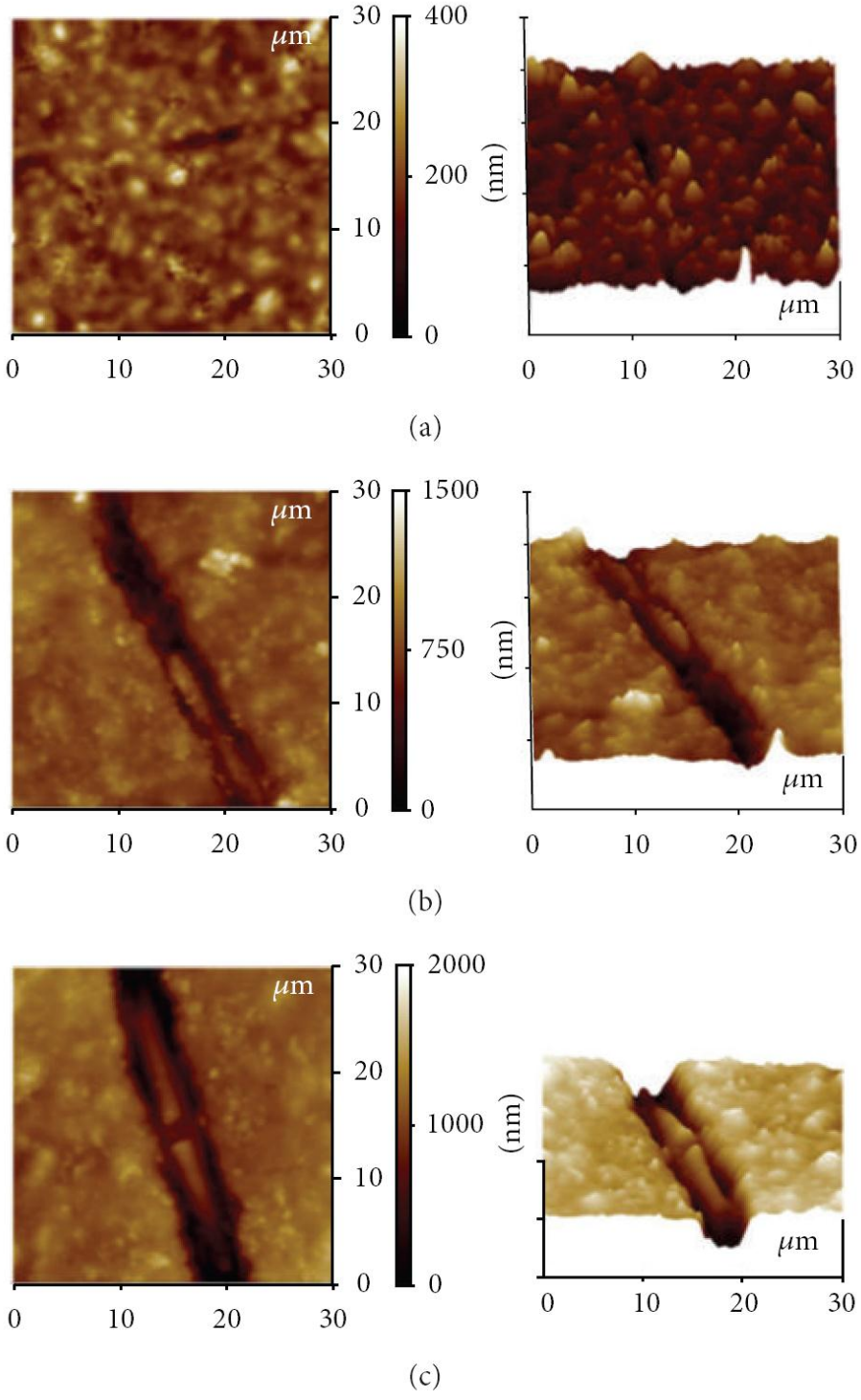

Figure 2.20. The SPM images of SiC coated with SiO_2 and healed for (a) Crack width of about 1 μm with crack healing of one time, (b) crack width of about 1.8 μm with crack healing of three times, and (c) crack width of about 4.05 μm with crack healing of three times. Reprinted with the permission from [94].

2.21 SiC/Al_2O_3

SiC/Al_2O_3 composite is one of the most extensively studied composites in the field of self-healing ceramics [111-144]. Addition of SiC to monolithic ceramics such as alumina significantly increased the mechanical properties of the base matrix at the room and high temperatures as a result of crack deflection, crack size reduction, healing of the surface cracks and also a decrease in the grain-boundary fracture during cooling [145-150]. Chou et al. [115] investigated the influence of annealing environment on the crack healing and mechanical behavior of SiC-reinforced (5 vol% 0.2 μm SiC) alumina annealed at 1300 °C for 2h. They observed a partial closure of the radial cracks and rebonding of the crack tip for those specimens annealed in argon atmosphere as shown in figure 2.21 part a and b.

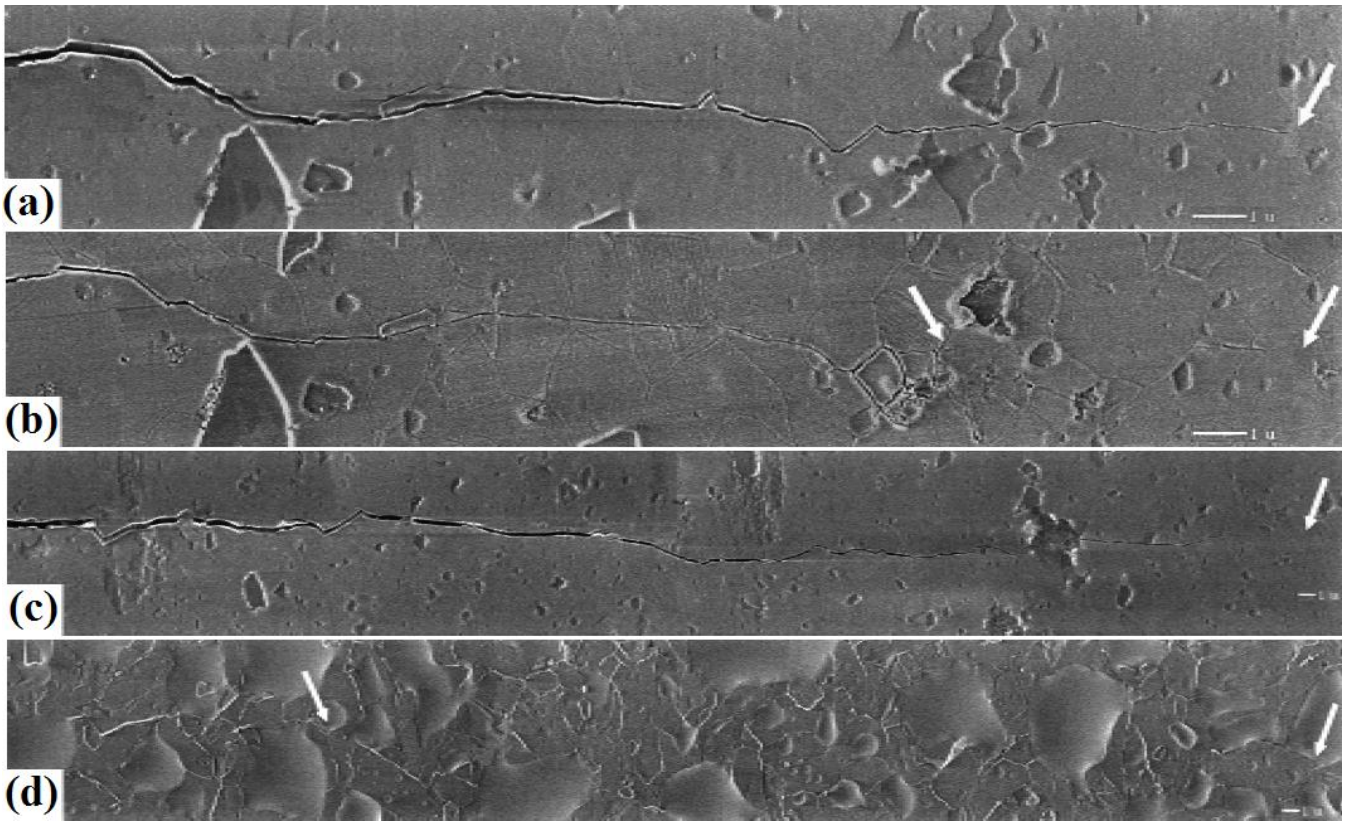

Figure 2.21. SEM micrographs showing a radial crack emanating from a corner of (a and b) a 10 N Vickers indentation (a) before and (b) after annealing in argon and (c and d) a 50 N Vickers indentation (c) before and (d) after annealing in air at 1300°C for 2h. Reprinted with the permission from [115].

Also they found that pinch-off occurs in the crack tip and leaves a line of isolated pores which is the characteristics of diffusional healing process (figure 2.22). The indentation strength of the healed specimens in argon atmosphere increased ~50%, as compared to the pre-cracked samples. On the other

hand, for those samples annealed in air the healing occurred completely and the strength of the healed samples was almost the same as initial specimens (figure 2.21, see c and d). Further studies showed that the formation of aluminosilicate glass and crystalline mullite (depends on the annealing temperature) is responsible for such a behavior [112,113 ,151,152]. Thompson et al. [111] also reported that the produced crack in SiC/Al_2O_3 nanocomposite (containing 5 vol% 0.15µm SiC) was healed after annealing the pre-cracked specimens at 1300 °C for 2h in an *argon atmosphere* (figure 2.23). They reported that the crack healing mechanism is adhesion of the crack surfaces to each other rather than a diffusion mechanism. This conclusion was based on their observation that the pinch-off and isolated pores which are the characteristics of diffusional healing mechanism were not detected on the healed specimens. Nevertheless, almost all other researchers reported that a complete self-healing of SiC/Al_2O_3 composite can only be achieved in air as a result of the oxidation of SiC in air and the formation of SiO_2 which is accompanied with 80% volume expansion. This volume expansion is necessary to fill and subsequently to heal the cracks [133,135].

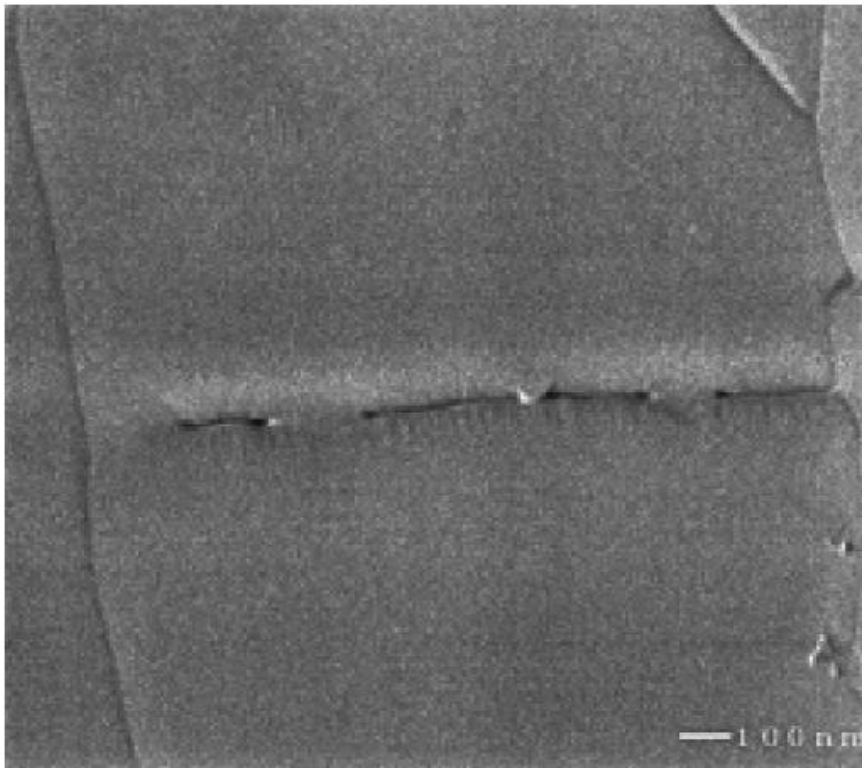

Figure 2.22. Micrograph showing the crack-tip region of a 50 N Vickers indentation radial crack after annealing in argon at 1300°C for 2h in argon atmosphere. Reprinted with the permission from [115].

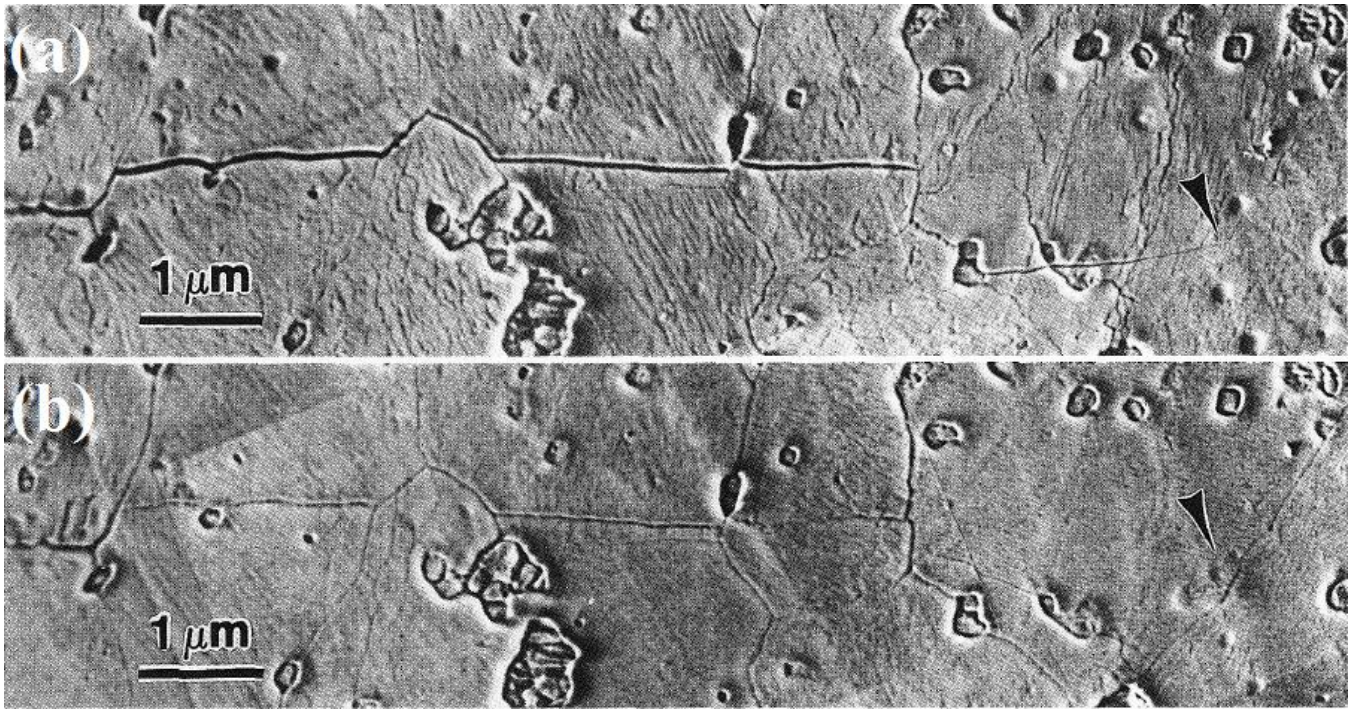

Figure 2.23. SEM images of $A1_2O_3$-SiC nanocomposite (a) prior to, and (b) after annealing for 2 h at 1300°C in argon. Reprinted with the permission from [111].

Takahashi et al. [117] reported that the healing temperature of SiC-whiskers (20 vol% 5-20μm) reinforced alumina composite is above 1200 °C (annealed for 1h in air). They just observed partial healing in those samples annealed at 1100 °C. Jun et al. [43] investigated the self-healing behavior and strength recovery of three types of alumina matrix composite: SiC_w/Al_2O_3, TiC_p/Al_2O_3, and ZrO_2/Al_2O_3. According to their observation the healing mechanism of SiC_w/Al_2O_3 and TiC_p/Al_2O_3 composites was chemical reactions while for the ZrO_2/Al_2O_3 composite the healing occurred through the rearrangement of grains due to the transformation of monoclinic zirconia to tetragonal zirconia at above 1170 °C. SiC_w/Al_2O_3 composite showed much higher strength recovery than that of TiC_p/Al_2O_3. The reasons for such a behavior were explained as follow: on the surface of SiC_w/Al_2O_3 composite a dense aluminusilicate layer was formed which in turn decreased the diffusion of oxygen through the formed layer and stopped the oxidation of inner SiC_w, while in TiC_p/Al_2O_3 a porous Al_2TiO_5 layer was formed and hence oxidation continued with increasing the holding time at high temperature. On the other hand, in the SiC_w/Al_2O_3 composite a glassy phase was formed on the surface of the composite, which increased the transfer of the matter and filled the cracks while no glassy phase was observed in TiC_p/Al_2O_3 composites [43].

Lee et al. [119,120] studied the fatigue strength of crack-healed SiC_w/Al_2O_3 composite (20 vol% SiC, 30-100μm in length) at room and high temperatures. The bending strength of pre-cracked samples was completely recovered after annealing the specimens at 1300 °C for 1h. The value of the static fatigue

limit of the crack healed specimens was 750, 550 and 450 MPa at room, 900 and 1100 °C, respectively. The obtained values were about 70% in comparison to bending strength at each temperature. The value of the cyclic fatigue limit of the crack healed specimens was 850, 700 and 500 MPa at room, 900 and 1100 °C, respectively which was more that 75% of bending strength at each temperature. The obtained results showed that the prepared composite is not sensitive to static and cyclic fatigue at room and high temperature. Also they found that a complete healing can be achieved under static stresses below 250 MPa at 1200 °C. They reported the threshold static and cyclic stresses during crack healing of SiC_w/Al_2O_3 composite to be 250 and 300 MPa, respectively [120]. Kim et al. [125] investigated the self-healing behavior of alumina, SiC/Al_2O_3 composite (containing 15 wt.% SiC with particle size of about 0.27 μm), and SiC/Al_2O_3 composite in the presence of 1, 2 and 3 wt.% Y_2O_3 as an additive. In alumina ceramic crack self-healing occurs by secondary sintering phenomenon. In SiC/Al_2O_3 composite, reaction of SiC with oxygen and production of SiO_2 is responsible for self-healing behavior. While, in the presence of Y_2O_3, first SiC is oxidized to either amorphous or cristobalite silica. Then mullitization takes place as a result of the reaction between alumina and the produced silica at 1400 °C, although in the presence of yttria, the mullitization temperature decreases by about 100 °C. Therefore, in the Y_2O_3-SiO_2-Al_2O_3 ternary system, a liquid eutectic compound ($Y_2Si_2O_7$) forms with low viscosity which successively flows into the crack sites and heals the structure. The results showed that the SiC/Al_2O_3 composite containing 3 wt.% Y_2O_3 has the best crack self-healing ability [125,137].

Nakao et al. [129] produced alumina/nanometer-sized SiC particles (18.4 vol% SiC) composite through the reaction of mullite ($3Al_2O_3.2SiO_2$) with aluminum and carbon powders. The grain size of the intra SiC particles was around 10-30 nm and hence self-healing was achieved in much lower temperature in comparison to previous studies (at around 950 °C). However in another work [133] they investigated the self-healing ability of the same composite with SiC particles with the size of less than 10nm. They found that the healing cannot be achieved completely probably due to the small volume fraction of SiC particles between the crack walls and subsequently formation of insufficient oxide to fill the crack [133].

In order to utilize SiC/Al_2O_3 composite as a thermal barrier coating or ceramic in gas turbine, its self-healing behavior should be evaluated in actualized condition. Hence Kim [113] investigated the influence of oxygen pressure (from 5×10^{-7} to 1×10^{-3} MPa) on the strength of SiC-wisker (20 vol%) reinforced alumina after heat treatment at 1400 °C for various periods of times. To adjust the oxygen pressure, argon gas with various amount of oxygen was introduced into the furnace. It was found that in low oxygen pressure ($P_{O2} < 1 \times 10^{-5}$ MPa), the strength of the samples decreased as a result of the formation of volatile SiO. It should be noticed that the transition pressure from active to passive oxidation of monolithic SiC is 1×10^{-5} MPa [89,90]. On the other hand, the strength of the samples heat treated at higher P_{O2} was increased. At higher oxygen pressure, SiO_2 forms instead of SiO and reacts with the Al_2O_3 matrix. Subsequently an increase in the strength occurs due to the blunting and self-healing of the surface cracks as a result of the formation of aluminosilicate glass.

Osada et al. [135,136] also studied the crack-healing behavior of SiC/Al_2O_3 composite (containing 15 vol% SiC with mean particle size of about 270 nm) in the combustion gas atmosphere with a low oxygen partial pressure. To adjust the oxygen pressure, they utilized nitrogen gas. The healing behavior was investigated from 1000 to 1500 °C for different oxygen pressures. They found that in oxygen pressure of more than 50 Pa (corresponding to 0.24% of air) a complete strength recovery can be achieved due to the passive oxidation of SiC.

2.22 SiC/Si_3N_4

Another composite that has been widely studied in the field of self-healing ceramics is SiC/Si_3N_4 composite. All of the studies on this composite were performed by Ando's team [153-179]. In the first work [153], the prepared composite consisted of Si_3N_4 containing 20 vol% SiC with the particle size of 270 nm and 8 wt.% Y_2O_3 as an additive. This sample was called SNC-Y8. The powders were ball milled and then hot pressed at 1850 °C for 1h under 35 MPa pressure in nitrogen gas. They found that the microstructure consisted of $Y_{20}N_4Si_{12}O_{18}$, $Y_2Si_3N_4O_3$ and $YNSiO_2$ phases crystallized in grain boundaries. The results showed that the pre-cracked samples can be healed completely after annealing at high temperature in the range of 900 to 1400 °C. In those samples healed at temperature more than 1200 °C fracture occurred outside the healed zone after bending test. Consequently the best healing condition was reported for those specimens annealed at 1200 and 1300 °C for 1h in air. In a similar work the influences of the SiC grain size and annealing atmosphere were evaluated on the healing behavior of SiC/Si_3N_4 composite [154]. SiC with four different grain sizes of 30, 270 and 600 and 1200 nanometer was utilized. It was found that the healing capability of the composite increased with increasing the grain size of SiC. Also it was found that the SiC/Si_3N_4 composite can heal the crack only in air environment but not in a vacuum, argon or nitrogen gas. In their next work [155] the crack healing behavior of SiC/Si_3N_4 composite containing 20 vol% SiC with the particle size of about 270nm, 5 wt% yttria and 3 wt% alumina as sintering additives was studied. This sample is called SNC-Y5A3. The powder mixture of the initial materials was hot pressed at 1850 °C for 2h under 35 MPa pressure in nitrogen gas. They found that all the pre-cracked samples heat treated at 1100 °C for 1h in air fractured from the indentation location. However, half of the specimens healed between 1200 and 1400 °C for 1h failed outside the crack healed zone. The results showed that, in comparison with previous work [153], substitution of 3 wt.% of yttria with alumina caused a decrease in the bending strength of the healed specimens at temperatures above 1000 °C. It can be concluded that the addition of a small amount of Al_2O_3 as a sintering aid can have detrimental effects on the high temperature bending strength of the healed samples. Also it was reported that the oxidation rate of SNC-Y5A3 was significantly higher than that of SNC-Y8 and the formed oxidize layer on the surface of SNC-Y5A3 was thicker than that of SNC-Y8 [156]. However SNC-Y5A3 shows lower crack healing ability in comparison with SNC-Y8. There are several hypotheses for this inconsistent behavior: (1) Due to the different compositions of SNC-Y8 and SNC-Y5A3, the oxidation mechanisms should be different between the sample surface and crack walls. (2) The formation of more oxygen products on the surface of SNC-Y5A3 may disturb the diffusion of oxygen into the crack surface. (3) Due to the higher roughness of SNC–Y5A3, a thicker

oxide layer is needed to fill out the crack. (4) The formed oxides should be different in each composite and hence the required thickness of the oxidized layer to heal the crack should be different [156].

It is found that the healed SNC-Y5A3 specimens are sensitive to static fatigue at 1000 °C but not at 800 °C [155]. In other works [157, 158], Ando's team investigated the crack-healing behavior of SiC/Si_3N_4 composite under cyclic stress at high temperatures. The composition of the composite was similar to what was reported in [153]. The hot pressing procedure was performed at 1800 °C for 2h under 35 MPa pressure in nitrogen gas. The results showed that the surface cracks can be healed completely under cyclic stress at 1100 and 1200 °C due to the crystallization of SiO_2 and $Y_2Si_2O_7$ [155, 159]. The healed samples showed similar bending strength to parent ceramic before indentation. Also it was found that the healing behavior of this composite is not dependent on the holding time at high temperature. Those samples healed after 0.5 h almost showed similar behavior to that one healed for 5h. Also the cyclic fatigue limit of healed samples at 900 °C was 550 MPa, and at 1000, 1100 and 1200°C was 650 MPa which was 80% of the bending strength of the non-cracked samples (800 MPa) [157,158]. They found that the threshold cyclic and static stresses in which the pre-cracked samples can be healed were 300 MPa at 1000 and 1200 °C, about 75% of the bending strength of the pre-cracked specimens. Figure 2.24 part a shows the SEM micrograph of the fracture surface of the healed sample at 1300 °C for 1h.

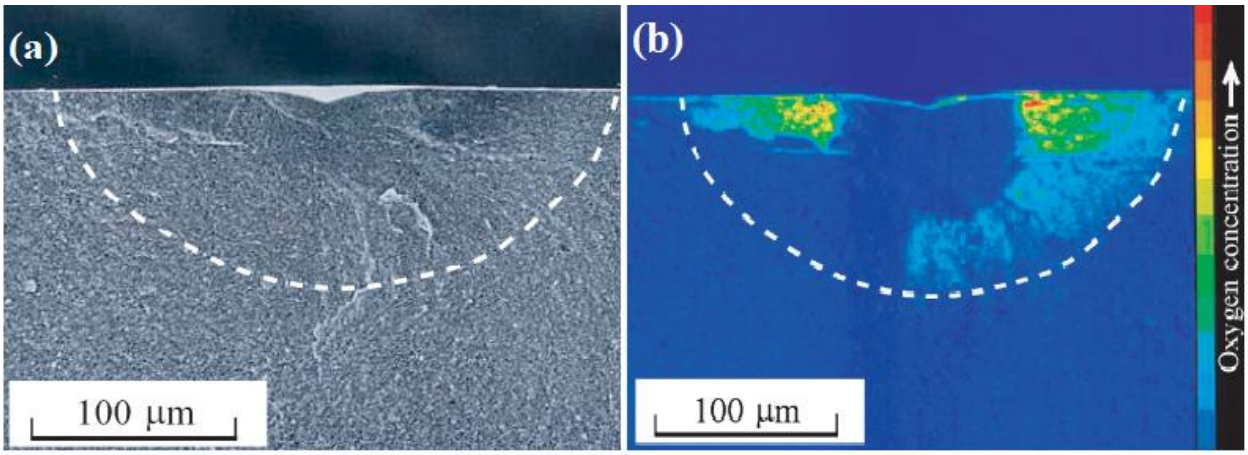

Figure 2.24. (a) SEM micrograph and (b) distribution of oxygen element measured by EMPA in the fracture surface of crack-healed SiC/Si_3N_4 composite. The pre-cracked specimen was healed in air at 1300 °C for 1h followed by bending test at room temperature. Reprinted with the permission from [158].

The white dotted line shows the front of the pre-cracked specimen. The results of EPMA analysis of the same location for the elemental mapping of oxygen is shown in figure 2.24 part b. As can be seen in this figure, the concentration of oxygen is high in the crack location which demonstrates the formation of oxide (SiO_2) in this region [158]. They also evaluated the influence of partial pressure of oxygen on the

healing behavior of SiC/Si_3N_4 composite to simulate the condition of micro-gas turbine blades which works under tensile stress at high temperature [160, 161]. The results showed that in the absence of any external stresses, oxygen pressure as low as 50 Pa is enough to heal the pre-cracked samples at 1300 °C for 10h [160]. However under constant stress of 200 MPa, at least the oxygen pressure of 500 Pa is required to achieve complete healing (performed at 1200 °C for 5h) [161].

2.23 SiC/ZrB_2

ZrB_2 is utilized in ultrahigh-temperature applications; therefore it is really important to engineer its oxidation behavior at high temperature. SiC/ZrB_2 shows good oxidation resistance at high temperature due to the formation of less volatile silica-rich surface layer rather than boria [44,45,180]. Zhang et al. [181] investigated the crack healing ability of SiC_w/ZrB_2 composite (containing 20 vol.% SiC whisker with the diameter of 0.2–1.0 μm and a length of 10–50 μm). A semicircular crack with a length of 70 μm was made on the specimens. The samples were healed in air and in a vacuum at 1000 °C for 1h. The bending strength of the un-cracked samples was 799 MPa. The produced crack decreased the bending strength of the samples to 279 MPa. After crack healing in air, the flexural strength of the specimens was recovered indicating a complete healing of the pre-cracked specimens. On the other hand, those samples healed in a vacuum only showed a small amount of strength recovery (351 MPa) as a result of removal of the residual stress ahead of the cracks [156]. Almost no crack healing was observed in those samples annealed in a vacuum. The oxidation of ZrB_2 to ZrO_2 and B_2O_3 at 800 °C, and SiC to SiO_2 at higher temperature and the formation of borosilicate glass is responsible for the healing behavior. Borosilicate layer is more protective than B_2O_3 due to its higher melting point and lower vapor pressure [182]. Consequently it fills the cracks and prevents the diffusion of oxygen into the structure and subsequently increases the oxidation resistance of the composite [181]. They also investigated the crack-healing behavior of the composite at 1200 °C for various holding times in air atmosphere. The strength of the specimens heat treated for 30 and 60 min showed a decrease and then an increase in comparison with parent specimens.

Figures 2.25 and 2.26 show the surface morphology of the heat treated samples at 1200 °C for 30 and 60 min, respectively. After annealing for 30 min, a river-style surface structure was formed as can be seen in figure 2.25 part a. It was found that zirconium-rich crystals gathered in the river valley. A porous zirconia structure with small SiO_2 flakes was observed as a result of the evaporation of oxidation products such as B_2O_3 and CO. The zirconia grains do not form a compact layer and consequently cannot seal the surface of the sample. When gases escape from the structure, they leave a channel of porosity and holes behind (figure 2.25, see d) which causes a decrease in the strength of the samples. With increasing the holding time to 60 min, more silica and borosilicate glass were formed which sealed the channels and pores between zirconia grain and subsequently increase the strength of the specimens [183].

Liang et al. [184] studied the oxidation healing of ZrB_2 -20 vol.% SiC-10 vol.% AlN composite. The average particle size of ZrB_2 , SiC and AlN was 2µm, 1µm and 100 nm, respectively. The powder mixture was hot pressed at 1850 ° C for 1h under the pressure of 30 MPa in an argon atmosphere. They found that oxidizing the specimens at 1000 °C for 1h (the optimum oxidizing time) can heal the cracks and prevent the penetration of oxygen into the interior layers due to the formation of a noticeable amount of SiO_2-rich borosilicate glass containing ZrO_2 and Al_2O_3.

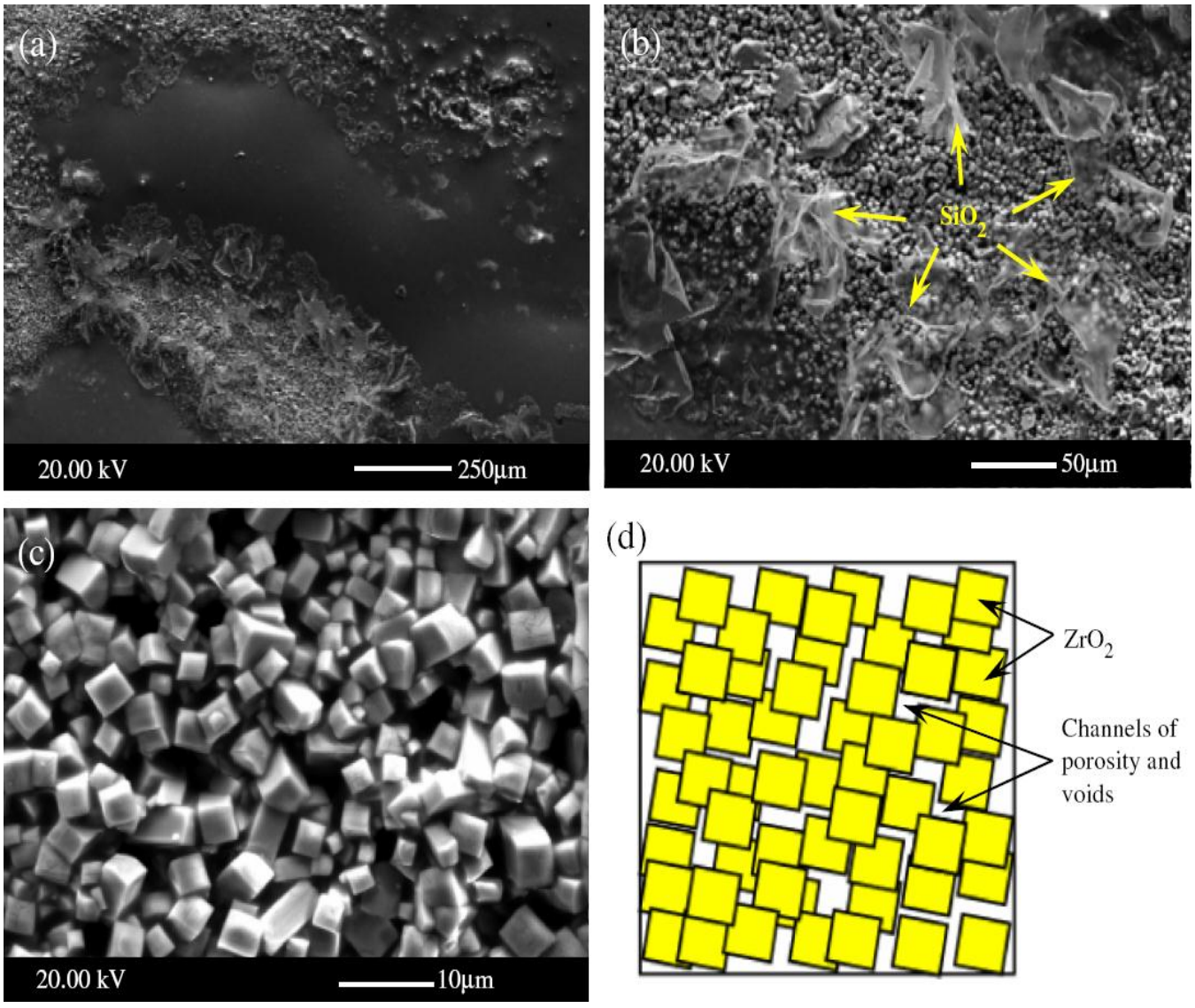

Figure 2.25. Scanning electron micrographs from the surface of ZrB_2–SiC after preoxidation at 1200 °C for 30 min. Reprinted with the permission from [183].

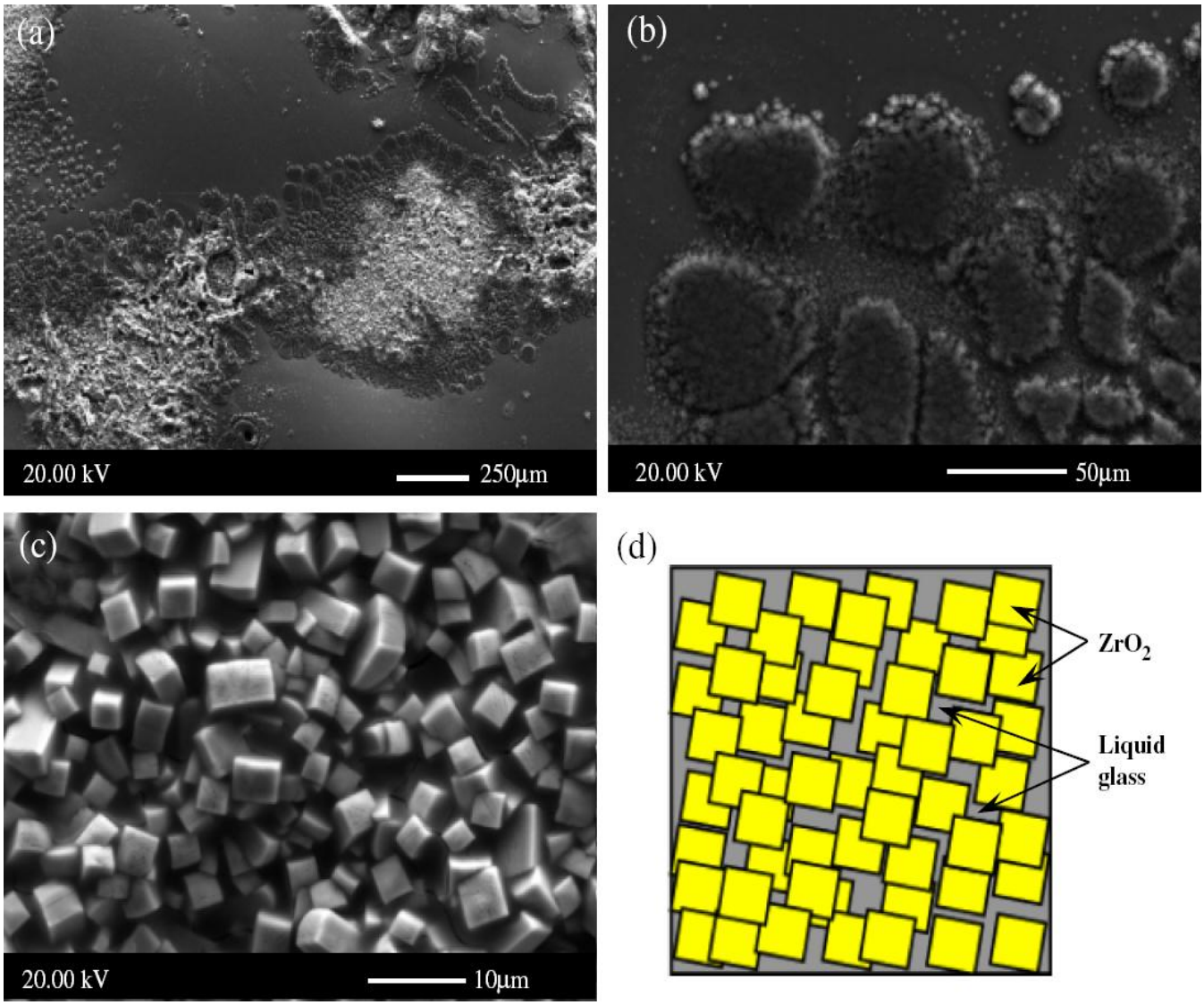

Figure 2.26. Scanning electron micrographs from the surface of ZrB_2–SiC after preoxidation at 1200 °C for 60 min. Reprinted with the permission from [183].

2.24 $SiC/Al_6Si_2O_{13}$

SiC/mullite ($Al_6Si_2O_{13}$) is another interesting composite in the field of self-healing ceramics which is the subject of many studies performed by Ando and his colleagues [185-206]. In the first study [185], the influences of particle size and volume fraction of SiC on the self-healing behavior of SiC/mullite composite was investigated. Those samples heat treated at 1300 °C for 1h in air showed the best crack healing behavior. It was found that an oxide layer formed on the surface of the ceramic after heat treatment in air. The best SiC/mullite composition (for self-healing and to recover the bending strength

of the pre-cracked samples) was reported as mullite containing 20 vol% SiC with particle size of about 0.56 µm. In the next study [186] the crack-healing behavior of SiC/mullite composite (15 vol% SiC with particle size of about 270 nm) was investigated under the static and cyclic stresses. It was found that in the absence of any external stress, the samples with semicircular cracks having length of 200 µm can be completely healed at 1300 °C for 1h in air. For those samples healed at 1300 °C with the crack diameter of less than 100 µm, most of the fatigue cracks occurred outside the crack-healed zone. However in those specimens with the crack diameter of about 200 µm, fracture occurred in the indentation location due to the stress concentration on the tip of the large indentation. Furthermore, with decreasing the annealing temperature to 1000 °C, 100 h heat treatment is required to heal a pre-cracked sample with crack diameter of about 100 µm. It was reported that the static and cyclic fatigue strengths of the healed samples are not dependent on the healing temperature and are similar to those samples healed at 1000 and 1300 °C. The crack-healed specimens showed higher static and fatigue strengths than those of non-cracked specimens due to the crack-healing phenomenon [186]. The SEM micrograph of the SiC/mullite composite (containing 20 vol% SiC with particle size of about 0.27 µm) after heat treatment at 1300 °C for 1h is shown in figure 2.27 part a [187].

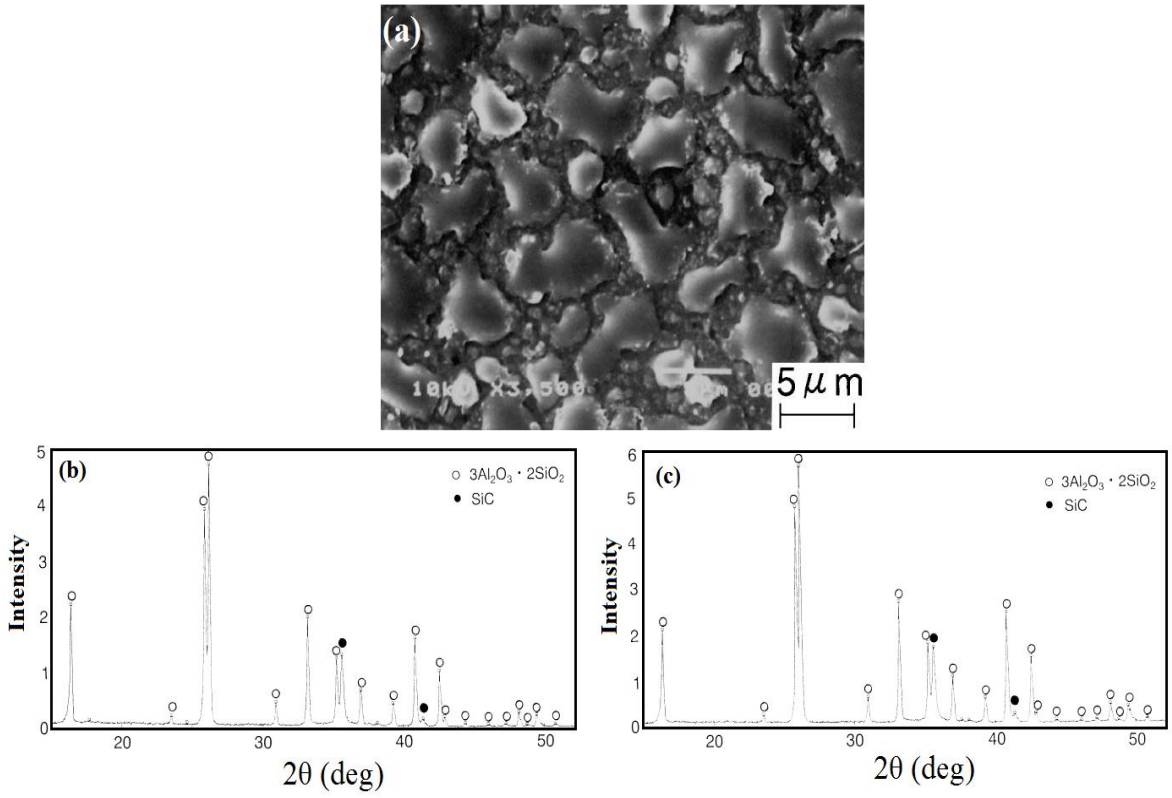

Figure 2.27. (a) SEM micrograph of the surface of the SiC/mullite composite heat treated at 1300 °C for 1 h in air. XRD patterns (b) before and (c) after heat treatment of the SiC/mullite composite at 1300 °C for 1 h in air. Reprinted with the permission from [187].

As can be seen some glassy phases are formed on the surface of the specimens. Also parts b and c in figure 2.27 show the XRD patterns of the specimens before and after annealing at 1300 °C for 1h. There is no difference in the XRD patterns and no new phase was observed after heat treatment. It can be concluded that some glassy phases formed during the annealing of the specimens which fill the cracks and heal the specimens [187]. In their next study the influence of Y_2O_3 was investigated on the crack-healing behavior of SiC/mullite composite [188]. For this purpose a composite of mullite containing 15 vol% SiC (with particle size of 0.27 µm) and 1.5 vol% Y_2O_3 (with particle size of 0.4 µm) was prepared. The powder mixture was hot pressed at 1650 °C and 35 MPa for 4h in nitrogen gas. It was found that the best crack-healing condition can be obtained after heat treatment at 1300 °C for 1h in air. Crack healing occurs by the oxidation reaction of SiC and Y_2O_3 and the formation of SiO_2 and $Si_2Y_2O_7$. It was found that in a similar condition, the bending strength of the healed Y_2O_3/SiC/mullite composite is lower than that of healed SiC/mullite composite. Consequently it can be concluded that the healing capability of Y_2O_3/SiC/mullite composite is less than SiC/mullite composite [188]. In another study the self-healing ability of mullite/SiC particle/SiC whisker multi composites was evaluated [189]. The results showed that in Mullite/15 vol% SiC whisker/10 vol% SiC particle the cracks can be completely healed at lower temperatures in comparison with mullite/25 vol% SiC whisker composites due to the different SiC distribution and geometry [142,189]. The bending strength of SiC/mullite (containing more than 20 vol% SiC) was higher than that of the base materials at room temperature. With increasing the SiC content in the matrix the fracture toughness of the composite increased. The best crack healing ability in mullite composites was reported for Mullite/15 vol% SiC whisker/10 vol% SiC particle composite with a shear deformation of about two times greater than that of monolithic mullite [189]. The threshold stresses at the healing temperature of 1200 °C, were 170 MPa for this composite for both constant and cyclic stresses, corresponding to 77% of the bending strength of the pre-cracked specimens (about 220 MPa) at room temperature. The cyclic and static fatigue strengths of the healed samples under the threshold stresses at 1200 °C for 100 h were 350 and 200 MPa, respectively which were higher than the threshold constant or cyclic stresses. The interesting result was that under cyclic fatigue the healing materials decreased the crack opening through a viscous flow. However under static fatigue, these bridging effects would not occur [190].

2.25 TiC/Si_3N_4

The crack self-healing behavior of TiC/Si_3N_4 composite under microwave and conventional heating procedures was studied by Li et al. [207]. Si_3N_4 containing 10 wt.% TiC (with particle size of 5 µm) and 3 wt.% MgO (as a sintering additives) were mixed and hot pressed at 1800 °C for 90 min in nitrogen atmosphere. The prepared specimens were quenched from 400 or 500 °C in ice water to produce microcracks. A 2.45 MHz microwave was utilized to heat the specimens at 1100 °C for 10 min in nitrogen gas (to avoid the oxidation of the specimens). Also specimens were heat treated in a conventional furnace at 1100 °C for 1h. Thermal shock decreased the bending strength of the specimens from 560 MPa to 320 and 350 MPa for those specimens quenched from 400 and 500 °C, respectively. The strength of those specimens heat treated in conventional furnace was partially recovered (between

67 to 85% for specimens quenched from 400 and 500 °C, respectively). However microwave heating completely recovered the bending strength of the samples in both groups. Through monitoring the electrical resistance of the specimens the healing mechanism was revealed. The resistance which is inversely proportional to the bending strengths increased from 300 to 1200 Ω in shocked specimens and then decreased to 400-600 Ω in heat treated samples. The resistance is dependent on the connectivity of the conductive phase (TiC and interfacial phases) inside the composite. When the microcracks are healed the resistance decreased. Investigations showed that TiC particles (with a high dielectric constant) and the regions with low density and abundant defects (such as porous areas, cracking zones, and grain boundaries), which have higher microwave-energy absorption ability, reach higher temperature than the surrounding matrix and may subsequently melt, diffuse and rebond with the surrounding glassy phase or matrix [207]. This type of selective heating may be considered as the main reason for the strength-recovery of the specimens heat treated with microwave [208]. Thus the mechanism of crack self-healing of TiC/Si_3N_4 composite was considered as the localized melting and chemical reaction between the TiC phase and the matrix occurred by microwave heating due to its much higher dielectric loss factor and good microwave-energy absorption ability than Si_3N_4 [207].

2.26 Si-B-C

The major limitation of carbon-containing composites at high-temperature applications is their poor oxidation resistance [209]. Carbon oxidizes at temperatures above 450 °C. In the presence of boron particles, heating the composite in an oxidizing environment causes the formation of a liquid phase such as B_2O_3 (in the range of 600 to 1200 °C) or a ternary phase containing boron and oxygen which flows into the cracks and heals them [210-225]. Also this phase acts as a barrier and prevents the penetration of oxygen into the interior layers, hence increases the oxidation resistance. Wang et al. [210] reported that the weight loss of boron-bearing specimens decreased from about 36 to 16 wt% after oxidizing the samples at 800 °C for 10 h in air. Zuo et al. [211] investigated the self-healing behavior of C/SiC composite modified with Si-B-C. They found an excellent oxidation resistance for the modified samples. Three different samples were prepared and their oxidation behavior was studied below and above 1000 °C. Figure 2.28 shows the oxidation models of C/SiC composites with different kinds of coatings. As can be seen in figure 2.28 part a, a layer of borosilicate glass is formed on the surface of specimen A due to the reaction between B_2O_3 and SiO_2 and subsequently the formation of $B_2O_3.xSiO_2$. The formed borosilicate flows into the cracks and consequently prevents the diffusion of oxygen into the interior layers and therefore slows down the oxidation of carbon which causes the weight loss. It should be noted that the volatilization of the formed borosilicate glass is below 1000 °C and hence the thickness of the Si-B-C layer almost remain constant. However in sample B less borosilicate glass is formed and as a result the cracks cannot be sealed completely. Subsequently more oxygen can penetrate into the structure and oxidize the carbonaceous materials. In specimen C there is no Si-B-C coating therefore no glassy phase is formed and a severe oxidation occurs.

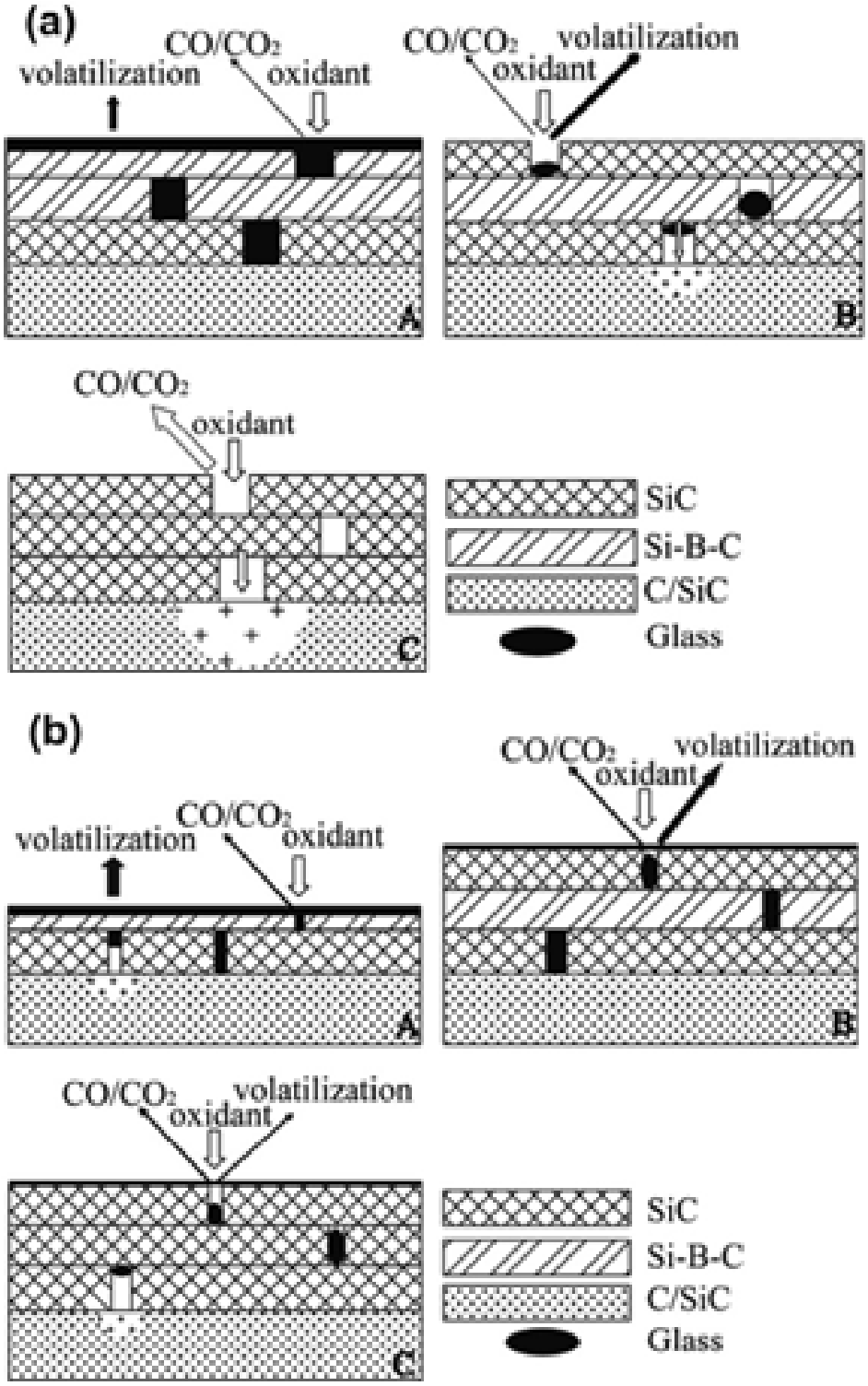

Figure 2.28. Oxidation models for specimens with different kinds of coatings in static air. (a) Specimens oxidized at low temperature (below 1000 °C), (b) specimens oxidized at high temperature (above 1000 °C). Reprinted with the permission from [211].

With increasing the temperature above 1000 °C (figure 2.28 part b), some cracks will be closed due to the thermal mismatch between the matrix and the fibers. Moreover, more borosilicate glass is produced which heals the cracks. As a result the diffusion of oxygen decreases. However, the volatilization of borate and borosilicate glass are aggravated at temperature higher than 1000 °C and therefore the thickness of the Si-B-C layer decreased which causes the oxidation of C/SiC substrate. In specimen B, SiO_2 forms on the surface of the samples (due to the oxidation of exterior SiC layer). The formed silica is highly viscos and hence decreases the volatilization of the borosilicate glass. Again specimen C cannot prevent the oxidation of carbonaceous materials; however, because the high temperature silica glass is formed, it partly seals the cracks and decreases the diffusion of oxygen into the interior layers. Figure 2.29 shows the formed borosilicate glass on the specimen B after annealing at 1300 °C for 50h in air [211]. Kobayashi et al. [212] investigated the self-healing ability and oxidation resistance of different carbon composites containing B_4C and SiC particles. They found that the healing behavior improved with increasing the B_4C and SiC volume fraction. The prepared composite was oxidized at 800 and 1200 °C and it was found that those samples oxidized at 1200 °C can provide an impact protective borosilicate glass layer which can heal the cracks and prevent the penetration of oxygen into the substrate. Figure 2.30 shows the oxidation model for the carbon- B_4C-SiC composite proposed by Kobayashi et al. [212].

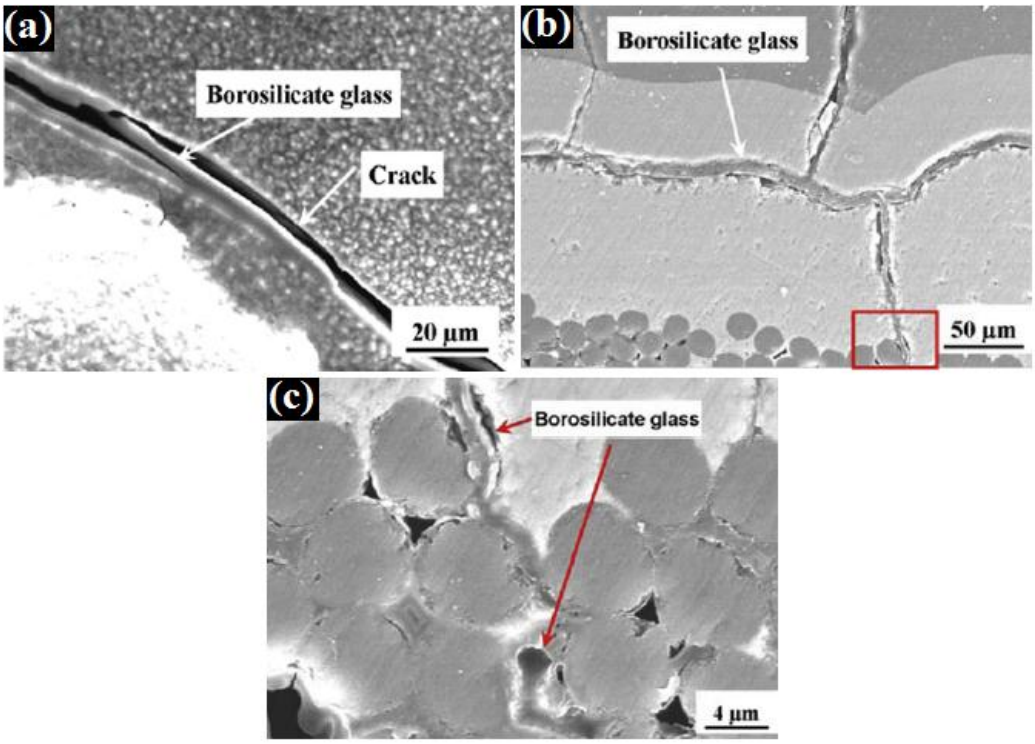

Figure 2.29. (a) Surface morphology and (b and c) cross-section morphology of C/SiC composite modified with Si-B-C (specimen B in figure 2.25) after oxidizing at 1300 °C for 50h in static air. Reprinted with the permission from [211].

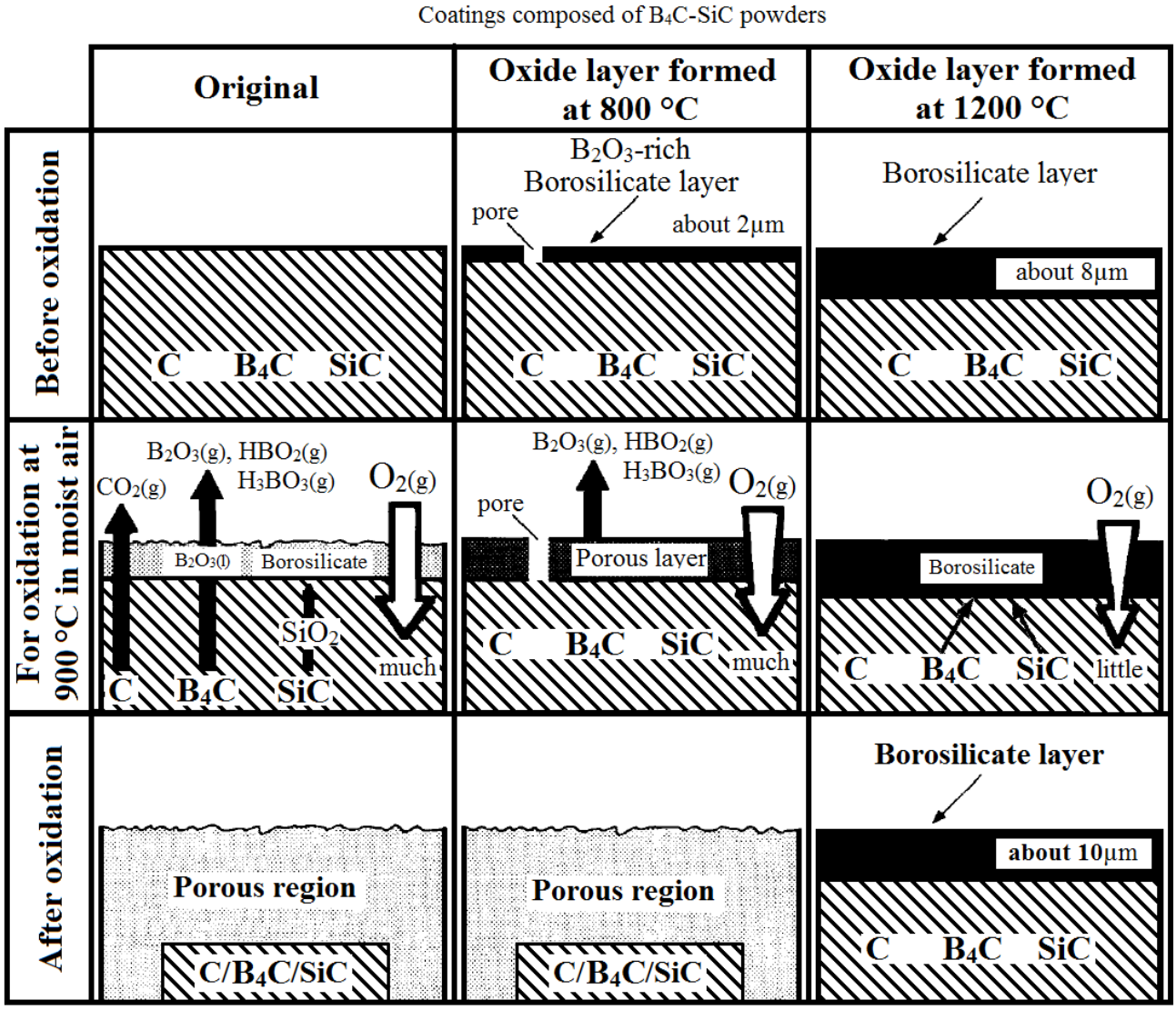

Figure 2.30. Oxidation model at 900°C in moist air for carbon-B_4C-SiC composites with and without oxide layer pre-formed at 800°C and 1200°C. Reprinted with the permission from [212].

2.27 Summary and future perspectives

Structural integrity of ceramics especially in high temperature application is a very important issue from safety and performance point of views. Inherently ceramics are brittle materials and are very sensitive to flaws which may develop many microcracks under thermal shocks and/or static or cyclic stresses. These microcracks can degrade the strength of the ceramic structure and cause the failure of the components in service. Therefore to increase the reliability of the ceramic components, the produced cracks should be controlled and managed in some way. The best known practical solution for this challenge is the capability of crack self-healing. Crack self-healing occurs through various mechanisms in different

ceramics. Grain growth at high temperatures, mass transportation phenomenon such as grain-boundary diffusion, bulk diffusion, surface diffusion, or evaporation and condensation, sintering phenomena, grain rearrangement and phase transformation (such as what happened in zirconia), chemical reactions such as oxidation of the composite constituents which is accompanied with a volume expansion, adhesion of the crack surfaces to each other, formation of glassy phase at high temperature and rebonding the crack surfaces are some examples of crack-healing mechanisms in ceramics. Ceramics with crack self-healing ability can guarantee the structural integrity and open a new horizon for application of ceramic materials in high temperature application.

Further development may be a combination of shape memory effect with the existing healing mechanisms, which is particularly important for those ceramics that only partial crack closing is achieved. The concept has been well demonstrated in self-healing of polymers. For example, Li's team proposed a bio-inspired two-step close-then-heal (CTH) approach by mimicking the self-healing process of human skin based on shape memory polymers (SMPs) [226-238]. It is further divided into two subgroups: SMPs as matrix [226-234] or SMP fibers as embedded sutures [235-238]. When SMP serves as matrix, it is first programmed by compression to reduce its volume. When a crack is created during service, the SMP is heated up to above its transition temperature, leading to shape recovery, i.e., volume expansion. Due to the constraint by surrounding cold materials or structure boundary, this volume expansion is not free, leading to closure of internal cracks. Further heating leads to melting of the embedded thermoplastic healing agent, which is sucked into the narrowed crack by capillary force, diffused into the fractured matrix by concentration gradient and shape recovery pressure, and entangled with the matrix molecules to form molecule level healing. In the second subgroup, SMP fibers were embedded in conventional polymer matrix, which does not have shape memory capability. The fibers were pre-stretched before embedding into the polymer matrix. When a crack is created in the matrix, heating leads to shape recovery (shrinkage) of the SMP fibers bridging over the crack. Due to the constraints by the matrix, this shrinkage is not free, pulling the fractured matrix surfaces marching towards each other and leading to closure of the crack. Again, further heating leads to the molecular healing process, similar to the other subgroup. We believe this proven mechanism can be transferred to self-healing ceramics. For example, volume expansion during phase transformation can be used in closing crack, and healing agent such as SiC [92,239], can heal crack molecularly. Because the crack has been closed or significantly narrowed due to phase transformation, only a small amount of healing agent is needed. Similar to SMP fibers, if pre-stretched shape memory alloy (SMA) fibers are embedded in ceramic matrix, they may be used as embedded suture to close cracks in ceramic matrix because they can survive high temperature environment [240,241]. Some ceramics such as ZrW_2O_8 have negative coefficient of thermal expansion [242]. If they are used in the form of whiskers in ceramic matrix, they may have similar function as SMA wires.

2.28 References

[1] Madhan M, Prabhakaran G. Self healing ability of structural ceramics - a review. Trends in Intelligent Robotics, Automation, and Manufacturing Communications in Computer and Information Science 2012;330:466-74.

[2] van der Zwaag S. Routes and mechanisms towards self healing behavior in engineering materials. Bull Pol Ac Tech 2010;58:227-36.

[3] Bush EA, Hummel FA. High temperature mechanical properties of ceramic materials: I, magnesium dititanate. J Am Ceram Soc 41 (1958) 189-95.

[4] Bain AS. Cracking and bulk movement in irradiated uranium oxide fuel elements. Trans Am Nucl Soc 1963;6:352-3.

[5] Ellington JP. Temperatures, thermal stresses and displacements in solid uranium dioxide rods. Brit J Appl Phys 1960;11:33.

[6] Roberts JTA, Wrona BJ. Crack healing in UO_2. J Am Ceram Soc 1973;56:297-9.

[7] Dutton R. Comments on "Crack Healing in UO_2". J Am Ceram Soc 1973;56:660-1.

[8] Dutton R. Comments on "Crack Healing in UO_2". J Am Ceram Soc 1976;59:88.

[9] Bandyopadhyav G, Kennedy CR. Isothermal crack healing and strength recovery in UO_2 subjected to varying degrees of thermal shock. J Am Ceram Soc 1977;60:48-50.

[10] Bandyopadhyav G, Kennedy CR. Crack healing and strength recovery in UO_2. J Am Ceram Soc 1976;59:415-9.

[11] Ainscough JB, Rigby F. Measurements of crack sintering rates in UO_2 Pellets. J Nucl Mater 1973;47:246-50.

[12] Singh RN, Routbort JL. Fracture and crack healing in (U, Pu)C. J Am Ceram Soc 1979;62:128-33.

[13] Heuer AH, Roberts JP. The influence of annealing on the strength of corundum. Cryst Proc Br Ceram Soc 1966;6:17–27.

[14] Kim BS, Ando K, Chu MC, Saito S. Crack-healing behavior of monolithic alumina and strength of crack-healed member. J Soc Mater Sci Jpn 2003;52:667-73.

[15] Gupta TK. Crack healing and strengthening of thermally shocked alumina. J Am Ceram Soc 1976;59:259-62.

[16] Lange FF, Radford KC. Healing of surface cracks in polycrystalline Al_2O_3. J Am Ceram Soc 1970;53:420-1.

[17] Choi SR, Tikare V. Crack healing of alumina with a residual glassy phase: strength, fracture toughness and fatigue. Mater Sci Eng A 1993;171:77-83.

[18] Wilson BA, Lee KY, Case ED. Diffusive crack-healing behavior in poly crystalline alumina: a comparison between microwave annealing and conventional annealing, Mater Res Bull 1997;32:1607-16.

[19] Nightingale SA, Dunnie DP, Worrier HK. Sintering and grain growth of 3 mol% yttria zirconia in a microwave field. J Mater Sci 1996;31:5039.

[20] Moffatt J, Plumbridge WJ, Hermann R. High temperature crack annealing effect on fracture toughness of alumina and alumina–SiC composite. Br Ceram Trans 1996;95:23-9.

[21] Mitomo M, Nishmura T, Tsutsumi M. Crack healing in silicon nitride and alumina ceramics. J Mater Sci lett 1996;15:1976-8.

[22] Yen CF, Coble RL. Spheroidization of tubular voids in Al_2O_3 crystals at high temperatures. J Am Ceram Soc 1972;55:507-9.

[23] Gupta TK. Crack Healing in $A1_2O_3$, MgO, and related materials. Advances in Ceramics, Vol. 10, Structure and Properties of MgO and $A1_2O_3$ Ceramics. In: Kingery WD, editor. Columbus, OH: American Ceramic Society; 1984, p. 750-66.

[24] Gupta TK. Instability of cylindrical voids in alumina. J Am Ceram Soc 1978;61:191-5.

[25] Hockey BJ, Lawn BR. Electron microscopy of microcracking about indentations in aluminum oxide and silicon carbide. J Mater Sci 1975;10:1275-84.

[26] Gupta TK. Alteration of cylindrical voids during crack healing in alumina. In: Fulrath RM, Pask JA, editors. Boulder, CO: Westview Press; 1977, p. 354-65.

[27] Maruyama O, Komatsu W. Observations on the grain-boundary of Al_2O_3 Bicrystals. Ceramurgia Int 1979;5:51-5.

[28] Rodel J, Glaeser AM. Application of controlled interfacial pore structures to kinetic studies in alumina. Mater Res Soc Proc 1988;122:485-90.

[29] Mallinder FP, Proctor BA. Preparation of high-strength sapphire crystals. Proc Br Ceram Soc 1966;6:9-16.

[30] Davies LM. The effect of heat treatment on the tensile strength of sapphire. Proc Br Ceram Soc 1966;6:29-35.

[31] Evans AG, Charles EA. Strength recovery of diffusive crack healing. Acta Metall 1977;25:919-27.

[32] Huang FH, Henrichsen RA, Li CY. A study of the capillarity and mass transport on the $A1_2O_3$ Surface, in Sintering and Catalysis. In: Kuczynski GC, editor. New York: Plenum Press; 1975, p. 173-86.

[33] Rodel J, Glaeser AM. High temperature healing of lithographically introduced cracks in sapphire. J Am Ceram Soc 1990;73:592-601.

[34] Powers JD, Glaser AM. High temperature healing of crack like flaws in Mg- and Ca-ion-implanted sapphire. J Am Ceram Soc 1992;75:2547-58.

[35] Powers JD, Glasser AM. High-temperature healing of crack like flaws in titanium ion-implanted sapphire. J Am Ceram Soc 1993;76:2225-34.

[36] Matsuo Y, Ogasawara T, Kimura S, Sato S, Yasuda E. The effect of annealing on surface machining damage of alumina ceramics. J Ceram Soc Jpn 1991;99:384-9.

[37] Rodel J, Glaeser AM. Production of controlled-morphology pore arrays: implications and opportunities. J Am Ceram Soc 1987;70:172-5.

[38] Kirchner HP, Gruver RM, Walker RE. Strength effects resulting from simple surface treatments; in The Science of Ceramic Machining and Surface Finishing. In: Schneider SJ, Rice RW, editors. Washington, DC: U.S. Government Printing Office; 1972, p. 353-63.

[39] Lange FF, Clarke DR. Morphological changes of an intergranular thin film in a polycrystalline spinel. J Am Ceram Soc 1982;65:502-6.

[40] Case ED, Smyth JR, Hunter O, Microcrack healing during the temperature cycling of single phase ceramics; in Fracture Mechanics of Ceramics. Vol. 5. In: Bradt RC, Evans AG, Hassleman DPH, Lange FF, editors. New York: Plenum; 1983, p. 507-30.

[41] Ando K, Shirai Y, Nakatani M, Kobayashi Y, Sato S. [Crack- healing _ proof test] to guarantee the reliability of ceramics components. in Structural Integrity in the 21st Century. In: Edwards JH, Flewitt PEJ, Gasper BC, Mclarty KA, Smith RA, Stanley P, Temple JAG, Tomkins B, editors. West Midlands, U.K.: EMAS Publishing; 2000, p. 345–55.

[42] Wang J, Stevens R. Modification of indentation cracks in TZP ceramics by thermal treatment. J Mater Sci Lett 1988;7:560-2.

[43] Jun L, Zheng ZX, Ding HF, Jin ZH. Preliminary study of the crack healing and strength recovery of Al_2O_3-matrix composites. Fatigue Fract Eng Mater Struct 2004;27:89-97.

[44] Houjou K, Ando K, Takahashi K. Crack-healing behavior of zirconia/SiC composite ceramics. J Soc Mat Sci Jpn 2009;58:510-5.

[45] Houjou K, Sudo S, Takahashi K. Crack-healing behavior of zirconia/SiC composite ceramics and strength properties of crack-healing specimens. J Soc Mat Sci Jpn 2011;60:742-7.

[46] Lange FF, Gupta TK. Crack healing by heat treatment. J Am Ceram Soc 1970;53:54-5.

[47] Gupta TK. Crack healing in thermally shocked MgO. J Am Ceram Soc 1975;58:143.

[48] Sangwal K, Gorostiza P, Sanz F. In situ study of the recovery of nanoindentation deformation of the (100) face of MgO crystals by atomic force microscopy, Surf Sci 1999;442:161-78.

[49] Bronisz SE, Deuglass DL. Grain growth in thin films of ThO_2, NpO_2, and PuO_2. Phys Status Solidi 1968;29:95- 7.

[50] Petrovic JJ, Jacobson LA, Talty PK, Vasudevan AK. Controlled surface flaws in hot-pressed Si_3N_4. J Am Ceram Soc 1975;58:113-6.

[51] Choi SR, Tikare V. Crack healing behavior of hot pressed silicon nitride due to oxidation. Scr Metall Mater 1992;26:1263-8.

[52] Wilson SR, Tikare V, Pawlik R. Crack healing in silicon nitride due to oxidation. Ceram Eng Sci Proc 1991;12: 2190-202.

[53] Tighe TJ, Wiederhorn SM. Fracture mechanics of ceramics. Vol 5. New York: Plenum Press; 1983, p. 403.

[54] Easler TE, Bradt RC, Tressler RE. Effects of oxidation under load on strength distribution of Si_3N_4. J Am Ceram Soc 1982;65:317-20.

[55] Zhang YH, Edwards L, Plumbridge WJ. Crack healing in a silicon nitride ceramic. J Am Ceram Soc 1998;81:1861-8.

[56] Wiederhorn SM, Tighe NJ. Structural reliability of yttria-doped hot-pressed silicon nitride at elevated temperatures. J Am Ceram Soc 1983;66:884-9.

[57] Klemm H. Silicon nitride for high-temperature applications. J Am Ceram Soc 2010;93:1501-22.

[58] Ando K, Sato S, Kobayashi Y, Chu MC. Crack healing behaviour of Si_3N_4 ceramics and its application to structural integrity. in Fracture from Defects, EFC-12. In: Brown MW, de los Rios ER, Miller KJ, Editors. Sheffield, U.K.: Engineering Materials Advisory Services; 1998, p. 497–502.

[59] Ando K, Chu MC, Sato S, Yao F, Kobayashi Y. The study on crack healing behavior of silicon nitride ceramics. Jpn Soc Mech Eng 1998;64:1936-42.

[60] Ando K, Chu MC, Kobayashi Y, Yao F, Sato S. Crack healing behavior and high temperature strength of silicon nitride ceramics. Jpn Soc Mech Eng 1999;65:1132-9.

[61] Chu MC, Ando K, Sato S, Hirasawa T, Kobayashi Y. Crack-healing behavior of silicon nitride ceramics (effect of chemical composition on crack healing ability). High Pressure Inst Jpn 1998;36:82-9.

[62] Kim BA, Ando K, Sato S. Effect of grinding on cracks and the strength of ceramics. Fatigue Fract Eng Mater Struct 1994;17:187-200.

[63] Ogasawara T, Hori T, Okada A. Threshold stress intensity for oxidative healing in silicon nitride. J Mater Sci Letts 1994;13:404-6.

[64] Takahashi K, Kim BS, Chu MC, Sato S, Ando K. Self crack-healing behavior under stress of silicon nitride ceramics and resultant strength at the crack-healing temperature. Jpn Soc Mech Eng 2002;68:1063-70.

[65] Nakatani M, Ando K, Houjou K. Oxidation behavior of Si_3N_4/Y_2O_3 system ceramics and effect of crack-healing treatment on oxidation. J Eur Ceram Soc 2008;28:1251-7.

[66] Hickman SH, Evans B. Influence of geometry upon crack healing rate in calcite. Phys Chem Miner 1987;15:91-102.

[67] Chikada T, Suzuki A, Yao Z, Sawada A, Terai T, Muroga T. Basic study on self-healing of Er_2O_3 coating for vanadium–lithium blanket system. Fusion Eng Des 2007;82:2572-7.

[68] Lamaka SV, Zheludkevich ML, Yasakau KA, Montemor MF, Cecílio P, Ferreira MGS. TiOx self-assembled networks prepared by templating approach as nanostructured reservoirs for self-healing anticorrosion pre-treatments, Electrochem Commun 2006;8:421-8.

[69] Lamaka SV, Zheludkevich ML, Yasakau KA, Serra R, Poznyak SK, Ferreira MGS. Nanoporous titania interlayer as reservoir of corrosion inhibitors for coatings with self-healing ability. Prog Org Coat 2007;58:127-35.

[70] Park M, Oboyle DR. Observation of crack healing in sodium chloride single crystals at low temperatures, J Mater Sci 1977;12:840-1.

[71] Song GM, Pei YT, Sloof WG, Li SB, De Hosson JTM, van der Zwaaga S. Oxidation-induced crack healing in Ti_3AlC_2 ceramics. Scripta Mater 2008;58:13-6.

[72] Song GM, Pei YT, Sloof WG, Li SB, De Hosson JTM, van der Zwaag S. Early stages of oxidation of Ti_3AlC_2 ceramics. Mater Chem Phys 2008;112:762-8.

[73] Zhou YC, Sun ZM, Wang XH, Chen S. Ab initio geometry optimization and ground state properties of layered ternary carbides, Ti_3MC_2 (M=Al Si and Ge). J Phys Condens Matter 2001;13:10001-10.

[74] Legzdina D, Robertson IM, Birnbaum HK. Oxidation behavior of a single phase γ-TiAl alloy in low-pressure oxygen and hydrogen. Acta Mater 2005;53:601-8.

[75] Wang XH, Zhou YC. Stability and selective oxidation of aluminum in nano-laminate Ti_3AlC_2 upon heating in argon. Chem Mater 2003;15:3716-20.

[76] Sun Z, Zhou Y, Li M. Oxidation behaviour of Ti_3SiC_2-based ceramic at 900 - 1300°C in air. Corros Sci 2001;43:1095-109.

[77] Yang HJ, Pei YT, Rao JC, De Hosson JTM, Li SB, Song GM. High temperature healing of Ti_2AlC: On the origin of inhomogeneous oxide scale. Scripta Mater 2011;65:135-8.

[78] Li S, Song G, Kwakernaak K, van der Zwaag S, Sloof WG. Multiple crack healing of a Ti_2AlC ceramic. J Eur Ceram Soc 2012;32:1813-20.

[79] Li S, Xiao L, Song G, Wu X, Sloof WG, van der Zwaag S. Oxidation and crack healing behavior of a fine-grained Cr_2AlC ceramic. J Am Ceram Soc 2013;96:892-9.

[80] Huang XX, Wen GW. Mechanical properties of Al_4SiC_4 bulk ceramics produced by solid state reaction. Ceram Int 2007;33:453-8.

[81] Chen G, Zhang R, Zhang X, Zhao L, Han W. Oxidation-induced crack healing in $Zr_2Al_4C_5$ ceramic. Mater Des 2009;30:3602-7.

[82] Rao YK. Stoichoimetry and thermodynamics of metallurgical processed. Cambridge, UK: Cambridge University Press; 1985.

[83] Gao J, Zhang D, Suo J. Tritium permeation barrier based on self-healing composite materials. Fusion Eng Des 2010;85:1618-23.

[84] Gao J, Suo J. Effects of heating temperature and duration on the microstructure and properties of the self-healing coatings. Sur Coat Technol 2011;206:1342-50.

[85] You XQ, Si TZ, Liu N, Ren PP, Xu YD, Feng JP. Effect of grain size on thermal shock resistance of Al_2O_3-TiC ceramics. Ceram Int 2005;31:33-8.

[86] Ohya Y, Nakagawa Z, Hamano K. Crack healing and bending strength of aluminum titanate ceramics at high temperature J Am Ceram Soc 1988;71:232-3.

[87] Lange FF. Healing of surface cracks in SiC by oxidation. J Am Ceram Soc 1970;53:290.

[88] Petrovic JJ, Jacobson LA. Controlled surface flaws in hot-pressed SiC. J Am Ceram Soc 1976;59:34-7.

[89] Gulbransen EA, Jansson SA. High-temperature oxidation, reduction and volatilization reactions of silicon and silicon carbide. Oxid Metals 1972;4:181-201.

[90] McLean AF, Fisher EA, Bratton RJ. Brittle materials design, high temperature gas turbine. Tech Rept AMMRC CTR 1973;73:169-210.

[91] Korouš J, Chu MC, Nakatani M, Ando K. Crack healing behavior of silicon carbide ceramics. J Am Ceram Soc 2000;83:2788-92.

[92] Kim HW, Kim HE, Song H, Ha J. Effect of oxidation on the room-temperature flexural strength of reaction-bonded silicon carbides. J Am Ceram Soc 1999;82:1601-4.

[93] Chu MC, Cho SJ, Lee YC, Park HM, Yoon DY. Crack healing in silicon carbide. J Am Ceram Soc 2004;87:490-2.

[94] Nam KW. Effect of crack healing of SiC according to times of SiO_2 Colloid Coating. J Powder Technol 2013;Article ID 695895, http://dx.doi.org/10.1155/2013/695895.

[95] Magnani G, Beaulardi L, Brentari A, Toyoda T, Takahashi K. Crack healing in liquid-phase-pressureless-sintered silicon carbide-aluminum nitride composites. J Eur Ceram Soc 2010;30:769-73.

[96] Lee SK, Ishida W, Ando K. Strength properties of crack-healed silicon carbide ceramics. J Soc Mater Sci Jpn 2002;52:674-80.

[97] Lee SK, Ishida W, Lee SY, Nam KW, Ando K. Crack-healing behavior and resultant strength properties of silicon carbide ceramic. J Eur Ceram Soc 2005;25:569-76.

[98] Ohji T, Yamauchi Y, Kanematsu W, Ito S. Dynamic and static fatigue strength and crack propagation of engineering ceramics. Nippon Seramillusu Kyokai Gakujutsu Ronbunshi 1990;98:521-8.

[99] Ando K, Takahashi K, Nakao W, Osada T, Iwanaka K. New Technology for Increasing Through-life reliability ceramics components using self-crack-healing ability. J Powder Technol 2013;Article ID 937312, http://dx.doi.org/10.1155/2013/937312.

[100] Maity A, Kalita D, Kayal N, Goswami T, Chakrabarti O, Rao PG. Oxidation behavior of SiC ceramics synthesized from processed cellulosic bio-precursor. Ceram Int 2012;38:4701-6.

[101] Lee SK, Ando K, Kim YW. Effect of heat treatments on the crack-healing and static fatigue behavior of silicon carbide sintered with Sc_2O_3 and AlN. J Am Ceram Soc 2005;88:3478-82.

[102] Chu MC, Matushita S, Sato S, Ando K, [Crack-healing+ Proof test] to guarantee the reliability of ceramics composites. Bulletin of the Faculty of Engineering, Yokohama National University 2001;50:13–22.

[103] Chen Y, Wang C, Zhao W, Lu W, Chen A, Tan T. Fabrication of a SiC/Si/$MoSi_2$ multi-coating on graphite materials by a two-step technique. Ceram Int 2012;38:2165-70.

[104] Smith DL, Evans B, Diffusional crack healing in quartz. J Geophys Res 1984;89:4125-35.

[105] Sprunt ES, Nur A, Microcracking and healing in granites: new evidence from cathodoluminescence. Science 1979;205:495-7.

[106] Wanamaker BJ, Evans B, Experimental diffusional crack healing in olivine. In: Schock RN, editor. Point Defects in Minerals, Geophysical Monograph 31. Washington, D.C: Am Geophys Union; 1985, p. 194-210.

[107] Kim YW, Ando K, Chu MC. Crack-healing behavior of liquid-phase-sintered silicon carbide ceramics. J Am Ceram Soc 2002;86:465-70.

[108] Federico S, Monica F, Milena S. Multilayer coating with self-sealing properties for the carbon–carbon composites. Carbon 2003;41:2105-11.

[109] Nakatani M, Nishimura J, Hanaki S, Uchida H. Crack healing behavior of SiN/SiC nano-laminated films, 13th International Conference on Fracture, Beijing, China, 2013.

[110] Fu Q, Zou X, Chu Y, Li H, Zou J, Gu C. A multilayer $MoSi_2$-SiC-B coating to protect SiC-coated carbon/carbon composites against oxidation. Vacuum 2012;86:1960-3.

[111] Thompson AM, Chan HM, Harmer MP. Crack healing and stress relaxation in Al_2O_3-SiC "nanocomposites". J Am Ceram Soc 1995;78:567-71.

[112] Chiu CC. Influence of surface oxidation on thermal shock resistance and flexural strength of SiC/Al_2O_3 composites. J Mater Sci 1994;29:2078-82.

[113] Kim HE. Oxidation behavior and effects of Oxidation on the strength of SiC-wisker reinforced alumina. J Mater Sci 1994;29:1656-61.

[114] Kim HE, Moorhead AJ, Kim SH. Strengthening of alumina by formation of a mullite/glass layeron the surface. J Am Ceram Soc 1997;80:1877-80.

[115] Chou IA, Chan HM, Harmer MP. Effect of annealing environment on the crack healing and mechanical behavior of silicon carbide-reinforced alumina nanocomposites. J Am Ceram Soc 1998;81:1203-8.

[116] Ando K, Furusawa K, Takahashi K, Chu MC, Sato S. Crack-healing behavior of structural ceramics under constant and cyclic stress at elevated temperature. J Ceram Soc Jpn 2002;110:741-7.

[117] Takahashi K, Yokouchi M, Lee SK, Ando K. Crack-healing behavior of Al_2O_3 toughened by SiC whiskers. J Am Ceram Soc 2003;86:2143-7.

[118] Ando K, Kim BS, Chu MC, Saito S, Takahashi K. Crack-healing and mechanical behaviour of Al_2O_3/SiC composites at elevated temperature. Fatigue Fract Eng Mater Struct 2004;27:533-41.

[119] Lee SK, Takahashi K, Yokouchi M, Suenaga H, Ando K. High-Temperature Fatigue Strength of Crack-Healed Al_2O_3 Toughened by SiC Whiskers. J Am Ceram Soc 2004;87:1259-64.

[120] Nakao W, Ono M, Lee SK, Takahashi K, Ando K. Critical crack-healing condition for SiC whisker reinforced alumina under stress. J Eur Ceram Soc 2005;25:3649-55.

[121] Ando K, Kim BS, Kodama S, Ryu SH, Takahashi K, Saito S. Fatigue strength of an Al_2O_3/SiC composite and a monolithic Al_2O_3 subjected to crack-healing treatment. J Soc Mat Sci Jpn 2003;52:1464-70.

[122] Ando K, Yokouchi M, Lee SK, Takahashi K, Nakao W, Suenaga H. Crack-healing behavior, high temperature strength and fracture toughness of alumina reinforced by SiC whiskers. J Soc Mat Sci Jpn 2004;53:599-606.

[123] Osada T, Nakao W, Takahashi K, Ando K, Saito S. Strength recovery behavior of machined Al_2O_3/SiC nano-composite ceramics by crack-healing. J Eur Ceram Soc 2007;27:3261-7.

[124] Ono M, Nakao W, Takahashi K, Nakatani M, Ando K. A new methodology to guarantee the structural integrity of Al_2O_3/SiC composite using crack healing and a proof test. Fatigue Fract Eng Mater Struct 2007;30:599-607.

[125] Kim HS, Kim MK, Kang SB, Ahn SH, Nam KW. Bending strength and crack healing behavior of Al_2O_3/SiC composites ceramics. Mater Sci Eng A 2008;483:672-5.

[126] Chlup Z, Flasar P, Kotoji A, Dlouhy I. Fracture behaviour of Al_2O_3/SiC nanocomposite ceramics after crack healing treatment. J Eur Ceram Soc 2008;28:1073-7.

[127] Ando K, Nakao W, Takahashi K, Osada T. Strength recovery behavior of machined alumina by crack healing, Mechanical Properties and Performance of Engineering Ceramics and Composites III. In: Lara-Curzio E, editor. The American Ceramic Society; 2009, p. 399-409.

[128] Ono IM, Nakao W, Takahashi K, Ando K, M Nakatani. A methodology to increase a strength and guarantee a reliability of a Al_2O_3/SiC composite ceramics component by crack healing and proof testing. J high Presure inst Jpn 2006;44:80-90.

[129] Nakao W, Tsutagawa Y, Takahashi K, Ando K. Self-crack-healing ability of alumia/SiC nanocomposite fabricated by self-propagating high-temperatures synthesis. Mechanical Properties and Performance of Engineering Ceramics and Composites III. In: Lara-Curzio E, editor. The American Ceramic Society; 2009, p. 443-8.

[130] Ando K, Ono M, Nakao W, Takahashi K. Through-life reliability management of structural ceramic components using crack-healing and proof test. Mechanical Properties and Performance of Engineering Ceramics and Composites III, In: Lara-Curzio E, editor. The American Ceramic Society; 2009, p. 449-59.

[131] Nakao W, Chiba Y, Ando K. New ceramics surface reinforcing treatment treatment using a combination of crack-healing and electron beam irradiation. Ceram Eng Sci Proc 2009;29:75-80.

[132] Sugiyama R, Yamane K, Nakao W, Takahashi K, Ando K. Effect of difference in Crack-healing ability on fatigue behavior of Alumina/SiC composites. J Intell Mater System Struct 2008;19:411-5.

[133] Nakao W, Abe S, Ando K. SiC nanometer sizing effect on self healing ability of structural ceramics. Mechanical Properties and Performance of Engineering Ceramics and Composites IV. In: Singh D, Kriven WM, editors. The American Ceramic Society; 2009, p. 137-42.

[134] Nakao W, Takahashi K, Ando K. Self-healing of Surface Cracks in Structural Ceramics. Self-healing Materials: Fundamentals, Design, Strategies, and Applications. In: Ghosh SK, editor. Weinheim: WILEY-VCH Verlag GmbH & Co. KgaA; 2009, p. 183- 217.

[135] Osada T, Nakao W, Takahashi K, Ando K. Self-crack healing behavior under combustion gas atmosphere. Mechanical Properties and Performance of Engineering Ceramics and Composites IV. In: Singh D, Kriven WM, editors. The American Ceramic Society; 2010**,** p. 155-166.

[136] Osada T, Nakao W, Takahashi K, Ando K. Kinetics of Self-Crack-Healing of Alumina/Silicon Carbide Composite Including Oxygen Partial Pressure Effect. J Am Ceram Soc 2009;92:864-9.

[137] Mohanty D, Sil A, Maiti K. Development of input output relationships for self-healing Al_2O_3/SiC, ceramic composites with Y_2O_3 additive using design of experiments. Ceram Int 2011;37:1985-92.

[138] Liu SP, Ando K, Kim BS, Takahashi K. In situ crack-healing behavior of Al_2O_3/SiC composite ceramics under cyclic-fatigue strength. Int Commun Heat Mass Transfer 2009;36:558-62.

[139] Liu SP, Ando K, Kim BS, Takahashi K. In situ crack-healing behavior of Al_2O_3/SiC composite ceramics under static fatigue strength. Int Commun Heat Mass Trans 2009;36:563-8.

[140] Ono M, Nakao W, Takahashi K, Ando K. Strength recovery of machined Al_2O_3/SiC composite ceramics by crack healing. Fatigue Fract Eng Mater Struct 2007;30:1140-8.

[141] Oki T, Yamamoto H, Osada T, Takahashi K. Improvement of the contact strength of Al_2O_3/SiC by a combination of shot peening and crack-healing. J Powder Technol, 2013, Article ID 946984, http://dx.doi.org/10.1155/2013/946984.

[142] Nakao W, Osada T, Yamane K, Takahashi K, Ando K. Crack- Healing mechanism by alumina/SiC particles/SiC whiskers multi-composite. J Jpn Inst Metal 2005;69:663-6.

[143] Osada T, Wataru N, Takahashi K, Ando K, Saito S. Strength recovery behaviore of machined alumina/SiC whisker composite by crack-healing. J Ceram Soc Jpn 2007;115:278-84.

[144] Cantrell JH, Qian M, Ravichandran MV, Knowles KM. Scanning electron acoustic microscopy and residual stresses in ceramics. Appl Phys Lett 1990;57:1870-72.

[145] Niihara K, Nakahira A. strengthening of oxide ceramics by SiC and Si_3N_4 dispersions. in proceedings of third international symposium on ceramic materials and components for engines. Westerville, OH: The American ceramic society; 1988, p. 919-926.

[146] Niihara K, Nakahira A, Sasaki G, Hirabayashi M. Development of strong Al_2O_3 composites, in 124the proceedings of the international meeting on advanced materials, vol 4. Kawasaki, Japan: The Materials Research Society of Japan; 1989, p. 134.

[147] Niihara K, Nakahira A. Particulate strengthened oxide nanocomposites. in advanced structural inorganic composites. In: Vincenzini P, editor. Trieste, Italy, Elsevier, 1990, p. 637-64.

[148] Niihara K. New design concept of structural ceramic-ceramic nanocomposites, The centennial issue of the ceramic society of japan. J Ceram Soc Jpn 1991;99:974-82.

[149] Zhao J, Steams LC, Harmer MP, Chan HM, Miller GA, Cook RF. Mechanical behavior of alumina-silicon carbide 'Nanocomposites'. J Ceram Soc Jpn 1993;76:503-10.

[150] Steams LC, Zhao J, Harmer MP. Processing and microstructure development in $A1_2O_3$-SiC 'Nanocomposites'. J Eur Ceram Soc 1992;10:473-7.

[151] Luthra KL, Park HD. Oxidation of silicon carbide-reinforced oxide-matrix composites at 1375° to 1575°C. J Am Ceram Soc 1990;73:1014-23.

[152] Wu HZ, Lawrence CW, Roberts SG, Derby B. The strength of Al_2O_3/SiC nanocomposites after girding and annealing. Acta Mater 1998;46:3839-48.

[153] Ando K, Chu MC, Yao F, Sato S. Fatigue strength of crack-healed Si_3N_4/SiC composite ceramics. Fatigue Fract Eng Mater Struct 1999;22:897-903.

[154] Ando K, Ikeda T, Sato S, Yao E, Kobayashi Y. A preliminary study on crack healing behavior of Si_3N_4/SiC composite ceramics. Fatigue Fract Eng Mater Struct 1998;21:119-22.

[155] Yao F, Ando K, Chu MC, Sato S. Crack-healing behavior, high-temperature and fatigue strength of SiC-reinforced silicon nitride composite. J Mater Sci Lett 2000;19:1081-3.

[156] Houjou K, Ando K, Liu SP, Sato S. Crack-healing and oxidation behavior of silicon nitride ceramics. J Eur Ceram Soc 2004;24:2329-38.

[157] Ando K, Takahashi K, Nakayama S, Saito S. Crack-healing behavior of Si_3N_4/SiC ceramics under cyclic stress and resultant fatigue strength at the healing temperature. J Am Ceram Soc 2002;85:2268-72.

[158] Takahashi K, Ando K, Murase H, Nakayama S, Saito S. Threshold stress for crack-healing of Si_3N_4/SiC and resultant cyclic fatigue strength at the healing temperature. J Am Ceram Soc 2005;88:645-51.

[159] Ando K, Chu MC, Matsushita S, Sato S. Effect of crack-healing and proof-testing procedures on fatigue strength and reliability of Si_3N_4/SiC composites. J Eur Ceram Soc 2003;23:977-84.

[160] Jung Y, Nakao W, Takahashi K, Ando K, Saito S. Crack healing behavior of Si_3N_4/SiC composite under low oxygen partial pressure. J Soc Mater Sci Jpn 2008;57:1132-7.

[161] Takahashi K, Jung YS, Nagoshi Y, Ando K. Crack-healing behavior of Si_3N_4/SiC composite under stress and low oxygen pressure. Mater Sci Eng A 2010;527:3343-8.

[162] Ando K, Shirai Y, Nakatani M, Kobayashi Y, Sato S. (Crack-healing+proof test): a new methodology to guarantee the structural integrity of a ceramics component. J Eur Ceram Soc 2002;22:121-8.

[163] Ando K, Takahashi K, Murase H, Sato S. A new methodology to guarantee the structural integrity of ceramics component using self-crack-healing ability. High Press Inst Jpn 2003;41:316-26.

[164] Takahashi K, Kim BS, Chu MC, Sato S, Ando K. Crack-healing behavior and static fatigue strength of Si_3N_4/SiC ceramics held under stress at temperature (800, 900, 1000 °C). J Eur Ceram Soc 2003;23:1971-8.

[165] Takahashi K, Murase H, Yoshida S, Houjou K, Ando K, Saito S. Improvement of static fatigue strength of Si_3N_4/SiC crack-healed under cyclic stress. J Eur Ceram Soc 2005;25:1953-9.

[166] Takahashi K, Mizobe Y, Ando K, Saito S. Effects of frequency on the crack-healing behavior of Si_3N_4/SiC composite under cyclic stress. JME Int J 2006;49: 307-13.

[167] Jung YS, Guo Y, Nakao W, Takahashi K, Ando K, Saito S. Crack-healing behavior and resultant high-temperature fatigue strength of machined Si_3N_4/SiC composite ceramic. Fatigue Frac Eng Mater Struc 2008;31:2-11.

[168] Jung YS, Nakao W, Takahashi K, Ando K, Saito S. Crack healing of machining cracks introduced by wheel grinding and resultant high-temperature mechanical properties in a Si_3N_4/SiC composite. J Am Ceram Soc 2009;92:167-73.

[169] Nam KW, Kim MK, Park SW, Ahn SH, Kim JS. Crack-healing behavior and bending strength of Si_3N_4/SiC composite ceramics by SiO_2 colloidal. Mater Sci Eng A 2007;471:102-5.

[170] Takahashi K, Nishio Y, Kimura Y, Ando K. Improvement of strength and reliability of ceramics by shot peening and crack healing. J Eur Ceram Soc 2010;30:3047-52.

[171] Takahashi K, Nishio Y. Improvement of the contact strength of Si_3N_4/SiC by a combination of shot peening and crack-healing. J Solid Mech Mater Eng 2012;6:144-53.

[172] Takahashi K, Takahashi K, Ando K. Improvement in contact strength of Si_3N_4/SiC composite by crack healing, J Powder Technol 2013, Article ID 598024, http://dx.doi.org/10.1155/2013/598024.

[173] Takahashi K, Nishio Y, Takahashi K, Ando K. Improvement of contact strength in ceramics by crack-healing, Trans Jpn Soc Mech Eng A 2010;76:1379-81.

[174] Jung Y, Nakao W, Takahashi K, Ando K, Saito S. Strength recovery of heavily machined Si_3N_4/SiC composite ceramic by crack-healing. Trans Jpn Soc Spring Eng 2007;52:98-102.

[175] Nam KW, Kim MK, Kim HS, Kim JW, Ahn SH. Bending strength of Si_3N_4 monolithic and Si_3N_4/SiC composite ceramics and elastic wave characteristics by wavelet analysis. Int J Mod Phys B 2006;20:4279-84.

[176] Yao F, Ando K, Chu MC, Sato S. Static and cyclic fatigue behavior of crack-healed Si_3N_4/SiC composite ceramics. J Eur Ceram Soc 2001;21:991-7.

[177] Ando K, Houjyou K, Chu MC, Takahashi K, Yao F, Sato S. Crack-healing behavior under stress and fatigue strength at elevated temperature of crack-healed Si_3N_4/SiC composite ceramics. Proceedings of 7th Conf. Brugge, Belgium: European Ceramics Society; 2001, p. 819-22.

[178] Ando K, Houjyou K, Chu MC, Takeshita S, Takahashi K, Sakamoto S, Sato S. Crack-healing behavior of Si_3N_4/SiC ceramics under stress and fatigue strength at the temperature of healing (1000 °C), J Eur Ceram Soc 2002;22:1339-46.

[179] Takahashi K, Yoshida S, Ando K, Saito S. Self-crack-healing behavior under cyclic stress of silicon nitride composite at elevated temperature. Smart Mater III 2004;5648:54-61.

[180] Zhang X, Xu L, Du S, Han W, Han J, Liu C. Thermal shock behavior of SiC-whisker-reinforced diboride ultrahigh-temperature ceramics. Scripta Mater 2008;59:55-8.

[181] Zhang X, Xu L, Du S, Han W, Han J. Crack-healing behavior of zirconium diboride composite reinforced with silicon carbide whiskers. Scripta Mater 2008;59:1222-5.

[182] Monteverde F, Bellosi A, Oxidation of ZrB_2-based ceramics in dry air. J Electrochem Soc 2003;150:552-9.

[183] Zhang X, Xu L, Du S, Han W, Han J. Preoxidation and crack-healing behavior of ZrB_2-SiC ceramic composite. J Am Ceram Soc 2008;91:4068-73.

[184] Liang J, Wang Y, Fang G, Wang G. Influence of oxidation healing for cracks on the strength of hot-pressed ZrB_2–SiC–AlN ceramics. Int J Appl Ceram Technol 2012;9:441-6.

[185] Chu MC, Sato S, Kobayashi Y, Ando K. Damage healing and strengthening behavior in intelligent mullite/SiC ceramics. Fatigue Fract Eng Mater Struct 1995;18:1019-29.

[186] Ando K, Furusawa K, Chu MC, Hanagata T, Tuji K, Sato S, Crack-healing behavior under stress of mullite/silicon carbide ceramics and the resultant fatigue strength. J Am Ceram Soc 2001;84:2073-8.

[187] Ando K, Chu MC, Tsuji K, Hirasawa T, Kobayashi Y, Sato S. Crack healing behaviour and high-temperature strength of mullite/SiC composite ceramics. J Eur Ceram Soc 2002;22:1313-9.

[188] Lee SK, Ono M, Nakao W, Takahashi K, Ando K. Crack-healing behaviour of mullite/SiC/Y_2O_3 composites and its application to the structural integrity of machined components. J Eur Ceram Soc 2005;25:3495-502.

[189] Nakao W, Mori S, Nakamura J, Takahashi K, Ando K. Self-crack-healing behavior of mullite/SiC particle/SiC whisker multi-composites and potential use for ceramic springs. J Am Ceram Soc 2006;89:1352-7.

[190] Takahashi K, Uchiide K, Kimura Y, Nakao W, Ando K, Yokouchi M. Threshold stress for crack-healing of mullite reinforced by SiC whiskers and SiC particles and resultant fatigue strength at the healing temperature. J Am Ceram Soc 2007;90, 2159-64.

[191] Chu M, Sato S. Study on strengthening of mullite by dispersion of carbide ceramics particles, Trans Jpn Soc Mech Eng A 1994;60:2829-34.

[192] Sato S, Chu MC, Kobayashi Y, Ando K. Strengthening of mullite by dispersion of carbide ceramics particles. Bull Japan Soc Mech Eng 1995;61:1023-30.

[193] Ando K, Tsuji K, Ariga M, Sato S. Fatigue strength properties of crack healed mullite/SiC composite ceramics. J Soc Mat Sci Jpn, 1999;48:1173-8.

[194] Ando K, Tsuji K, Furusawa K, Hanagata T, Chu MC, Sato S. Effect of pre-crack size and testing temperature on fatigue strength properties of crack healed mullite. J Soc Mater Sci Jpn 2001;50:920-5.

[195] Ando K, Tsuji K, Hirasawa T, Kobayashi Y, Chu MC, Sato S. Crack healing behavior and high temperature strength of mullite/SiC composite ceramics. J Soc Mater Sci Jpn 1999;48:484-94.

[196] Ando K, Furusawa K, Takahashi K, Sato S. Crack-healing ability of structural ceramics and a new methodology to guarantee the structural integrity using the ability and proof-test. J Eur Ceram Soc 2005;25:549-58.

[197] Furusawa K, Furumachi N, Takahashi K, Saito S, Ando K. In situ crack-healing behavior of mullite/SiC composite ceramics. Jpn Soc Mater Sci 2003;52:998-1005.

[198] Nakao W, Ono M, Lee SK, Takahashi K, Ando K. Mechanical properties of SiC reinforced alumina composites attached crack healing ability. In Proceedings of the 11th Materials and Processing Conference. Tokyo: The Japan Society of Mechanical Engineers; 2003, p. 59-60.

[199] Osada T, Nakao W, Takahashi K, Ando K. Healing behavior of machining cracks in oxide-based composite containing SiC particles. Corrosion, Wear, Fatigue, and Reliability of Ceramics. In: Salem J, Fuller ER, editors. The American Ceramic Society; 2009, p. 45-55.

[200] Ando K, Tsuji K, Hirasawa T, Kobayashi Y, Chu MC, Sato S. Crack healing behaviour and high temperature strength of mullite/SiC ceramics. Jpn Soc Mater Sci Jpn 1999;48:489-94.

[201] Ando K, Tsuji K, Nakatani M, Chu MC, Sato S, Kobayashi Y. Effects of Y_2O_3 on crack healing temperature strength of structural mullite. J Soc Mat Sci Jpn 2002;51:458-64.

[202] Ando K, Tsuji K, Ariga M, Sato S. Fatigue strength properties of crack healed mullite/SiC composite ceramics. J Soc Mater Sci Jpn 1999;48:1151-6.

[203] Ono M, Ishida W, Nakao W, Ando K, Mori S, Yokouchi M. Crack-healing behavior, high temperature strength and fracture toughness of mullite/SiC whisker composite ceramic. J Soc Mat Sci Jpn 2005;54:207-14.

[204] Nakao W, Takahashi K, Ando K. Threshold stress during crack-healing treatment of structural ceramics having the crack-healing ability. Mater Lett 2007;61:2711-3.

[205] Nakao W, Chiba Y, Iwata K, Nishi Y, Ando K. Strengthening of ceramics surface by crack healing and electron beam irradiation. Int J Appl Ceram Technol 2011;8:383-9.

[206] Takahashi K, Uchiide K, Nakao W, Ando K. Crack healing behavior of mullite /SiC multi-composite under stress. Proceedings of the First International Conference on Self Healing Materials. The Netherlands: Noordwijk aan Zee; 2007, p. 1-10.

[207] Li J, Kong X, Xie Z, Huang Y. Improved strength recovery of a titanium carbide/silicon nitride composite from thermal shock damage via microwave heating. J Am Ceram Soc 1999;82:1576-8.

[208] Meek TT. Proposed model for the sintering of a dielectric in a microwave field. J Mater Sci Lett 1987;6:638-40.

[209] Lee Y, Radovic L. Oxidation inhibition effects of phosphorus and boron in different carbon fabrics. Carbon 2003;41:1987-97.

[210] Wang Z, Dong S, He P, Gao L, Zhou H, Yang J, Jiang D. Fabrication of carbon fiber reinforced ceramic matrix composites with improved oxidation resistance using boron as active filler. J Eur Ceram Soc 2010;30:787-92.

[211] Zuo X, Zhang L, Liu Y, Cheng L, Xia Y. Oxidation behaviour of two-dimensional C/SiC modified with self-healing Si-B-C coating in static air. Vorros Sci 2012;65:87-93.

[212] Kobayashi K, Maeda K, Sano H, Uchiyama Y. Formation and oxidation resistance of the coating formed on carbon material composed of B_4C-SiC powders. Carbon 1995;33:397-403.

[213] Berjonneau J, Langlais F, Chollon G. Understanding the CVD process of (Si)–B–C ceramics through FTIR spectroscopy gas phase analysis. Surf Coat Technol 2007;201:7273-85.

[214] Carrère P, Lamon J. Creep behaviour of a SiC/Si-B-C composite with a self-healing multilayered matrix. J Eur Ceram Soc 2003;23:1105-14.

[215] Vandenbulcke L. Multilayered materials by ICVI in non-oxide self-healing ceramic matrix composites for high temperature applications. Ceram Trans 2005;175:13-26.

[216] Goujard S, Vandenbulcke L. Deposition of Si-B-C materials from the vapor phase for application in ceramic matrix composites. Ceram Trans 1994;46:925-35.

[217] Bouillon E, Abbe F, Goujard S, Pestourie E, Habarou G, Dambrine B. Mechanical and thermal properties of a self-sealing matrix composite and determination of the life time duration. Ceram Eng Sci Proc 2000;21:459-67.

[218] Forio P, Lamon J. Fatigue behaviour at high temperatures in air of a 2D SiC/Si-B-C composite with a self-healing multilayered matrix. Ceram Trans American Ceram Soc, 2001;128:127-41.

[219] Carrère P, Lamon J. The fatigue behaviour at high temperature of a ceramic matrix composite with a self-healing matrix. 8th International Spring Meeting, International Conference on Fatigue of Composites, ed. Degallaix S, Bathias C, Fougeres R. SF2M, 1997;74-81.

[220] Naslain R, Guette A, Rebillat F, Pailler R, Langlais F, Bourrat X. Boron-bearing species in ceramic matrix composites for long-term aerospace applications. J Solid State Chem 2004;177:449-56.

[221] Guo Q, Song J, Liu L, Zhang B. Relationship between oxidation resistance and structure of B_4C-SiC/C composites with self-healing properties, Carbon 1999;37:33-40.

[222] Kobayashi K, Miyazaki K, Ogawa I, Hagio T, Yoshida H. Carbon/ceramics composites - Preparation and properties. Mater Des 1988;9:10-21.

[223] Li J, Luo R, Lin C, Bi Y, Xiang Q. oxidation resistance of a gradient self-healing coating for carbon/carbon composite. carbon 2007;45:2471-8.

[224] Guo QG, Song JR, Liu L, Zhang BJ. Factors influencing oxidation resistance of B_4C/C composites with self-healing properties. Carbon 1998;36:1597-601.

[225] Quemard L, Rebillat F, Guette A, Tawil H, Louchet-Pouillerie C. Self-healing mechanisms of a SiC fiber reinforced multi-layered ceramic matrix composite in high pressure steam environments. J Eur Ceram Soc 2007;27:2085-94.

[226] Li G, John M. A self-healing smart syntactic foam under multiple impacts. Compos Sci Technol 2008;68:3337-43.

[227] Li G, Nettles D. Thermomechanical characterization of a shape memory polymer based self-repairing syntactic foam. Polymer 2010;51:755-62.

[228] Nji J, Li G. A self-healing 3D woven fabric reinforced shape memory polymer composite for impact mitigation. Smart Mater Struct 2010;19:1-9.

[229] Xu W, Li G. Constitutive modeling of shape memory polymer based self-healing syntactic foam. Int J Solid Struct 2010;47:1306-16.

[230] John M, Li G. Self-healing of sandwich structures with grid stiffened shape memory polymer syntactic foam core. Smart Mater Struct 2010;19:1-12.

[231] Li G, Uppu N. Shape memory polymer based self-healing syntactic foam: 3-D confined thermomechanical characterization. Compos Sci Technol 2010;70:1419-27.

[232] Nji J, Li G. A biomimic shape memory polymer based self-healing particulate composite. Polymer 2010;51:6021-9.

[233] Li G, Xu W. Thermomechanical behavior of thermoset shape memory polymer programmed by cold-compression: testing and constitutive modeling. J Mech Phys Solid 2011;59:1231-50.

[234] Nji J, Li G. Damage healing ability of a shape memory polymer based particulate composite with small thermoplastic contents. Smart Mater Struct 2012; 21:025011.

[235] Li G, Shojaei A. Viscoplastic theory of shape memory polymer fibers with application to self-healing materials. P Roy Soc A-Math Phy Eng Sci 2012; 468:2319-46.

[236] Li G, Meng H, Hu J. Healable thermoset polymer composite embedded with stimuli-responsive fibers. J Roy Soc Interface 2012;9:3279-87.

[237] Li G, Ajisafe O, Meng H. Effect of strain hardening of shape memory polymer fibers on healing efficiency of thermosetting polymer composites. Polymer 2013;54:920-8.

[238] Li G, Zhang P. A self-healing particulate composite reinforced with strain hardened short shape memory polymer fibers. Polymer 2013;54:5075-86.

[239] Greil P. Generic principles of crack-healing ceramics. J Adv Ceram 2012;1:249-67.

[240] Firstov GS, Van Humbeeck J, Koval YN. High-temperature shape memory alloys: some recent developments. Mater Sci Eng A, 2004;378:2-10.

[241] Hassan MR, Mehrpouya M, Emamian S, Sheikholeslam MN. Review of self-healing effect on shape memory alloy (SMA) structures. Adv Mater Res 2013;701:87-92.

[242] Holzer H, Dunand DC. Phase transformation and thermal expansion of Cu/ZrW_2O_8 metal matrix composites. J Mater Res 1999;14:780-9.

CHAPTER 3 MECHANICAL ACTIVATION ASSISTED SYNTHESIS OF NANOSTRUCTURE $MgAl_2O_4$ FROM GIBBSITE AND LANSFORDITE[1]

3.1 Introduction

Spinel is a ternary oxide with a chemical formula of AB_2O_4 in which a divalent metallic cation (A) is located at a tetrahedral site, a trivalent metallic cation (B) is located at an octahedral site and oxygen ions are arranged in cubic closed-packed structure [1,2] . The term of spinel is mostly referred to magnesium aluminate (MA) structure with the chemical formula $MgAl_2O_4$ which is one of the most attractive ceramic materials for many industries.

Spinel has interesting optical, thermal, mechanical, chemical and dielectric properties, and hence it has been used in many industries for a variety of applications such as mid-wave infrared windows, catalyst or catalyst support, dye adsorbents, refractory material, active elements in humidity sensors, insulating compound for fusion reactor core, resonators or oscillators in the range of microwave frequencies and excellent transparent ceramic material for high-temperature applications [1-5].

Spinel has been synthesized by various techniques including the conventional solid-state reaction of periclase (MgO) and alumina (Al_2O_3) [6,7], chemical coprecipitation [8-10], freeze–drying [11], sol–gel method [12,13], combustion [14] microwave [15] and metal–chitosan complexation method [2]. Each of these processes has some limitations. For example, the conventional solid-state reaction needs extremely high temperature (around two-third of the melting point) to be completed [16]. Controlling the sol-gel method is also difficult due to the sensitivity of chemicals to the environment. As a result, the chemical composition of the final product may alter and does not match with the stoichiometric amount. In the coprecipitation method normally aluminum and magnesium nitrate or chloride are used. A repeated washing procedure is required to remove the anions, which will alter the compositions of the precipitates and as a result the final product [4].

Mechanical activation is one of the widely used methods to produce nanomaterials. In this process, the contact surface area between the reacting materials increases as a result of an intense reduction of particles size. This mechanism is very important in the case of diffusion-controlled reactions. It also has other advantages over the conventional solid state reaction and chemical-based method. The mechanical activation process can enhance the speed of reaction in multi-component system by significantly decreasing the calcination temperatures. In this process there is no need to use expensive starting materials; instead low cost and widely available oxides can be used as the initial materials. In this chapter, the synthesis of spinel nanoparticle is reported using mechanical activation of gibbsite ($Al(OH)_3$) and lansfordite ($MgCO_3.5H_2O$). The production of spinel during mechanical activation and after subsequent annealing are studied. The formation mechanism of the spinel is discussed as well.

[1] This chapter previously appeared as Fariborz Tavangarian, Guoiqang Li, Mechanical activation assisted synthesis of nanostructure $MgAl_2O_4$ from gibbsite and lansfordite, *Powder Technology*, November, 2014. It is reprinted by permission of Elsevier (see the permission letter in Appendix A).

3.2 Experimental procedures

Lansfordite ($MgCO_3.5H_2O$) (99% purity, BulkSupplements) and gibbsite ($Al(OH)_3$) (99% purity, Alpha Chemicals) powders were used as raw materials. $MgCO_3.5H_2O$ and $Al(OH)_3$ powders with molar ratio of 1:2 were mixed to yield stoichiometric spinel. Powder mixture was mechanically activated in a planetary ball mill (Across International, PQ-N2) in air atmosphere, at room temperature. The milling media consisted of a zirconia vial with 5×20 mm and 10×10 mm zirconia balls. In all milling runs the ball-to-powder weight ratio was 10:1 and the rotational speed of the main disc was 500 rpm. Heat treatment of ball milled powders was carried out at 1000 and 1200 ºC for 1h in a tube furnace (MTI Corporation, GSL 1700x).

The phase transformations of ball milled and heat treated specimens were evaluated by X-ray diffractometry (MiniFlex XRD, Rigaku Corporation, Japan) with Cu Kα radiation (λ= 0.154178 nm). The XRD traces were recorded in the 2θ range of 20–80º (step size of 0.05º and time per step of 1 s). The morphology of powder particles was studied by field emission scanning electron microscopy (Quanta3D FEG, FEI Company, USA) at acceleration voltages between 5 and 30 kV. Image analyzing method was used to measure spinel powder particles size. The transmission electron microscopy (TEM; JEM-1400) technique was utilized to characterize the morphology and the structure of the prepared samples.

3.3 Results and discussions

Figure 3.1 shows the XRD patterns of the ball milled powders after various durations. The x-ray diffraction pattern of 0h ball milled sample corresponded to gibbsite (XRD JCPDS data file No. 12-0460) and lansfordite (XRD JCPDS data file No. 21-0959) phases. Milling the initial powders led to the broadening of XRD peaks and a significant decrease in their intensities due to the formation of smaller crystallite size and the formation of internal strains [17,18]. The characteristic peaks of gibbsite and lansfordite phases remained up to 10h ball milling time. No new crystalline phase was observed in the XRD patterns even after 10h of milling time. Hence, the ball milled powders were subjected to subsequent heat treatment to obtain spinel structure.

Figure 3.2 shows the XRD pattern of obtained powders after annealing at 1000 ºC for 1h in air. Annealing of sample milled for 0h led to the complete vanishing of both lansfordite and Gibbsite phases. On the other hand, some peaks of periclase (MgO) (XRD JCPDS data file No. 43-1022), alumina (Al_2O_3) (XRD JCPDS data file No. 10-0173), and spinel ($MgAl_2O_4$) (XRD JCPDS data file No. 01-075-1795) phases can be observed on the XRD pattern. With increasing the milling time up to 3h, no significant changes were observed except that the intensity of the characteristic peaks of spinel increased while those of alumina and periclase decreased. Mechanical activation process led to an increase in contact surface area and better reactivity of periclase and alumina after subsequent annealing. With increasing the ball milling time to 6 h only spinel phase can be detected in the XRD patterns. The spinel formation mechanism was studied by Carter [19]. He found that spinel forms through the counterdiffusion of the

Mg^{2+} and Al^{3+} ions through the rigid oxygen lattice of spinel. Reaction occurs at the interface of alumina and periclase. At the interface a layer of spinel forms and then the reaction continues at both the Al_2O_3-$MgAl_2O_4$ and the MgO-$MgAl_2O_4$ interfaces [19]. Murphy et al. [20] found that the Mg^{2+} ions are more mobile than the Al^{3+} ions. Also they reports that Al^{3+} ion diffuses through the vacancy sites in the magnesium sublattice [20].

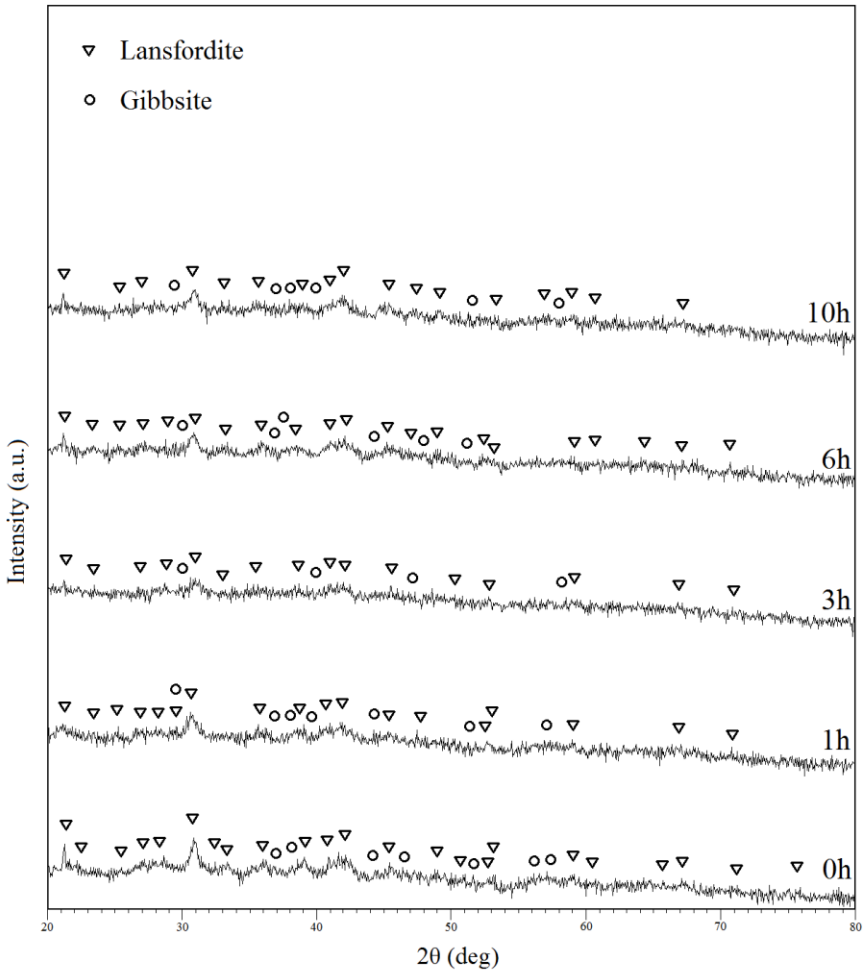

Figure 3.1. XRD patterns of initial materials after mechanical activation for various periods of time.

The rate-limiting step for a sequential reaction is determined by the slowest step in the sequence. If this slow step is mass transfer, the reaction is said to be diffusion-controlled [21]. Due to the fact that the mechanism of spinel formation is diffusion-controlled [19], using mechanical activation can affect the spinel formation rate via increasing the contact surface area through decreasing the particle size of the

reacting materials and homogenizing the powder mass. On the other hand, as reported by Sarkar et al. [22], mechanical activation can affect the subsequent densification of spinel bodies in both the single-stage and double-stage sintering processes.

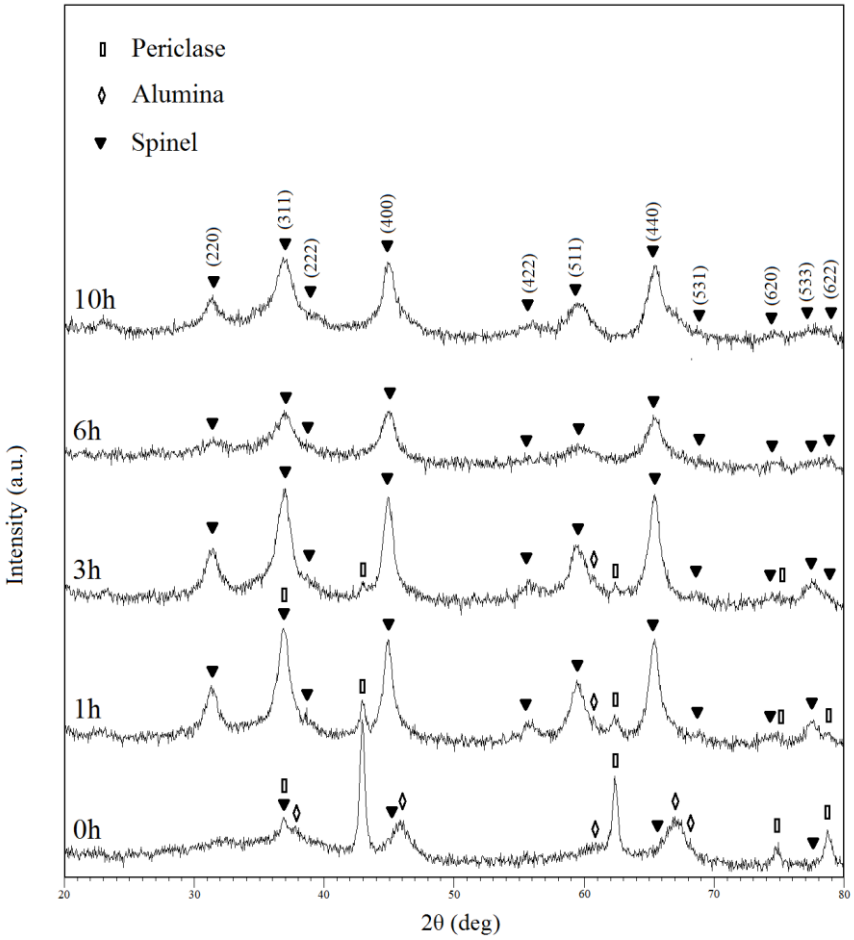

Figure 3.2. XRD patterns of obtained powders after mechanical activation for various periods of time and subsequent annealing at 1000 °C for 1 h.

Figure 3.3 shows the XRD patterns of powders milled for various times with subsequent annealing at 1200 ºC for 1h in air. As can be seen, periclase and alumina phases were remained up to 3h ball milled samples. But for those sample ball milled for more than 6h, only spinel can be detected in the XRD patterns. With increasing the annealing temperature from 1000 to 1200 ºC (please see figures 3.2 and 3.3), the peaks intensity increased and their widths decreased due to the recovery of internal strain and growth of crystallite size [23]. Conventionally, spinel powder was prepared by solid-state reaction which needs an annealing temperature of as high as 1400 to 1600 ºC [6,7]; however, as can be seen in the present work, utilizing mechanical activation method spinel can be formed after annealing the 6h ball

milled powder at 1000 ºC for 1 h due to the higher reactivity and contact surface area of the initial powders.

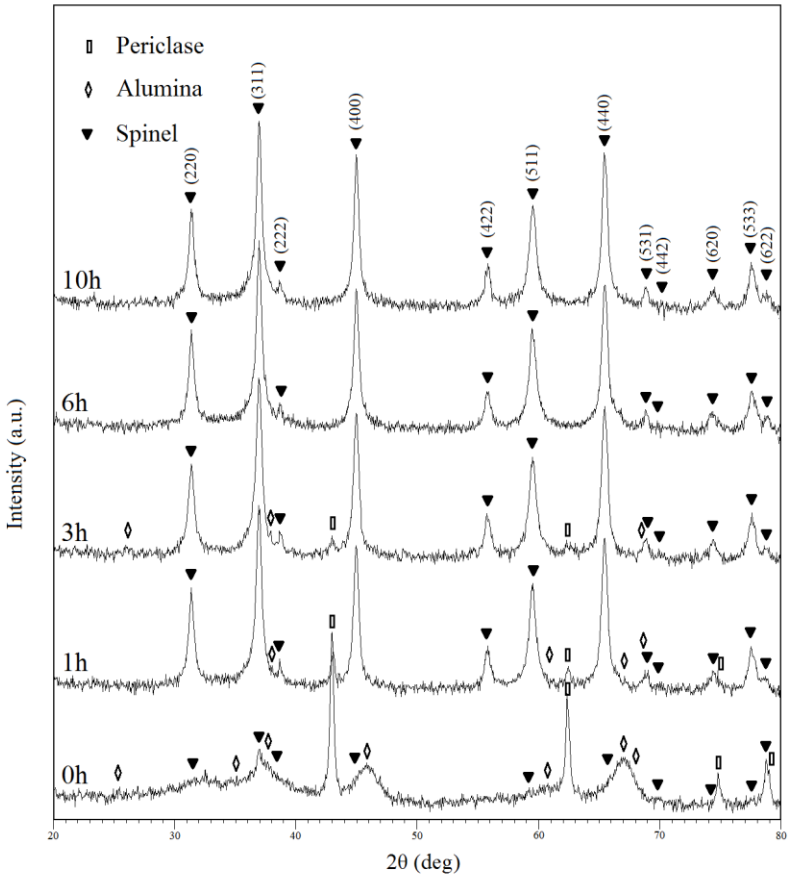

Figure 3.3. XRD patterns of obtained powders after mechanical activation for various periods of time and subsequent annealing at 1200 °C for 1 h.

Figure 3.4 shows the morphology of initial materials. As can be seen in figure 3.4 part a, lansfordite powder had a flake shape with mean particle size of about 3 µm. Gibbsite powder had a shapeless structure with mean particle size of about 5 µm (figure 3.4, see b). Because of the large size of particles of the initial materials, and due to the fact that the formation of spinel has a diffusion-control mechanism [19], spinel can be formed partially after heat treatment procedure of the reactants in the absence of mechanical activation. Hence ball milling can play a crucial role in the formation of spinel structure through mixing the initial materials and decreasing the diffusion paths.

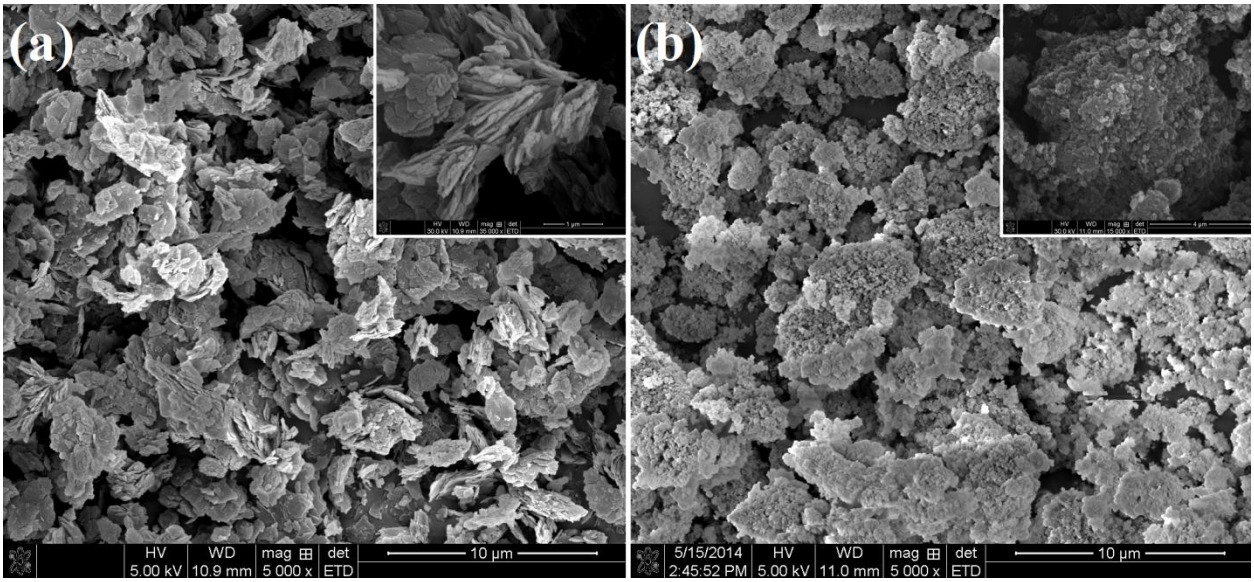

Figure 3.4. SEM micrographs of initial materials including: (a) lansfordite and (b) gibbsite.

Parts a and b in figure 3.5 show the ball milled powders after 6 and 10 h, respectively. As can be seen, a uniform powder mixture can be obtained after ball milling of the initial materials.

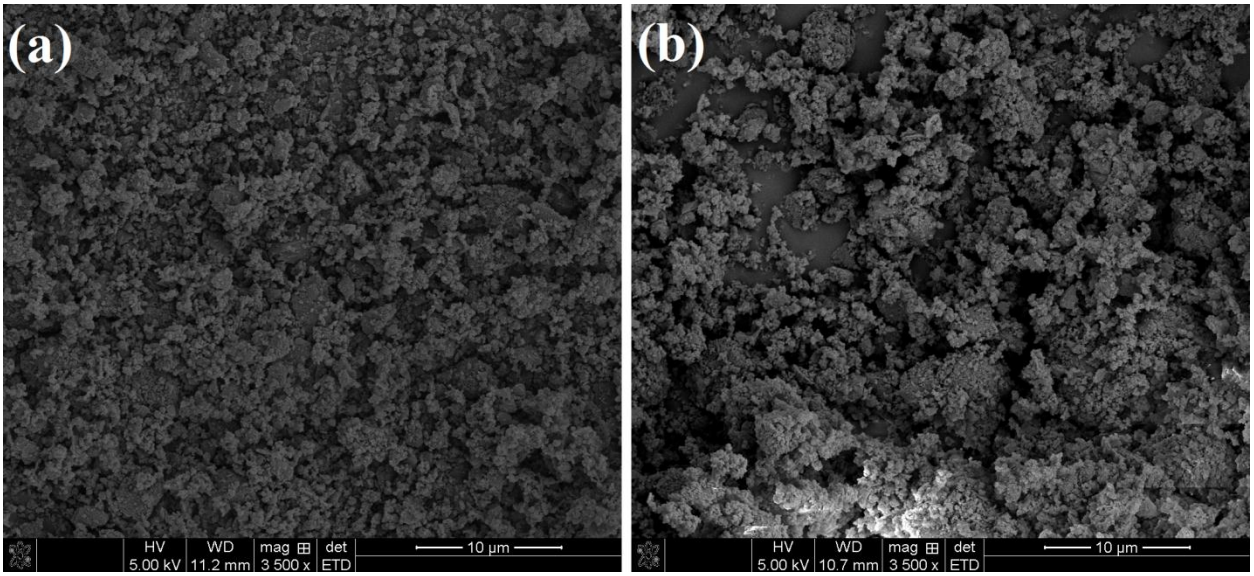

Figure 3.5. SEM micrographs of ball milled powders for (a) 6 h and (b) 10 h.

Parts a and b in figure 3.6 show the morphology of the obtained spinel structure after ball milling for 6 and 10h with subsequent annealing at 1200 °C for 1h, respectively. As can be seen in figure 3.6 part a, the obtained spinel powder has a mean grain size of about 35nm. However, with increasing the ball milling time to 10 h the mean grain size decreased to about 27nm. As milling time advances, the density of dislocation increases as a result of more nucleation sites are available during crystallization upon annealing which in turn led to the smaller final grain size.

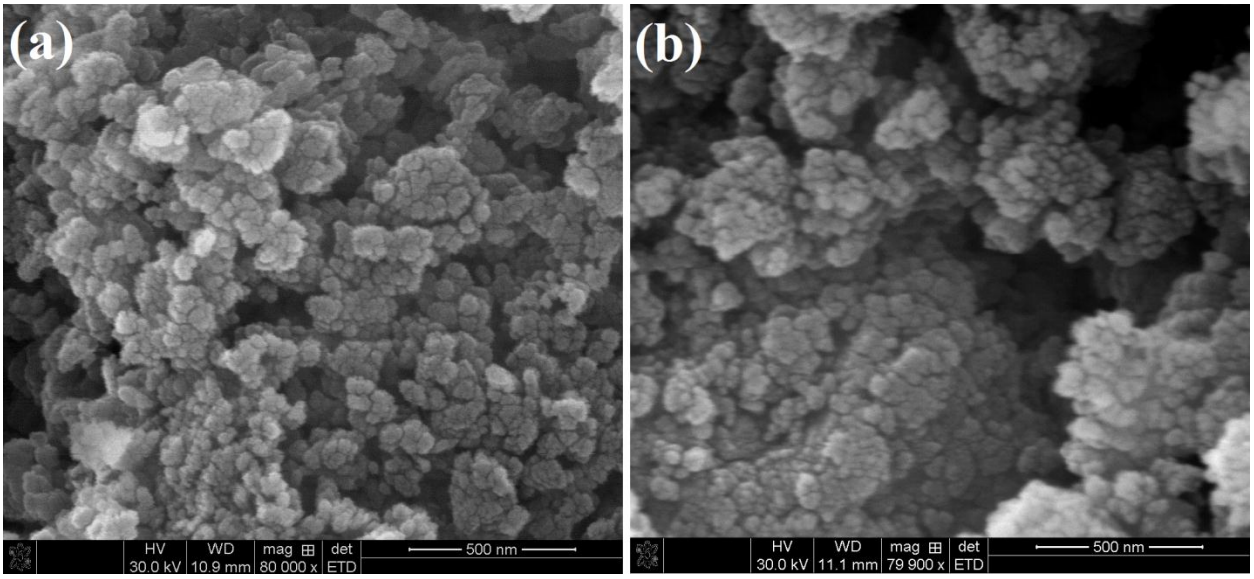

Figure 3.6. SEM micrographs of prepared spinel after (a) 6h and (b) 10h ball milling time with subsequent annealing at 1200 °C for 1h.

Parts a and b in figure 3.7 show the morphology and crystallite size of the prepared nanocrystalline spinel powder after 6 and 10h of mechanical activation with subsequent annealing at 1200 °C for 1 h, respectively. As can be seen, the obtained spinel powders had a nanostructure with round shape crystallites. Also with comparing parts a and b in figure 3.7, it is clear that the crystallite size of the obtained spinel powders after 10h ball milling is smaller than that of obtained after 6h. Mechanical activation introduces more defects and dislocations inside the structure. Hence, more nucleation sites are available during subsequent annealing and consequently smaller crystallite size was obtained [22-25].

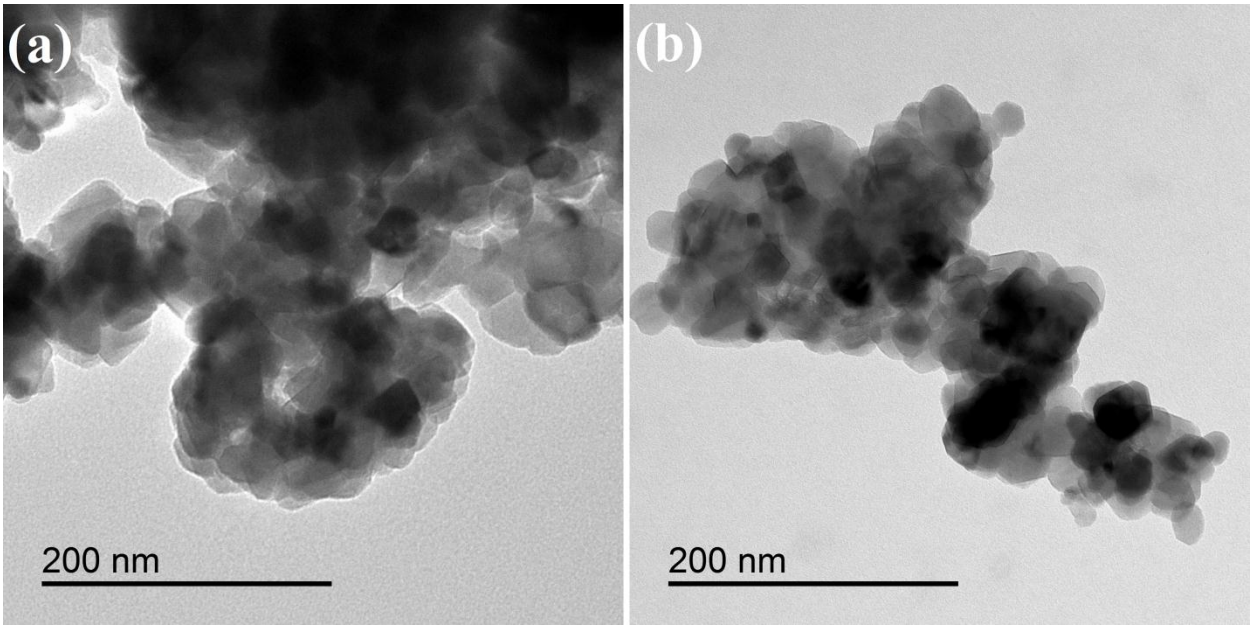

Figure 3.7. TEM micrographs of prepared spinel after (a) 6h and (b) 10h ball milling time with subsequent annealing at 1200 °C for 1h.

3.4 Conclusion

Single-phase nanostructure spinel powder was successfully synthesized by 6 and 10h of mechanical activation of gibbsite and lansfordite with respective annealing at 1000 and 1200 °C for 1 h. Mechanical activation advanced the spinel formation reaction through increasing the contact surface area and producing more dislocations and defects inside the reacting phases as a consequence of intense reduction of particles size, which is very important in the case of diffusion-controlled reactions. Spinel forms through the counterdiffusion of the cations through the rigid oxygen lattice of spinel. The mean grain size of the obtained spinel structure was below 50 nm according to the SEM and TEM evaluation.

3.5 References

[1] Stubičar N, Tonejc A, Stubičar M. Microstructural evolution of some MgO-TiO_2 and MgO-Al_2O_3 powder mixtures duering high-energy ball milling and post-annealing studied by X-ray diffraction. J Alloys Compd 2004;370:296-301.

[2] Nuernberg GDB, Foletto EL, Probst LFD, Campos CEM, Carreño NLV, Moreira MA. A novel synthetic route for magnesium aluminate ($MgAl_2O_4$) particles using metal–chitosan complexation method. Chem Eng J 2012;193:211–4.

[3] Gledhill AD, Li D, Mroz T, Goldman LM, Padture NP. Strengthening of transparent spinel/Si_3N_4 nanocomposites. Acta Mater 2012;60:1570–5.

[4] Kong LB, Ma J, Huang H. $MgAl_2O_4$ spinel phase derived from oxide mixture activated by a high-energy ball milling process. Mater Lett 2002;56:238–43.

[5] Zawrah MF. Investigation of lattice constant, sintering and properties of nano Mg–Al spinels. Mater Sci Eng A 2004;382:362–70.

[6] Bratton RJ. Sintering and grain-growth kinetics of $MgAl_2O_4$. J Am Ceram Soc 1971;52:141-3.

[7] Bhatia T, Chattopadhyay K, Jayaram V. Effect of rapid solidification on microstructural evolution in MgO-$MgAl_2O_4$. J Am Ceram Soc 2001;84:1873-80.

[8] Gusmano G, Nunziante P, Traversa E, Chiozzini G. The mechanism of $MgAl_2O_4$ spinel formation from the thermal decomposition of coprecipitated hydroxides. J Eur Ceram Soc 1991;7:31-9.

[9] Li J, Ikegami T, Lee J, Mori T. Fabrication of translucent magnesium aluminum spinel ceramics. J Am Ceram Soc 2000;83:2866-8.

[10] Bratton RJ. Coprecipitates yielding $MgAl_2O_4$ spinel powders. Am Ceram Soc Bull 1969;48:759-62.

[11] Wang CT, Lin L, Yang S. Preparation of $MgAl_2O_4$ spinel powders via freeze-drying of alkoxide precursors. J Am Ceram Soc 1992;75:2240-3.

[12] Varnier O, Hovnanian N, Larbot A, Bergez P, Cot L, Charpin J. Sol-gel synthesis of magnesium aluminum spinel from a heterometallic alkoxide. Mater Res Bull 1994;29:479-88.

[13] Yang N, Chang L. Structural inhomogeneity and crystallization behavior of aerosol-reacted $MgAl_2O_4$ powders. Mater Lett 1992;15:84-8.

[14] Ganesh I, Johnson R, Rao GVN, Mahajan YR, Madavendra SS, Reddy BM. Microwave-assisted combustion synthesis of nanocrystalline $MgAl_2O_4$ spinel powder. Ceram Int 2005;31:67-74.

[15] Gómez I, Hernández M, Aguilar J, Hinojosa M. Comparative study of microwave and conventional processing. Ceram Int 2004;30:893-900.

[16] Smart LE, Moore EA. solid state chemistry an introduction (4^{th} edition), CRC press, 2012, pp. 138.

[17] Tavangarian F, Emadi R. Mechanochemical synthesis of nanocrystalline forsterite powder. Int J Mod Phys B 2010;24:343-50.

[18] Tavangarian F, Emadi R. Effects of mechanical activation and chlorine ion on nanoparticle forsterite formation. Mater Lett 2011;65:126-9.

[19] Carter RE. Mechanism of solid-state reaction between magnesium oxide and aluminum oxide and between magnesium oxide and ferric oxide. J Am Ceram Soc 1961;44:116-20.

[20] Murphy ST, Uberuaga BP, Ball JB, Cleave AR, Sickafus KE, Smith R, RW Grimes. Cation diffusion in magnesium aluminate spinel. Solid State Ionics 2009;180:1-8.

[21] Marsden J, House I. The Chemistry of Gold Extraction, Ellis Harwood Ltd., London, UK, 1992.

[22] Sarkar R, Das SK, Banerjee G. Effect of attritor milling on the densification of magnesium aluminate spinel. Ceram Int 1999;25:485-9.

[23] Tavangarian F, Emadi R. Effects of fluorine ion and mechanical activation on nanostructure forsterite formation mechanism. Powder Technol 2010;203:180-6.

[24] Tavangarian F, Emadi R. Synthesis and characterization of spinel–forsterite nanocomposites. Ceram Int 2011;37:2543-8.

[25] Mirhadi SM, Tavangarian F, Emadi R. Synthesis, characterization and formation mechanism of single-phase nanostructure bredigite powder. Mater Sci Eng C 2012;32:133-9.

CHAPTER 4 CRACK SELF-HEALING IN SPINEL[1]

4.1 Introduction

In recent decades, design and production of a new generation of ceramics with crack self-healing capability have become a popular research and development topic in the scientific community. Ceramics with self-healing ability can prevent the catastrophic failure of structures, and subsequently increase the reliability of the structures in service.

The capability of crack-healing in various ceramics has been studied by many scientists. The crack self-healing behavior of UO_2 was investigated by Roberts and Wrona [1]. They observed a complete healing after 3h annealing at 2000 °C. Diffusion process was reported as a healing mechanism in UO_2. Kim et al. [2] studied the crack healing behavior in Al_2O_3. They found that a surface crack of 100 μm can be healed by sintering the specimens above 1400 ºC for 1h. Gupta [3] showed that crack healing in alumina is related to pore evolution in the microstructure and sintering phenomena. Wang and Stevens [4] investigated the crack healing behavior of partially stabilized zirconia. The results showed that the strength of the pre-cracked samples was recovered up to 60% after annealing at 1250 °C for 20 min. The phase transition from monoclinic to tetragonal at above 1170 °C, grain rearrangement, structural deformation and diffusion mechanisms are responsible for the strength recovery and healing in zirconia. Also the self-healing process in MgO was studied by several researchers [5, 6]. It was found that the mass transportation phenomenon is responsible for crack healing in magnesium oxide structures.

Although the crack healing behavior of alumina and magnesium oxide are reported in the literature, there is no report of the crack self-healing behavior of spinel. Because it has been shown that MgO and Al_2O_3 have the crack healing capability, it is reasonable to expect that $MgAl_2O_4$ (spinel) will also have similar crack healing capabilities at high temperature. The objective of this chapter is to investigate the crack-healing capability of the spinel ceramic. The involved crack-healing mechanism and also the healing efficiency of the spinel will be discussed.

4.2 Experimental procedures

Spinel powder was prepared according to what is reported in chapter 3. Briefly, $MgCO_3$ (99% purity, BulkSupplements) and $Al(OH)_3$ (99% purity, Alpha Chemicals) powders with molar ratio of 1:2 were mechanically activated for 6h in a planetary ball mill (Across International, PQ-N2) in air at ambient temperature and then the ball milled powders were heat treated at 1200 ºC for 1h in a tube furnace (MTI Corporation, GSL 1700x) to produce single-phase spinel. The obtained spinel powder was uniaxially pressed into cylindrical pellets with the height and diameter of 12 × 12 mm in a hardened steel mold at a

[1] This chapter has been submitted as Fariborz Tavangarian, Guoiqang Li, crack Self-healing in spinel, to ELSEVIER, *Materials Chemistry and Physics*, in October 2014 for peer reviewing process and currently is under review.

pressure of 200 MPa using 10 wt.% glycerol binder. In order to remove the glycerol and to increase the density, the pellets were sintered at 1200 °C for 1h. These samples are called green samples (GS). Two groups of samples were prepared. One group is to investigate the crack healing behavior of spinel and another group is to investigate the healing efficiency of spinel ceramic. To investigate the crack self-healing behavior of spinel, the Vickers indenter was used to produce surface cracks in the middle of GS at a load of 9.8N. Then the pre-cracked specimens were annealed at 1200, 1400 and 1600 ºC for 1, 10 and 100h in air. In order to study the self-healing efficiency of spinel ceramics, diametral tensile strength (DTS) test was performed on another series of specimens. Table 4.1 shows the designation and sintering procedures to prepare samples for DTS experiments.

Table 4.1. Designation and sintering procedures to prepare samples for DTS experiments.

Designation	Step 1	Step 2	Step 3
GS	Sintered at 1200 °C for 1h	Non-indented	-
GS-C	Sintered at 1200 °C for 1h	Indented	-
12-A	Sintered at 1200 °C for 1h	Non-indented	Sintered at 1200 °C for 1h
12-AC	Sintered at 1200 °C for 1h	Indented	Sintered at 1200 °C for 1h
12-B	Sintered at 1200 °C for 1h	Non-indented	Sintered at 1200 °C for 10h
12-BC	Sintered at 1200 °C for 1h	Indented	Sintered at 1200 °C for 10h
12-D	Sintered at 1200 °C for 1h	Non-indented	Sintered at 1200 °C for 100h
12-DC	Sintered at 1200 °C for 1h	Indented	Sintered at 1200 °C for 100h
14-A	Sintered at 1200 °C for 1h	Non-indented	Sintered at 1400 °C for 1h
14-AC	Sintered at 1200 °C for 1h	Indented	Sintered at 1400 °C for 1h
14-B	Sintered at 1200 °C for 1h	Non-indented	Sintered at 1400 °C for 10h
14-BC	Sintered at 1200 °C for 1h	Indented	Sintered at 1400 °C for 10h
14-D	Sintered at 1200 °C for 1h	Non-indented	Sintered at 1400 °C for 100h
14-DC	Sintered at 1200 °C for 1h	Indented	Sintered at 1400 °C for 100h
16-A	Sintered at 1200 °C for 1h	Non-indented	Sintered at 1600 °C for 1h
16-AC	Sintered at 1200 °C for 1h	Indented	Sintered at 1600 °C for 1h
16-B	Sintered at 1200 °C for 1h	Non-indented	Sintered at 1600 °C for 10h
16-BC	Sintered at 1200 °C for 1h	Indented	Sintered at 1600 °C for 10h
16-D	Sintered at 1200 °C for 1h	Non-indented	Sintered at 1600 °C for 100h
16-DC	Sintered at 1200 °C for 1h	Indented	Sintered at 1600 °C for 100h

Those specimens without the letter “C” at the end are control samples for those with the “C” letter at the end; for example,16-A (the sample without any indentation) is the control sample for 16-AC and the healing efficiency of 16-AC is obtained with regard to 16-A. Three samples were used for each test. Two series of specimens was prepared: one series without any indentations and another series containing

Vickers indentations. Figure 4.1 shows the schematic representation of the prepared samples containing Vickers indentations. 18 indentations with 0.6-mm increments were created along the diameter of the top surface. Figure 4.2 shows the surface morphology of the top face of a typical specimen. Then the pellet was rotated 180 ° and 18 more indentations were created subsequently on the opposite surface of the tablet. These indentations can be the onset points of cracks and hence decrease the DTS of the pellets.

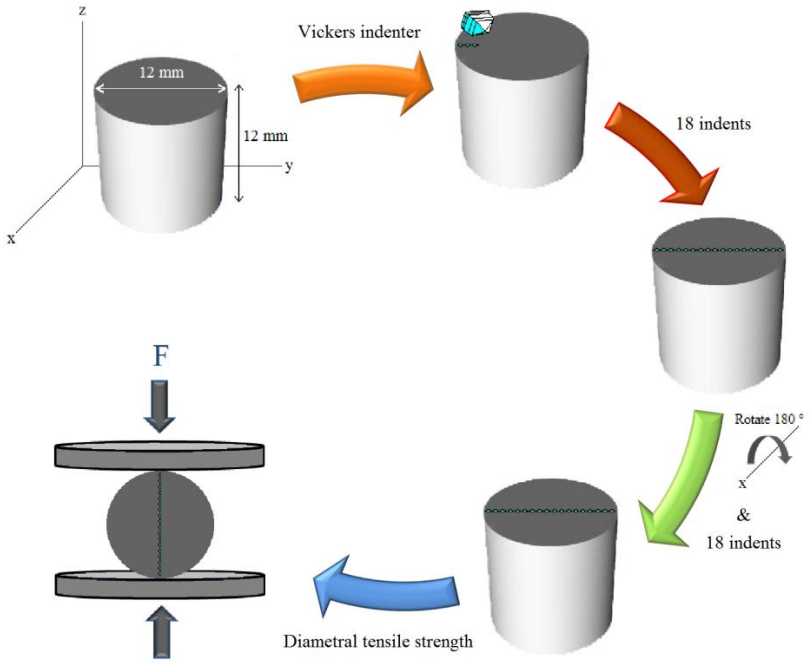

Figure 4.1. The schematic representation of the prepared samples containing Vickers indentations for diametral tensile strength.

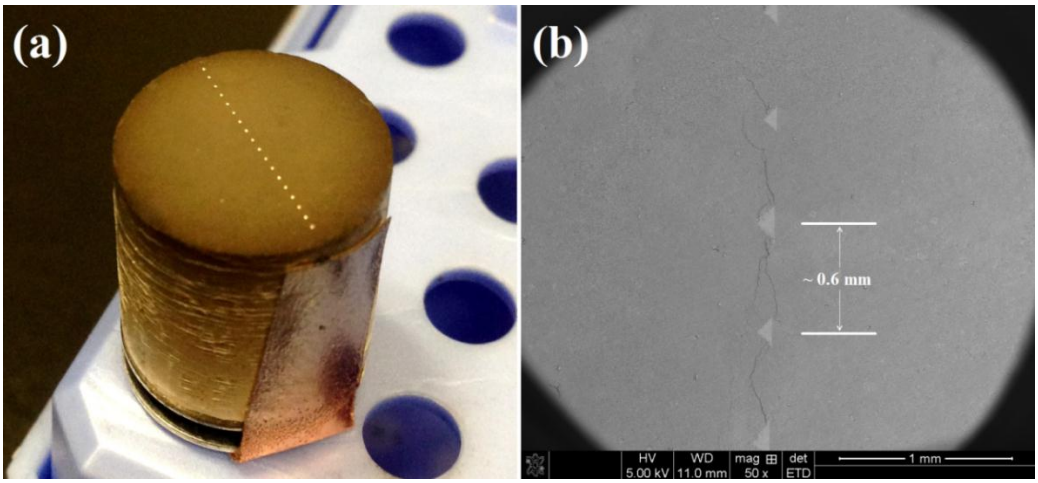

Figure 4.2. (a) The Vickers indentation trace of GS-C, (b) SEM micrograph of the surface of GS-C.

The morphology of the cracks before and after indentation was studied by field emission scanning electron microscopy (Quanta3D FEG, FEI Company, USA) at acceleration voltages between 5 and 30 kV. Nano-indentation tests were conducted using the Hysitron TI-900 Triboindenter (Minneapolis, USA) with a Berkovich tip to determine the hardness of the pellets sintered at various temperatures. Cold crushing strength (CCS) and diametral tensile strength (DTS) were obtained at room temperature using a Hydraulic Universal Testing Machine (Instron Model 5696, Canton, MA) at a rate of 5 mm/min. DTS was calculated according to equation (4-1) as follows [7]:

$$DTS = \frac{2F}{\pi Dt} \tag{4-1}$$

where F is the axial compressive load (figure 4.1), D is the specimen diameter and t is the specimen thickness. The healing efficiency of the spinel at each temperature was expressed as the percentage of the strength recovery of the specimens. To determine the strength recovery in the healed samples, first the percentage of diametral tensile strength reduction of samples due to the presence of a total of 36 indentations on both surfaces of the specimens before any healing process was calculated. For this purpose, the DTS of samples GS and GS-C was measured according to equation (4-1) and then the diametral tensile strength reduction of the initial samples in the presence of indentations ($DTSR_{initial}$) was calculated according to equation (4-2):

$$DTSR_{initial} = \left[1 - \frac{DTS_{GS-C}}{DTS_{GS}}\right] \times 100 \tag{4-2}$$

The diametral tensile strength reduction of the healed samples in the presence of indentations at each temperature ($DTSR_{healed}$) was calculated by dividing the DTS of indented samples by the DTS of non-indented specimens sintered at the same condition (for example by dividing 16-DC by 16-D) according to equation (4-3):

$$DTSR_{healed} = \left[1 - \frac{DTS_{indented+healed}}{DTS_{non-indented+healed}}\right] \times 100 \tag{4-3}$$

Finally, the strength recovery of the specimens which can be a criterion for the healing efficiency of the spinel samples at each temperature can be expressed as follow:

$$SR = \left[1 - \frac{DTSR_{healed}}{DTSR_{initial}}\right] \times 100 \quad (4\text{-}4)$$

Equation (4-4) shows that how much of the degraded strength due to the presence of the indentations (cracks) can be recovered by the healing process at each temperature.

4.3 Results and discussions

Parts a and b in figure 4.3 show the location of cracks before and after sintering at 1600 °C for 1h, respectively. As can be seen, in some locations the grains attached to each other and the crack was closed (arrows in figure 4.3 part b).

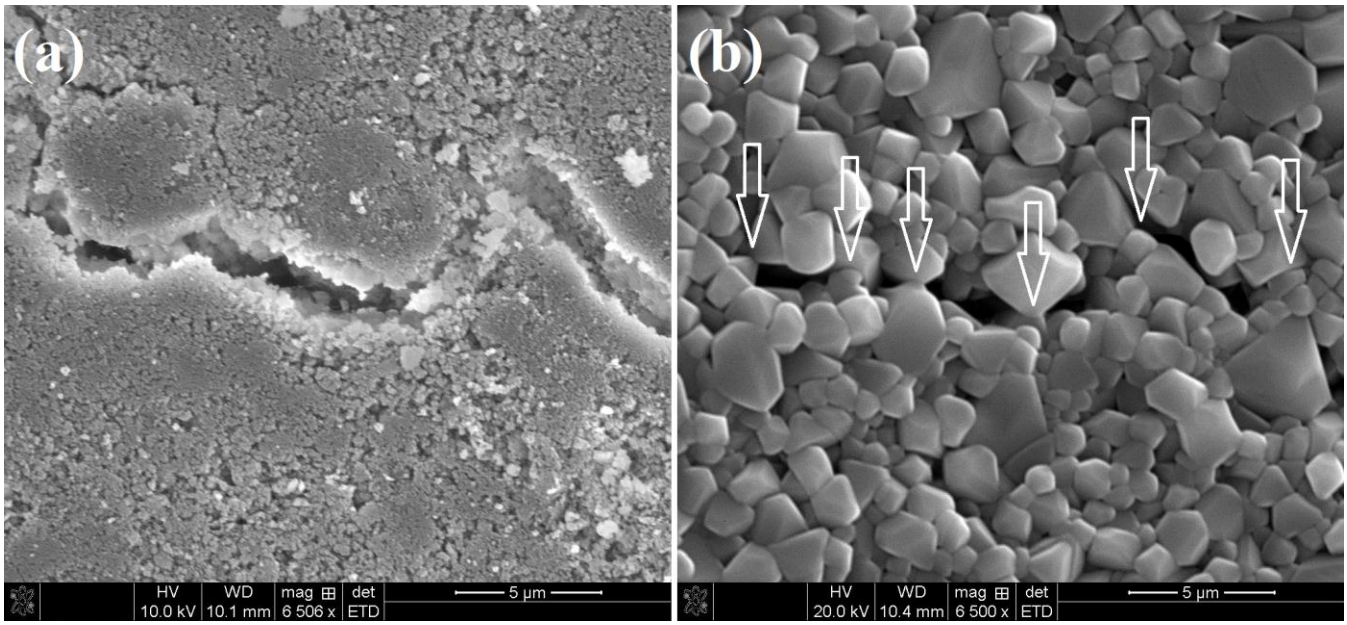

Figure 4.3. The location of a crack before and after sintering at 1600 °C for 1h.

Figure 4.4 shows the location of cracks before (left pictures) and after healing procedure (right pictures) at 1600 °C for 10h. Parts c and g in figure 4.4 show the location of the circles in parts a and e in figure 4.4, respectively. It can be seen that sintering the specimens for 10 h caused a partial healing of the cracks. Also the grain growth phenomenon can be clearly seen in the healed specimens. Figures 4.5 and 4.6 show the location of cracks before and after sintering at 1200 °C and 1400 °C for 100h, respectively. As can be seen, after 100 h sintering only partial healing was achieved in those specimens. Very minor healing was observed in those samples sintered at 1200 and 1400 °C for 1 and 10 h. Therefore it seems

that higher temperature and/or longer time are needed to achieve complete closure and healing of the cracks.

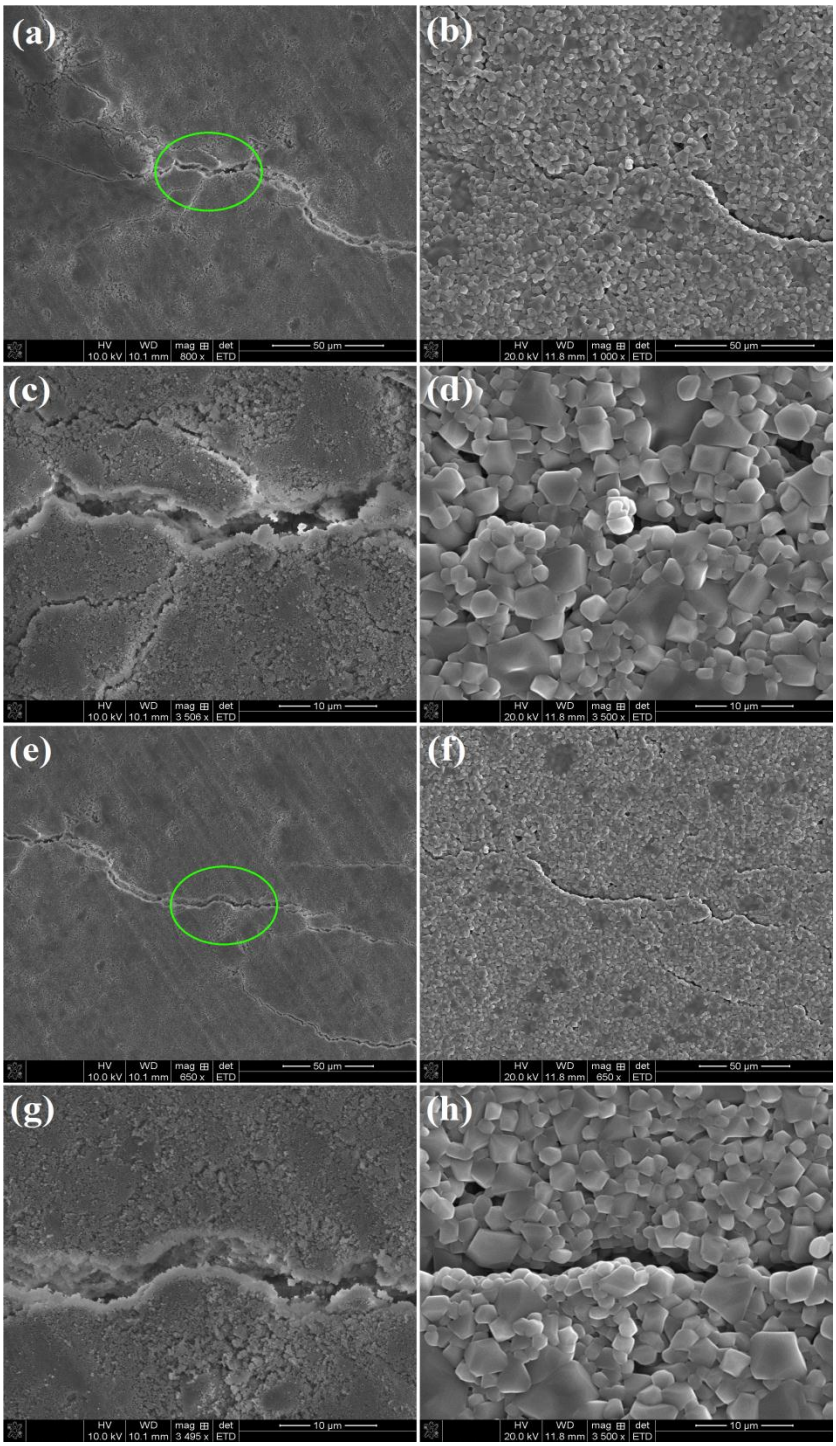

Figure 4.4. The location of cracks (a, c, e and g) before and (b, d, f, h) after sintering at 1600 °C for 10h, (a,b,e and f, scale bar = 50 µm)(c,d,g and h scale bar = 10 µm).

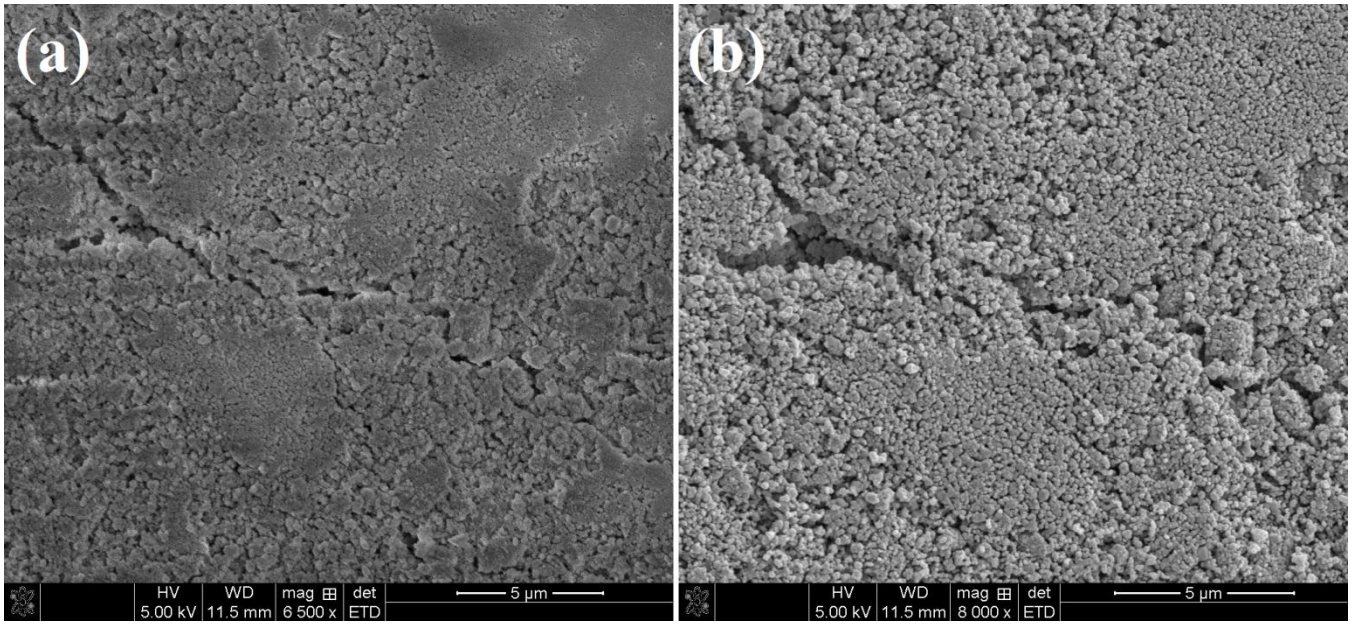

Figure 4.5. The location of a crack before and after sintering at 1200 °C for 100h.

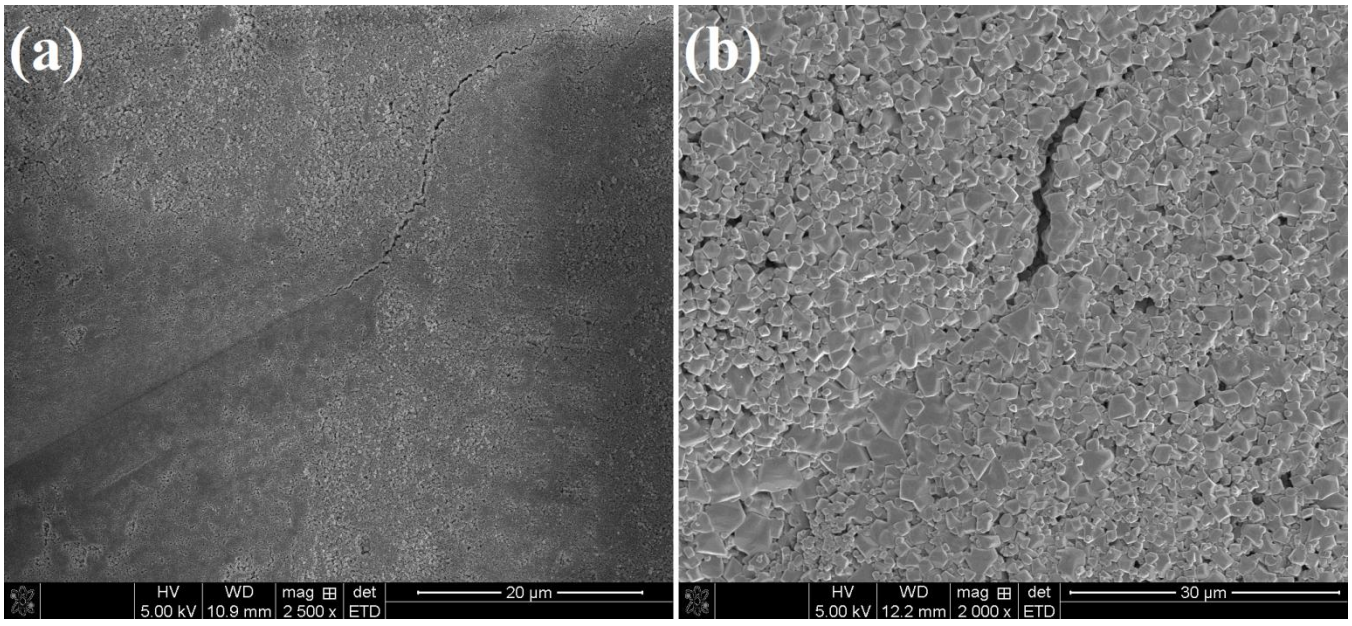

Figure 4.6. The location of a crack before and after sintering at 1400 °C for 100h.

Spinel has the chemical formula of $MgAl_2O_4$ ($MgO.Al_2O_3$). Hence in order to study the healing mechanism, it is a good idea to have a look at the healing procedure in MgO and Al_2O_3. According to the literature, the proposed healing mechanisms in MgO and Al_2O_3 are sintering, pore evolution, grain

growth, mass transport, and volume and surface diffusion processes. In monolithic alumina the sintering mechanism is responsible for the healing process. Gupta [8] demonstrated that crack healing in alumina is related to pores evolution in the microstructure during annealing. Cracks are healed via the disappearance of void space between adjacent grains. Also it is shown that cylindrical voids which are initially formed by the pinching of cracks, break up into spherical pores and then disappeared with increasing the holding times at elevated temperature [8]. Lange and Radford [9] reported that a complete healing of alumina can be ensured after sintering of the samples at 1700 °C for 1h. They suggested that the healing process is as a result of the grain growth which filled in and eliminated the crack. Choi and Tikare [10] investigated the crack healing of alumina in both air and inert environments. They found that crack healing occurred at temperatures higher than 800 ºC in both air and inert (argon) atmospheres, showing that the healing mechanism is due to the transport of existing materials to the crack surfaces.

The crack healing behavior of thermally shocked MgO was studied by Gupta [11]. It was found that crack healing can be completely reached after sintering the MgO specimens at 1500 °C for 7h as a result of a mass transportation phenomenon. The mechanism of healing is similar to what is explained in Al_2O_3 ceramic. In polycrystalline MgO, during the healing process cylindrical voids are first formed and then broken down into several spherical pores. With continuing the healing process, the produced spherical pores shrink and the strength of the structure increases [11]. Sangwal et al. [12] evaluated the surface morphology around nanoindentations (for loads up to 10μN) made on the (110) cleavage face of MgO crystals at room temperature by *in situ* atomic force microscopy. Kinetics studies suggested that the recovery of indented surfaces of MgO structure takes place by local reorganization, and volume and surface diffusion processes [12]. Therefore, similar mechanisms should be dominant on the crack self-healing in spinel. As can be seen in figure 4.3, the local healing of the cracks in the spinel structure can be assigned to the grain growth occurred from one side of the crack wall to the other side. When two growing grains come in contact with each other, the local sintering phenomenon happens (arrows in figure 4.3 part b) at high temperature which can finally result in crack closure. At high enough temperature, all the grains can grow from one side of the crack wall and come in contact with the grains on the opposite side. Then the sintering phenomena can close the whole crack and complete healing can be achieved.

Figure 4.7 shows the location of crack before and after sintering at 1600 °C for 100h. As can be seen in this figure, all the cracks are healed and no crack traces can be observed in the SEM micrographs. An interesting phenomenon which happened in this specimen is the abnormal grain growth that can be considered as one of the responsible mechanisms for the complete healing process. Abnormal grain growth is characterized by the excessive growth of a relatively small number of grains at the expense of the surrounding matrix grains and may lead to a bimodal distribution of grain sizes. In this phenomenon, a few large grains grow unusually quickly in a matrix of fine grains with a very slow growth rate. The driving force for grain growth is the decrease in free energy which is accompanied by a reduction in the total grain boundary area [13-16].

Therefore, in the case of spinel ceramic, grain growth and sintering phenomena are responsible for the crack healing process. At high enough temperature, the grains start to grow and when they come in

contact with each other, the sintering phenomenon happens which cause the formation of atomic bonding between two adjacent grains across the interface and cause the adhesion of the grains at the location of the crack (figure 4.3, see b).

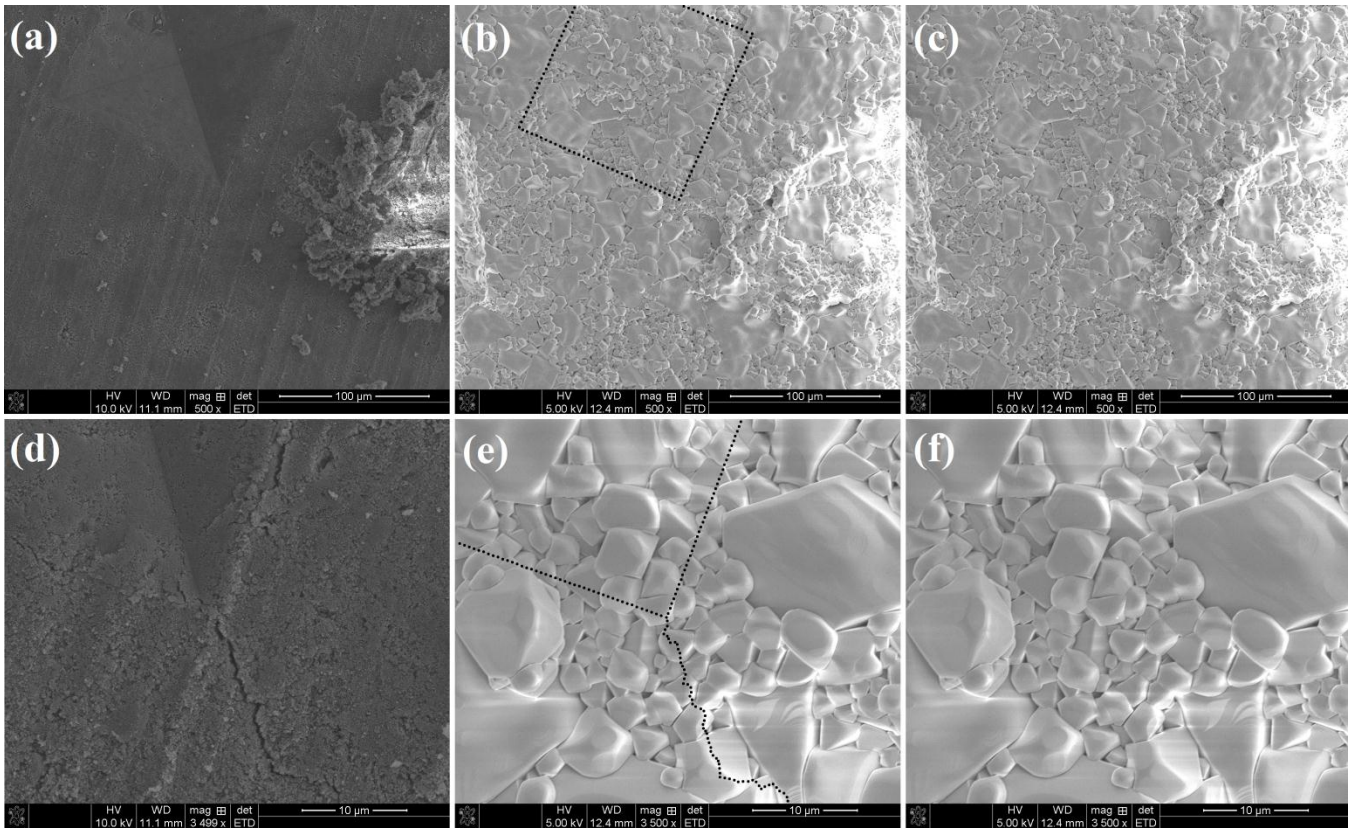

Figure 4.7. The location of cracks (a and d) before and (b, c, e, and f) after sintering at 1600 °C for 100h.

The cold crushing strength test was performed to measure the compressive strength of the specimens. The mean CCS of GS was 60.13MPa. The mean CCS of non-indented pellets which were sintered at various temperatures and times is shown in figure 4.8. As can be seen, in all specimens the CCS increased with increasing the holding time. The CCS of samples sintered at 1200 °C was very low indicating that the annealing temperature was not enough to sinter the adjacent grains. With increasing the sintering temperature to 1400 °C, the CCS increased, however increasing the holding time did not change the CCS noticeably, while those specimens sintered at 1600 °C showed a significant increase in the CCS. During the synthesis procedure of the pellets, some micro and macro cracks may form inside the structure which can have a detrimental influence on the mechanical properties of the pellets. At 1200 and 1400 °C the temperature is not enough for complete sintering of the structure and hence the CCS is low. With increasing the temperature to 1600 °C and holding time of up to 10h, the CCS increased due to the better sintering of the structure. The maximum CCS of 486.08 MPa was obtained for those

specimens sintered at 1600 °C for 100h (which was about 8 times of the GS) as a consequence of the abnormal grain growth and sintering phenomena which resulted in the complete closure of the micro- and macrocracks inside the structure.

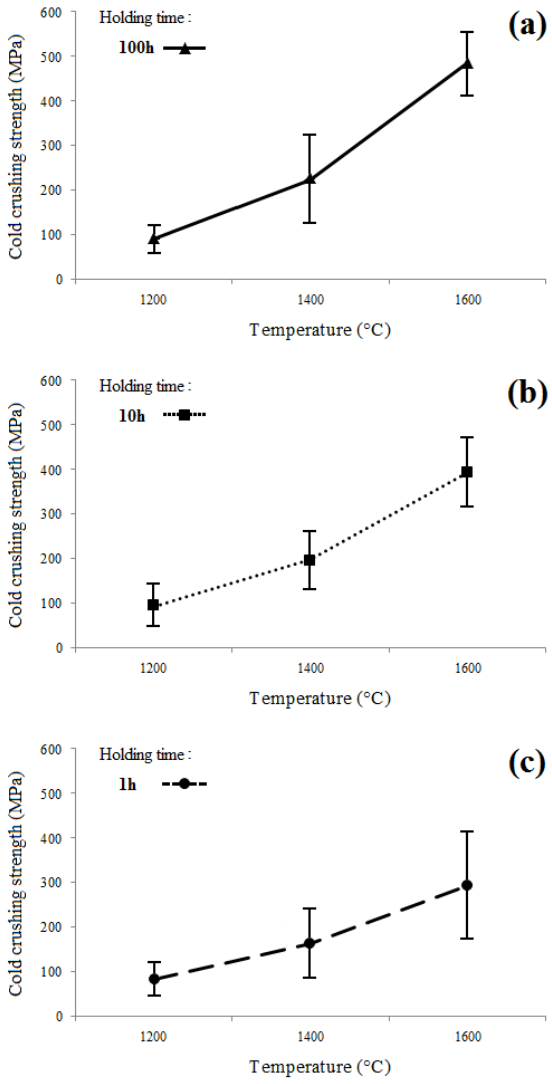

Figure 4.8. Cold crushing strength of sintered spinel pellets at various temperatures for (a) 100 h, (b) 10 h, (c) 1 h holdings times.

Figure 4.9 shows the hardness of annealed samples at various temperatures and times. Generally, sintering the samples for 1h did not have a great influence on the hardness of the specimens. The hardness of the specimens sintered at 1200 °C is very low which shows that the temperature is not enough for sintering. Those specimens sintered at 1400 °C for 10 and 100h shows a noticeable hardness;

however, their hardness is still lower than those samples sintered at 1600 °C for 10 and 100h, respectively. The maximum hardness of 4.39 GPa was obtained for the sample sintered at 1600 °C for 100h as a result of better sintering of the samples at higher temperatures for longer time.

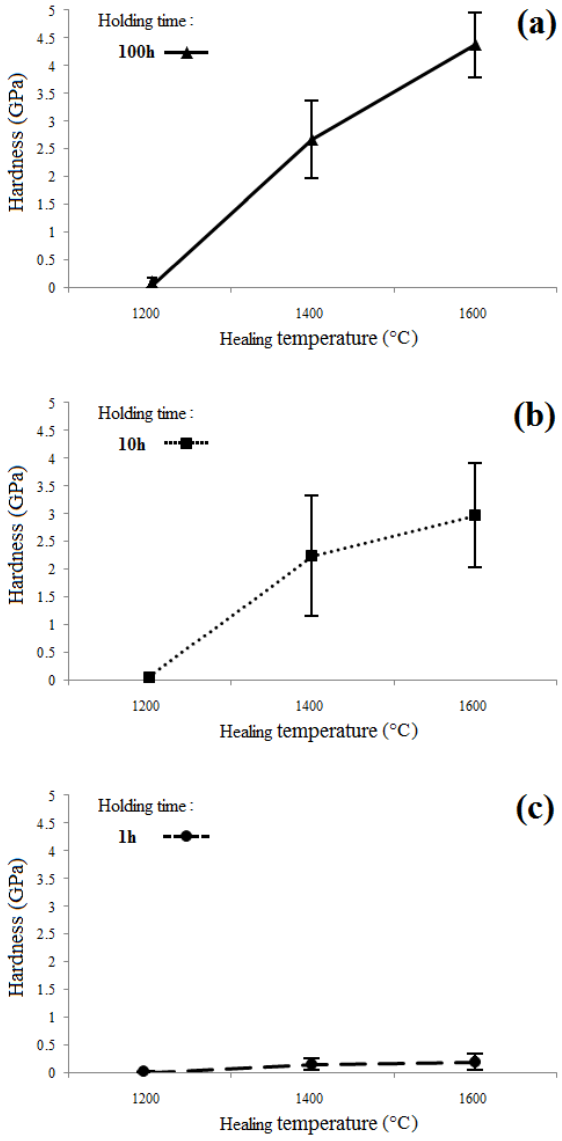

Figure 4.9. Hardness of sintered spinel pelleted at various temperatures for (a) 100 h, (b) 10 h, (c) 1 h holdings times.

Typically, to measure the tensile strength, tension test is performed; however, it can be difficult to perform tension test in the case of brittle materials due to the difficulties associated with the gripping of the samples. Diametral tensile strength (DTS) test is an alternative method to overcome this limitation. In this study, DTS test was performed on the specimens to determine the tensile strength of the pre-cracked and non-cracked specimens after sintering. In order to see if this experiment can be a useful method to determine the healing efficiency, first the DTS of GS and GS-C (table 4.1) was evaluated by this method. The mean DTS of GS was 6.20 MPa, while the mean DTS of GS-C was obtained as 4.01 MPa. According to equation (4-2), the $DTSR_{initial}$ is equal to 35.48 % which can be attributed to the presence of 36 indentations on both surfaces of the cylindrical specimens. The surface indentations can degrade the strength of the material by producing many micro- and macro-cracks inside the structure. Figure 4.10 shows the trace of crack in GS-C after the specimen is failed. As can be seen in figure 4.10 part a, the crack is on the line of indentations but at a certain point the direction of crack growth has changed (figure 4.10, see b). In three samples that were tested the cracks had the same behavior. Up to a location the crack was on the line of indentations and then the crack reached outside the indentation trace. The change in the direction of crack growth may be ascribed to the different orientation of crystal planes, the presence of surface or internal cracks, the presence of internal voids and defects inside the structure, and a small deviation of the line of indentations from vertical position when we put the samples in DTS testing machine. With comparing the amount of degradation of the DTS of the indented and non-indented samples after various healing procedures we can determine how much of the lost strength can be recovered.

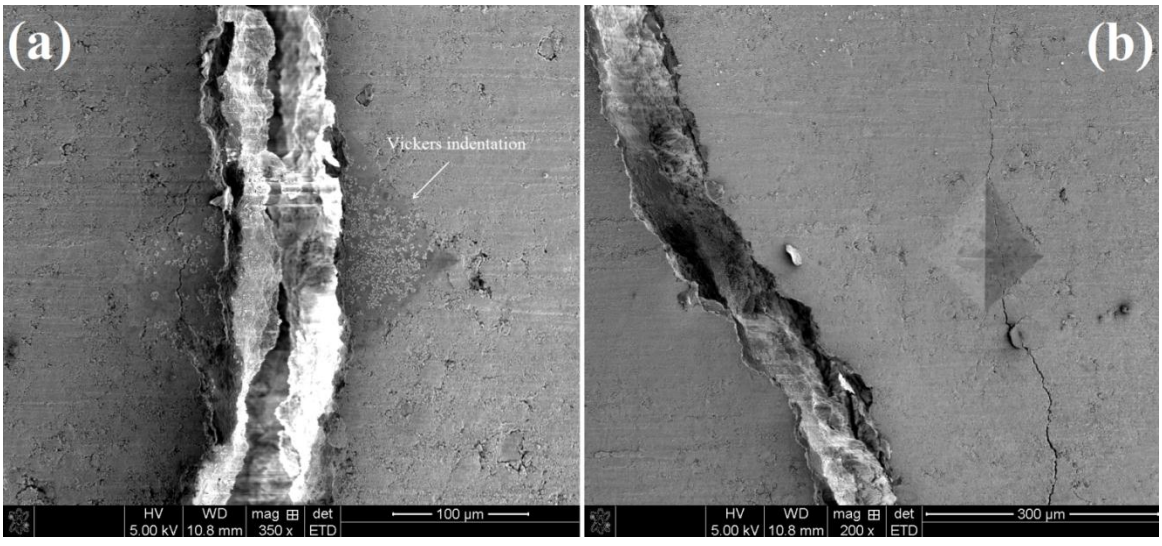

Figure 4.10. SEM micrograph of a crack propagated in the GS-C (a) crack passed through the line of indentations (b) change of the direction of the crack.

Figure 4.11 and table 4.2 show the strength recovery and the DTS of the indented and non-indented specimens after sintering at various temperatures, respectively. The maximum strength recovery of 91% was obtained for those samples heat treated at 1600 °C for 100h as a result of almost complete healing of the structure (figure 4.7). Those samples sintered at lower temperatures and/or sintered for less time showed less healing efficiency due to the partial healing phenomenon and insufficient time or temperature for sintering.

Table 4.2. Diametral tensile strength and DTSR of various specimens.

Sample	Mean diametral tensile strength (indented specimen) (MPa) (S.D.)	Sample	Mean DTS of the control sample (non-indented specimen) (MPa) (S.D.)	DTSR (%)
GS-C	4.01 (±0.37)	GS	6.20 (±0.58)	35.48
12-AC	4.13 (±0.47)	12-A	5.96 (±0.99)	30.70
12-BC	4.94 (±1.22)	12-B	6.45 (±0.52)	23.41
12-DC	5.55 (±0.63)	12-D	6.63 (±1.50)	16.28
14-AC	11.49 (±1.15)	14-A	15.20 (±1.98)	24.40
14-BC	13.70 (±1.62)	14-B	16.35 (±1.71)	16.20
14-DC	14.53 (±1.75)	14-D	15.73 (±1.66)	7.62
16-AC	11.37 (±0.73)	16-A	14.06 (±1.40)	19.13
16-BC	16.41 (±1.55)	16-B	18.97 (±1.97)	13.49
16-DC	20.10 (±2.70)	16-D	20.78 (±2.11)	3.27

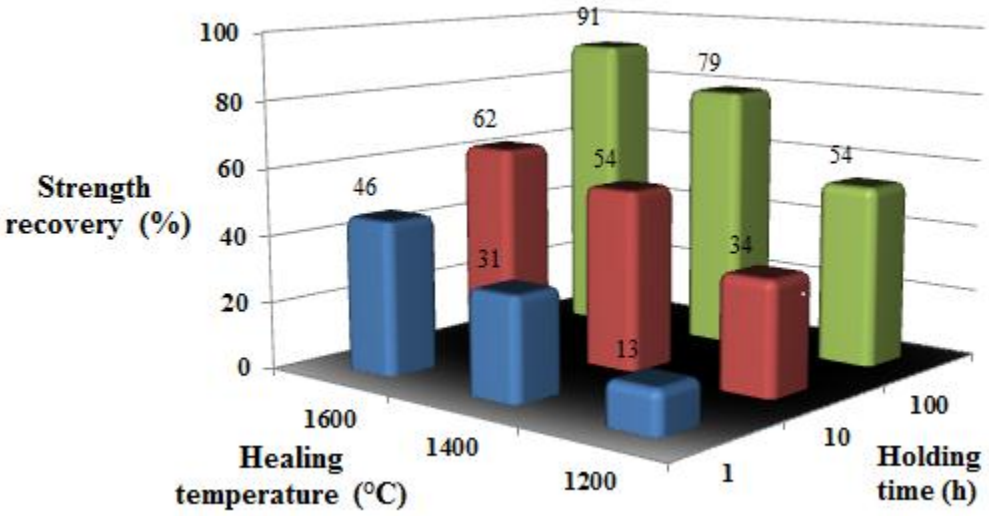

Figure 4.11. Strength recovery of different specimens.

4.4 Conclusion

The crack-healing behavior of spinel ceramic was investigated up to 1600 °C for 100h. Minor healing was observed in those specimens sintered at 1200 and 1400 °C. In those specimens sintered at 1600 °C for 1 and 10h, partial healing was observed. Complete healing was obtained only for those specimens sintered at 1600 °C for 100h. It was found that grain growth and sintering phenomena are two parameters that affect the healing procedure. Those specimens healed at 1600 °C for 100 h showed high CCS (486.08 MPa) and hardness (4.39 GPa) in comparison with those green samples as a result of the better sintering and adhesion of the grains in the structure. Also the healing efficiency of the samples was investigated by diametral tensile strength (DTS) test. The maximum strength recovery of 91% was obtained for those specimens healed at 1600 °C for 100 h as a result of almost complete healing of the structure.

4.5 References

[1] Li S, Xiao L, Song G, Wu X, Sloof WG, van der Zwaag S. Oxidation and crack healing behavior of a fine-grained Cr_2AlC ceramic. J Am Ceram Soc 2013;96:892-9.

[2] Liang J, Wang Y, Fang G, Wang G. Influence of oxidation healing for cracks on the strength of hot-pressed ZrB_2–SiC–AlN ceramics. Int J Appl Ceram Technol 2012;9:441-6.

[3] Zuo X, Zhang L, Liu Y, Cheng L, Xia Y. Oxidation behaviour of two-dimensional C/SiC modified with self-healing Si-B-C coating in static air. Corros Sci 2012;65:87-93.

[4] Yang HJ, Pei YT, Rao JC, De Hosson JTM, Li SB, Song GM. High temperature healing of Ti_2AlC: On the origin of inhomogeneous oxide scale. Scripta Mater 2011;65:135-8.

[5] Gao J, Suo J. Effects of heating temperature and duration on the microstructure and properties of the self-healing coatings. Sur Coat Technol 2011;206:1342-50.

[6] Roberts JTA, Wrona BJ. Crack healing in UO_2. J Am Ceram Soc 1973;56:297-9.

[7] Fahad MK. Stresses and failure in the diametral compression test. J Mater Sci 1996;31:3723-9.

[8] Gupta TK. Crack healing and strengthening of thermally shocked alumina. J Am Ceram Soc 1976;59:259-62.

[9] Lange FF, Radford KC. Healing of surface cracks in polycrystalline Al_2O_3. J Am Ceram Soc 1970;53:420-1.

[10] Choi SR, Tikare V. Crack healing of alumina with a residual glassy phase: strength, fracture toughness and fatigue. Mater Sci Eng A 1993;171:77-83.

[11] Gupta TK. Crack healing in thermally shocked MgO. J Am Ceram Soc 1975;58:143.

[12] Sangwal K, Gorostiza P, Sanz F. In situ study of the recovery of nanoindentation deformation of the (100) face of MgO crystals by atomic force microscopy. Surf Sci 1999;442:161-78.

[13] Rahaman MN. Ceramic processing and sintering second edition. CRC press, new york, 2003, page 543.

[14] Kang SJL. sintering, densification, grain growth, microstructure. 2005, Elsevier Butterworth-Heinemann, Linacre House, Jordan Hill, Oxford, Burlington, MA page 117.

[15] Humphreys FJ, Hatherly M, recrystallization and related annealing phenomena. Pergamon. 1995, 314-25.

[16] Somiya S, Aldinger F, Claussen N, Spriggs R.M, Uchino k, Koumoto K, kaneno M. Handbook of advanced ceramics: volume 1 materials science, 2003, page 204.

CHAPTER 5 SYNTHESIS, CHARACTERIZATION AND FORMATION MECHANISM OF SIC/SPINEL NANOCOMPOSITE[1]

5.1 Introduction

In many applications there is a need for a material with a combination of a series of properties simultaneously. Composite materials are made of two or more constituent materials with a desired properties of each one, while reduce the limitation of each components.

In recent years, it was found that SiC has a self-healing capability [1-6]. With initiating of a crack, SiC reacts with oxygen to form SiO_2 at high temperature and fills the crack. Lange [1] found that the flexural strength of pre-cracked SiC specimens were increased after annealing at 1400 °C for up to 100h while those samples annealed in a vacuum did not show a noticeable strength increase in comparison to pre-cracked samples. Further investigation showed that a film of SiO_2 is formed on the surface of the specimens and subsequently fills and heals the cracks. In another work [2], Petrovic and Jacobson examined the room-temperature fracture stress of SiC specimens annealed in air and in a vacuum. The results showed that the strength of those samples annealed in air was noticeably higher than that annealed in a vacuum. In the case of SiC, two kinds of oxidation may happen (depends on the partial pressure of the oxygen); passive oxidation and active one [3,4]. In passive oxidation, a layer of SiO_2 forms on the surface which is accompanied with a measurable weight gain. While in active oxidation volatile SiO gas forms which leaves the SiC substrate and hence the material is accompanied with a weight loss. Petrovic and Jacobson found that the oxidation occurred in their experiment is passive at all temperatures. Kim et al. [6] studied the strength change and oxidation behavior of four different types of reaction-bonded SiC (RBSC) ceramics after annealing at 1300 °C for up to 100h. RBSCs are composed of a combination of large SiC particles, a fine carbon source and liquid silicon and they are used to synthesize large bodies with complex shapes. The silicon and carbon react *in situ* to produce fine SiC particles. The results showed that the weight gain after oxidation increased by increasing the amount of free silicon. Also the flexural strength of the samples increased with increasing the oxidation time up to 50 h and then decreased. The increase in the strength can be ascribed to the healing process of the cracks while the decrease in strength is as a result of the formation of new cracks due to the thermal mismatch between the substrate and the produced SiO_2 oxide layer.

Magnesium aluminate spinel ($MgAl_2O_4$) is one of the most attractive materials in the field of ceramics engineering. Spinel, with a melting point of 2135 °C, shows high strength at both elevated and normal temperature and good chemical stability regarding to acids and alkalis, and is recommended as a great refractory material [7]. Also, due to its low electrical losses, spinel is used in microwave communication systems such as radar detectors, cellular telephones and global positioning systems (GPS) [8].

[1] This chapter previously appeared as Fariborz Tavangarian, Guoiqang Li, Synthesis, characterization and formation mechanism of SiC/spinel nanocomposite, *Journal of Alloys and Compounds*, June, 2014. It is reprinted by permission of Elsevier (see the permission letter in Appendix A).

Furthermore, its application in mid-wave infrared (IR) windows is being studied to protect high-velocity missiles and transparent armor screens against IR seekers [9].

The conventional synthesis procedure of spinel is reaction of the initial materials (oxides, hydroxides or salts) of aluminum and magnesium at temperature higher than 1400 ºC [10]. Due to the fact that the formation of spinel is accompanied with 5-8% volume expansion [11,12], producing dense bodies of spinel from initial materials through one step sintering is very difficult. To produce a dense body of spinel in practice, spinel powders are first synthesized to complete the spinelization process and then the produced powder is utilized to form dense body through a second sintering procedure [11]. These sintering procedures at elevated temperatures will result in the formation of a coarse grain microstructure (100-200 µm) with low mechanical properties and low thermal-shock resistance [9]. Some researchers produced nanostructured spinel with higher strength, however the produced nanostructured spinel is brittle and its mechanical properties degrade due to the formation of cracks in service [9,10]. To overcome this problem, SiC may be utilized as a secondary phase to increase the fracture toughness of the matrix and also to heal the produced cracks during the synthesis procedure as well as in service [13-15]. Prof. Ando's team investigated the crack self-healing behavior of the SiC/Al_2O_3 composite [16,17]. They found that alumina matrix containing 15 wt.% SiC can be completely healed after heat treatment at 1300 °C for 1h in air. The responsible reaction for the healing procedure in this composite is the formation of SiO_2 as a result of the reaction between SiC and oxygen at high temperature [16]. In another work [17] they studied the self-healing behavior of alumina reinforced by SiC whiskers under static and cyclic stresses. They found that cracks with length of up to 100 µm can be healed completely under static and cyclic stresses up to 250 MPa and 300 MPa, respectively. Zuo et al. [18] utilized Si-B-C coating on C/SiC substrate as a oxidation barrier coating. Formation of borosilicate glass at temperature between 700 and 1300 °C can heal the produced cracks on the surface of the coating and improve the oxidation resistance of C/SiC substrate. Lee et al. [19] studied the crack-healing behavior of mullite /SiC/Y_2O_3 composites and found that cracks can be healed after sintering the specimens from 1200 to 1400 °C in air with 40 to 200% increase in the sample strength.

Currently there is a lack of study on the synthesis and formation of SiC/spinel nanocomposite. The objective of this chapter is to produce SiC/spinel nanocomposite powder as a potential composite for high temperature applications with self-healing capabilities. Talc powder was used as a source of silicon and magnesium to synthesize SiC/spinel composite. The SiC/spinel formation mechanism was studied in detail and the reaction pathways were revealed as well.

5.2 Experimental procedures

Talc ($Mg_3Si_4O_{10}(OH)_2$) (99% purity, Sigma Aldrich), aluminum (Al) (99.5% purity, Alpha Chemicals) and graphite (C) (99% purity, Sigma Aldrich) powders were used as raw materials. Figure 5.1 shows the morphology of the initial powder particles. The talc powder particles were lamellar in shape with a mean

particle size of about 15 µm. Aluminum powder had a spherical shape with a mean particle size of about 2 µm. Graphite powder particles had a flake shape with a mean particle size of about 50 µm. Talc, Al and graphite powders with molar ratio of 1:6:4 were mixed to yield SiC/spinel composite containing 27.26 wt.% SiC. Powder mixture (27 g) was mechanically activated in a planetary ball mill (Across International, PQ-N2) in an argon atmosphere, at room temperature. The milling media consisted of a hardened steel vial with 5×20 mm, 20×10 mm, and 50×6 mm steel balls. In all milling runs the ball-to-powder weight ratio was 10:1 and the rotational speed of the main disc was 500 rpm. Heat treatment of ball milled powders was carried out at 1000, 1200 and 1400 ºC for 1h in a vacuum in a tube furnace (MTI Corporation, GSL 1700x). In all heat treatment procedures the starting pressure of the tube furnace was below 100 mTorr.

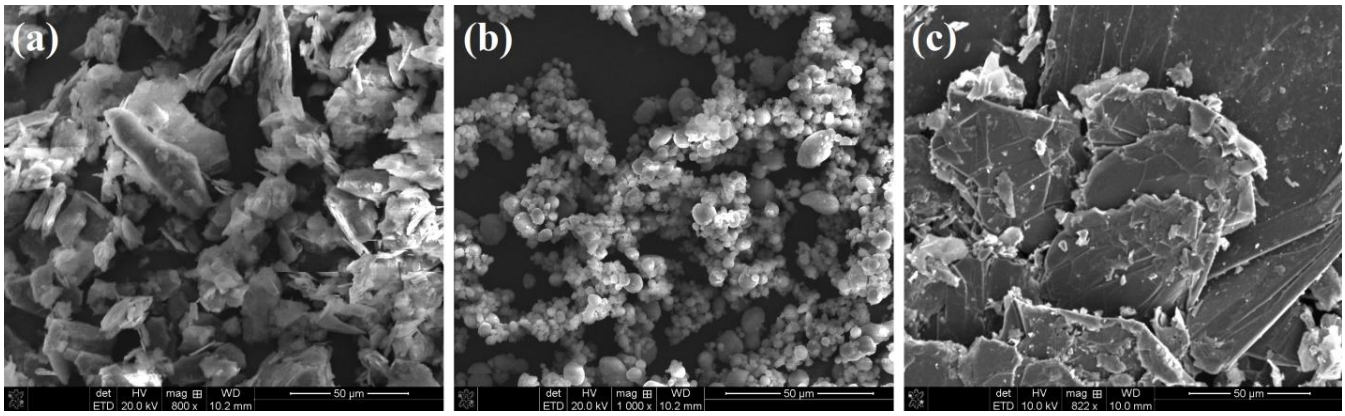

Figure 5.1. SEM micrographs of initial materials including: (a) talc, (b) aluminium and (c) graphite powders.

The phase transformations of different specimens were investigated by X-ray diffractometry (MiniFlex XRD, Rigaku Corporation, Japan) with Cu Kα radiation (λ= 0.154178 nm). The XRD traces were recorded in the 2θ range of 20–80º (step size of 0.05º and time per step of 1 s). The morphology of powder particles was studied by field emission scanning electron microscopy (Quanta3D FEG, FEI Company, USA) at acceleration voltages between 5 and 30 kV. Image analyzing method was used to measure spinel and SiC powder particles size. The transmission electron microscopy (TEM; JEM-1400) technique was utilized to characterize the morphology and the structure of the prepared samples.

5.3 Results and discussions

Figure 5.2 shows the XRD patterns of powders after various ball milling times. The x-ray diffraction pattern of as mixed powders (0h ball milled sample) corresponded to Talc ($Mg_3Si_4O_{10}(OH)_2$) (XRD JCPDS data file No. 13-0558), aluminum (Al) (XRD JCPDS data file No. 01-1176) and graphite (C)

(XRD JCPDS data file No. 01-0640) phases. Milling the initial powders led to the broadening of XRD peaks and a significant decrease in their intensities due to the formation of smaller crystallite size and the formation of internal strains [20,21]. The characteristic peaks of graphite and talc phases were vanished after 5 and 6h ball milling times, respectively. The characteristic peaks of aluminum phase were observed up to 6h ball milling time. No new crystalline phase was detected on the XRD patterns even after 6h of milling time. Exposure of the 7h ball milled powders to air led to an explosive reaction probably due to the formation of Al_2O_3. Hence, one limiting factor is the milling time. Since working with the ball milled powders is not possible in ambient condition for those samples milled for more than 6h, we have to select 6h ball milled samples for next step as the talc and graphite were in the form of amorphous phase and initial powders were well mixed together.

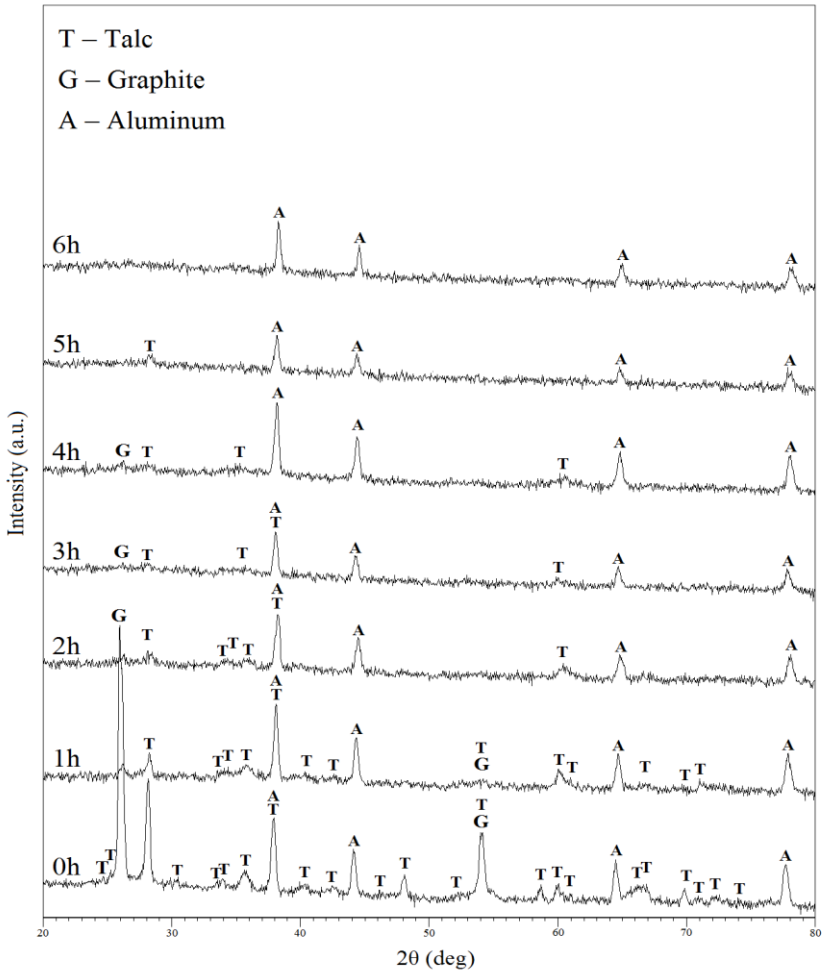

Figure 5.2. X-ray diffraction patterns of initial materials after mechanical activation for various periods of time.

To evaluate the formation of SiC/spinel composite in the ball milled sample during subsequent heat treatment, the milled powders were annealed at 1000, 1200 and 1400 ºC for 1h in a vacuum. Figure 5.3 shows the structure of specimens after annealing at 1000 ºC for 1h in a vacuum. Annealing of sample milled for 0h led to the complete vanishing of talc. Additionally some peaks of enstatite ($MgSiO_3$) (XRD JCPDS data file No. 03-0696), forsterite (Mg_2SiO_4) (XRD JCPDS data file No. 03-1117), silicon carbide (SiC) (XRD JCPDS data file No. 03-1146), serpentine ($3MgO.2SiO_2.2H_2O$) (XRD JCPDS data file No. 02-0092), alumina (Al_2O_3) (XRD JCPDS data file No. 10-0173), and spinel ($MgAl_2O_4$) (XRD JCPDS data file No. 01-1154) phases were appeared on the XRD pattern. With increasing the milling time up to 6h, no significant changes were observed except for a decrease in the intensity of graphite and aluminum phases and an increase in the intensity of enstatite and spinel phases. This can be ascribed to the consumption of initial materials and the formation of higher fraction of enstatite and spinel. But even after 6h of milling, enstatite and serpentine phases were remained in the structure of produced powder.

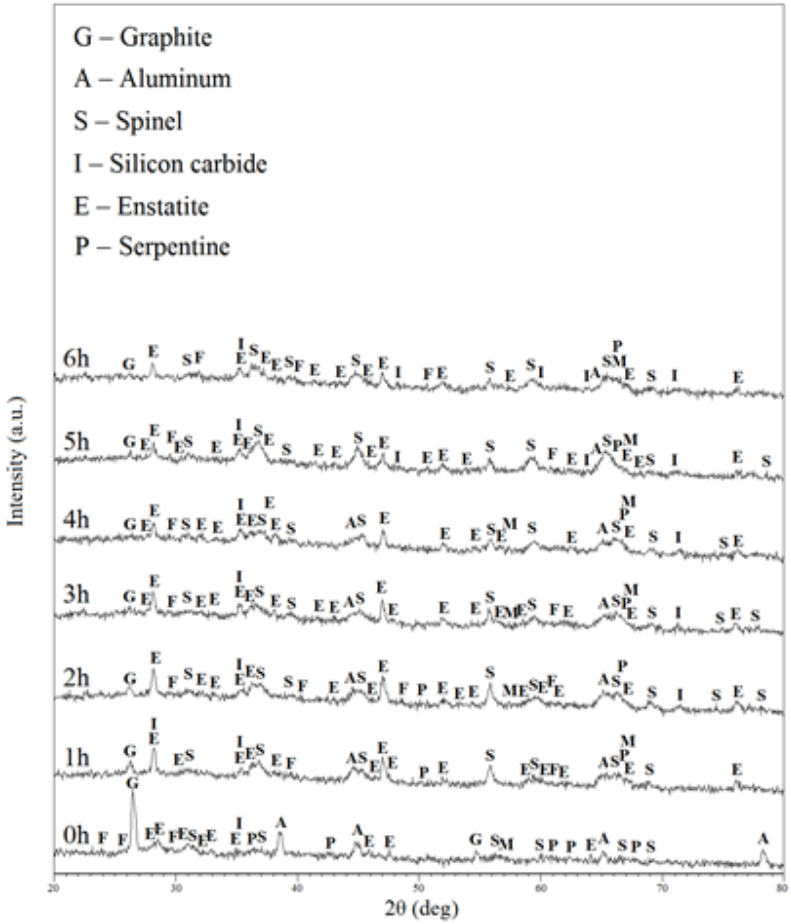

Figure 5.3. XRD patterns of obtained powders after mechanical activation for various periods of time and subsequent annealing at 1000 °C for 1 h in a vacuum.

Figure 5.4 shows the XRD patterns of powders milled for various times with subsequent annealing at 1200 ºC for 1h in a vacuum. As can be seen, graphite phase was detected up to 2h ball milled samples. Alumina and serpentine phases were vanished after 3h of milling. All the other phases such as enstatite, forsterite, aluminum phases was observed for those samples milled up to 4h of ball milling. For those samples milled for 5 and 6h, only spinel and silicon carbide phases were detected in the XRD patterns. Increasing the annealing temperature from 1000 to 1200 ºC speeded up the rate of reactions such that the SiC/spinel composite could form completely after 5 and 6h ball milling time.

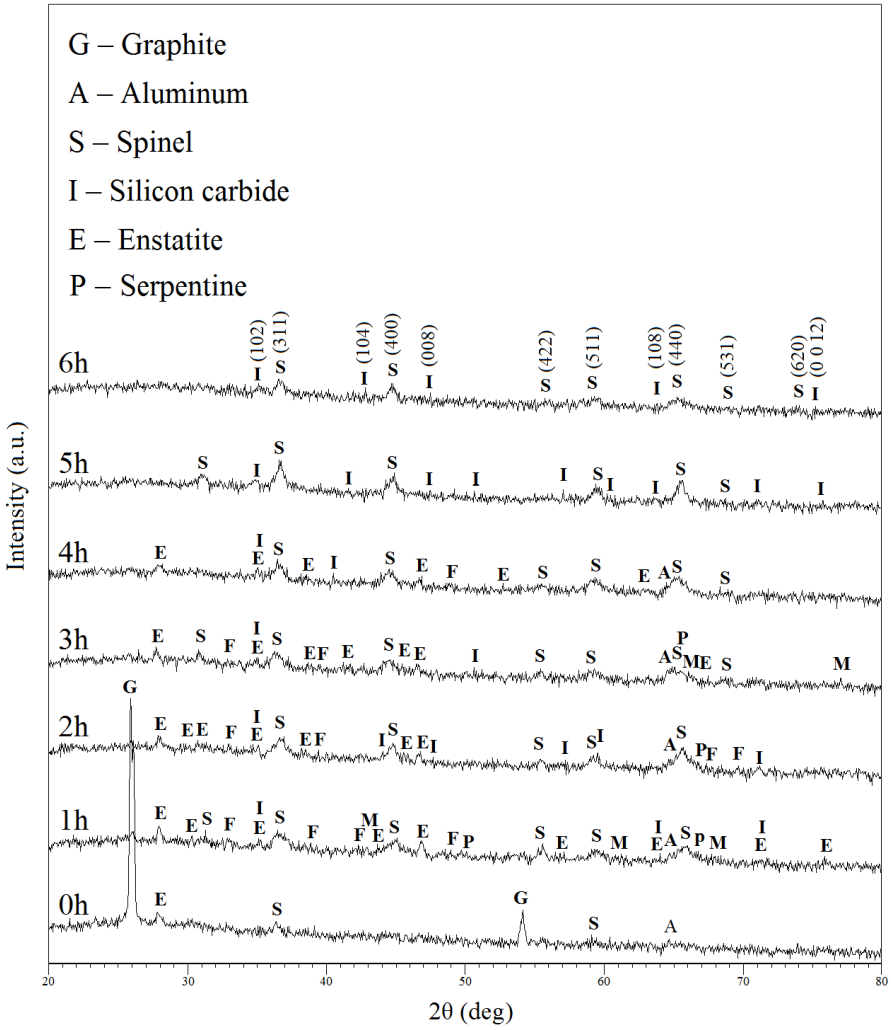

Figure 5.4. XRD patterns of obtained powders after mechanical activation for various periods of time and subsequent annealing at 1200 °C for 1 h in a vacuum.

To investigate the formation mechanism of SiC/spinel composite, first we monitored the inside vacuum pressure of the tube furnace with increasing the annealing temperature at a heating rate of 10 ºC/min. To achieve this goal, 1g of 6h ball milled sample was placed in the furnace. As soon as the inside pressure of the tube furnace reached 50 mtorr, the furnace was turned on and the vacuum pressure was monitored with increasing the temperature. Furthermore, in order to make sure that the vacuum pressure changes are due to the powder and not the tube, seals, vacuum flanges and valves of the furnace, the same experiments was carried out exactly in the same condition in the absence of any powder and crucible (control experiment). The results of vacuum pressure changes for 6h ball milled sample and the control are shown in figure 5.5. With increasing the annealing temperature from 50 to 250 ºC, the vacuum pressure increased slightly from 50 to 382 mtorr which can be ascribed to the loss of hydration water and also liberation of structural water of talc [20]. There is a very intensive peak at around 726 ºC in which the vacuum pressure suddenly increase from 220 to 2368 mtorr. This can be attributed to the occurrence of a reaction at this temperature which can be approved by obtained XRD patterns of powders around this temperature. Another important stage was observed from 1300 to 1425 ºC in which the vacuum pressure increased from 165 to 533 mtorr which can be a sign of another reaction around these temperatures. The only thing that should be noticed in the control experiment is that for those temperatures higher than 1300 ºC, the vacuum pressure increased and air could penetrate into the tube furnace. Consequently the obtained powders may react with the oxygen and this in turn may affect the final products.

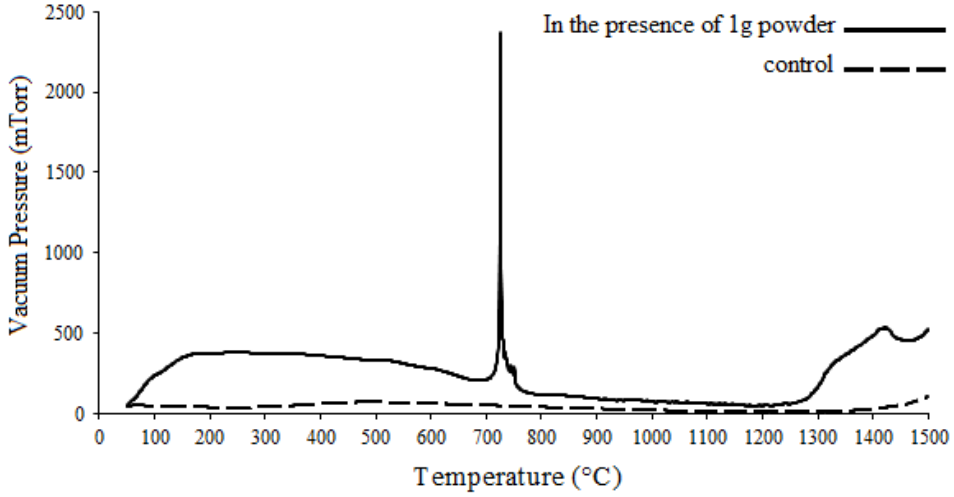

Figure 5.5. Vacuum pressure changes in the tube furnace with increasing the temperature in the presence and absence of 1g of initial ball milled powders.

Figure 5.6 shows the XRD patterns of 6h ball milled samples with 1h holding time at various temperatures in a vacuum. As can be seen, the XRD patterns of those samples annealed at 25 and 600 ºC corresponded to the aluminum phase. No new phases were detected in the XRD patterns. In fact the temperature was not enough to initiate any reaction up to 600 ºC. With increasing the annealing temperature to 700 ºC, a totally different pattern was observed. The intensity of aluminum peaks decreased enormously while other peaks such as enstatite, forsterite, serpentine, alumina, spinel and SiC phases were observed in the XRD pattern. At the beginning stage it seems that the structural water of talc released and then one mole of Si comes out from the talc structure, leaves enstatite behind and reacts with one mole graphite to form SiC. On the other hand two moles of aluminum reacts with three moles oxygen from talc to form alumina. Hence the general reaction in the first stage may be expressed as follows:

$$Mg_3Si_4O_{10}(OH)_2 + 6Al + 4C \rightarrow 3MgSiO_3 + SiC + 4Al + 3C + Al_2O_3 + H_2(g) \quad (5\text{-}1)$$

One can understand the above reaction as follows: the composition of talk can be expressed as $3MgO.4SiO_2.H_2O$. In the first stage one mole of SiO_2 and one mole of H_2O come out from the structure of talk and what remains is $3MgO.3SiO_2$ which is another form of enstatite ($3MgSiO_3$). The released Si reacts with C to form SiC and the released oxygen reacts with aluminum to form alumina. H_2O also comes out from talc and causes an increase in the internal pressure of the tube furnace. The next stage seems to occur as follow: another mole of SiO_2 may come out from the produced enstatite ($3MgO.3SiO_2$) and what remains is serpentine with the formula $3MgO.2SiO_2.2H_2O$. It should be noticed that the XRD patterns were obtained from the samples in ambient condition which means that the obtained powders can absorb water from the environment before XRD analysis. Hence the next stage in the SiC/spinel composite formation can occur according to the following reaction:

$$3MgSiO_3 + SiC + 4Al + 3C + Al_2O_3 \rightarrow 3MgO.2SiO_2 + 2SiC + \frac{8}{3}Al + 2C + \frac{5}{3}Al_2O_3 \quad (5\text{-}2)$$

Produced serpentine may dissociate into enstatite ($2MgO.2SiO_2$) and MgO and the obtained MgO may react with the existing alumina to produce spinel as follows:

$$3MgO.2SiO_2 + 2SiC + \frac{8}{3}Al + 2C + \frac{5}{3}Al_2O_3$$

$$\rightarrow 2MgSiO_3 + 2SiC + \frac{8}{3}Al + 2C + \frac{2}{3}Al_2O_3 + MgAl_2O_4 \quad (5\text{-}3)$$

The spinel formation mechanism is first studied by Carter [22]. He indicated that the spinelization reaction mechanism is by the counter diffusion of the Al^{3+} and Mg^{2+} ions through the rigid oxygen lattice.

It seems that the next stage is the formation of forsterite phase. This can happen when the obtained enstatite in reaction (3) loses one mole SiO_2 and in this way what remains is forsterite ($2MgSiO_3 \rightarrow MgO + Mg_2SiO_4$). As a result, the fourth stage of SiC/spinel composite formation may be expressed as follows:

$$2MgSiO_3 + 2SiC + \frac{8}{3}Al + 2C + \frac{2}{3}Al_2O_3 + MgAl_2O_4$$

$$\rightarrow\ Mg_2SiO_4 + 3SiC + \tfrac{4}{3}Al + C + \tfrac{4}{3}Al_2O_3 +\ MgAl_2O_4 \qquad (5\text{-}4)$$

Again the produced forsterite can be dissociated into enstatite and magnesium oxide and the produced MgO may react with alumina to yield spinel as follow:

$$Mg_2SiO_4 + 3SiC + \frac{4}{3}Al + C + \frac{4}{3}Al_2O_3 +\ MgAl_2O_4$$

$$\rightarrow MgSiO_3 + 3SiC + \tfrac{4}{3}Al + C + \tfrac{1}{3}Al_2O_3 + 2MgAl_{\ 2}O_4 \qquad (5\text{-}5)$$

The last stage is again the decomposition of enstatite to MgO and SiO_2 and the production of SiC and spinel according to the following reactions:

$$MgSiO_3 + 3SiC + \tfrac{4}{3}Al + C + \tfrac{1}{3}Al_2O_3 + 2MgAl_{\ 2}O_4 \rightarrow MgO + 4SiC + Al_2O_3 + 2MgAl_{\ 2}O_4 \qquad (5\text{-}6)$$

$$MgO + 4SiC + Al_2O_3 + 2MgAl_{\ 2}O_4 \rightarrow 3MgAl_{\ 2}O_4 +\ 4SiC \qquad (5\text{-}7)$$

In summary, the general reaction can occur as reaction (8):

$$Mg_3Si_4O_{10}(OH)_2 + 6Al + 4C \rightarrow 3MgAl_2O_4 + 4SiC + H_2(g) \quad (5\text{-}8)$$

With increasing the annealing temperature the above reaction advanced such that for the sample annealed at 1200 ºC only spinel and SiC can be detected in the XRD pattern.

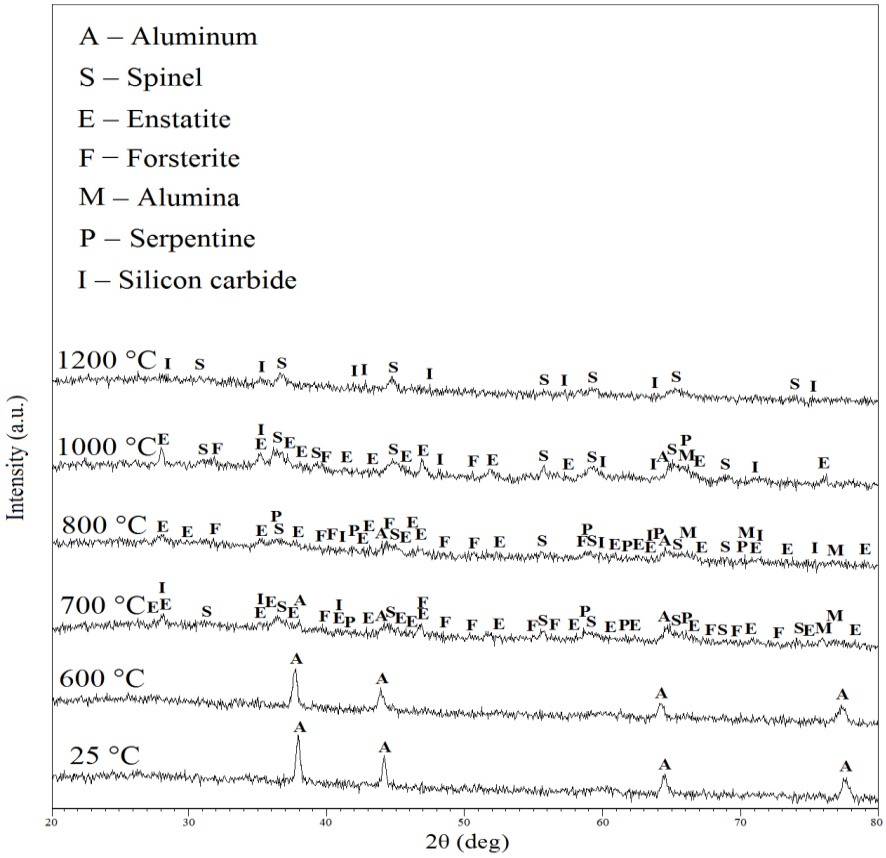

Figure 5.6. XRD patterns of obtained powders after 6h ball milling with subsequent annealing at various temperatures for 1h in a vacuum.

Figure 5.7 shows the XRD patterns of powders milled for various times with subsequent annealing at 1400 ºC for 1h in a vacuum. With increasing the annealing temperature to 1400 ºC for 0h ball milled powder, besides graphite and aluminum, enstatite, alumina and spinel phases can be observed in the

XRD pattern. The characteristic peaks of aluminum and graphite phases were vanished after 1 and 5h ball milling, respectively. It should be noticed that for the sample ball milled for 0h there is a considerable amount of spinel in the XRD pattern while with increasing the ball milling time the fraction intensity of characteristics peaks of spinel decreased and those of alumina increased. Regarding the results obtained from figure 5.5 for those temperatures above 1300 ºC, it seems that with penetration of air into the tube furnace, spinel is decomposed and also the available graphite may react with oxygen to produce CO_2 and hence increases the interior pressure of the tube furnace (figure 5.5). Therefore, another possible reaction that may occur can be described as follows:

$$MgAl_2O_4 + SiC + 2O_2(g) \rightarrow MgSiO_3 + CO_2(g) + Al_2O_3 \quad (5\text{-}9)$$

Hence during the synthesis of SiC/spinel composite, it is crucially important to be aware of the possible environmental factors and practical limitations of equipment that may influence the experimental results.

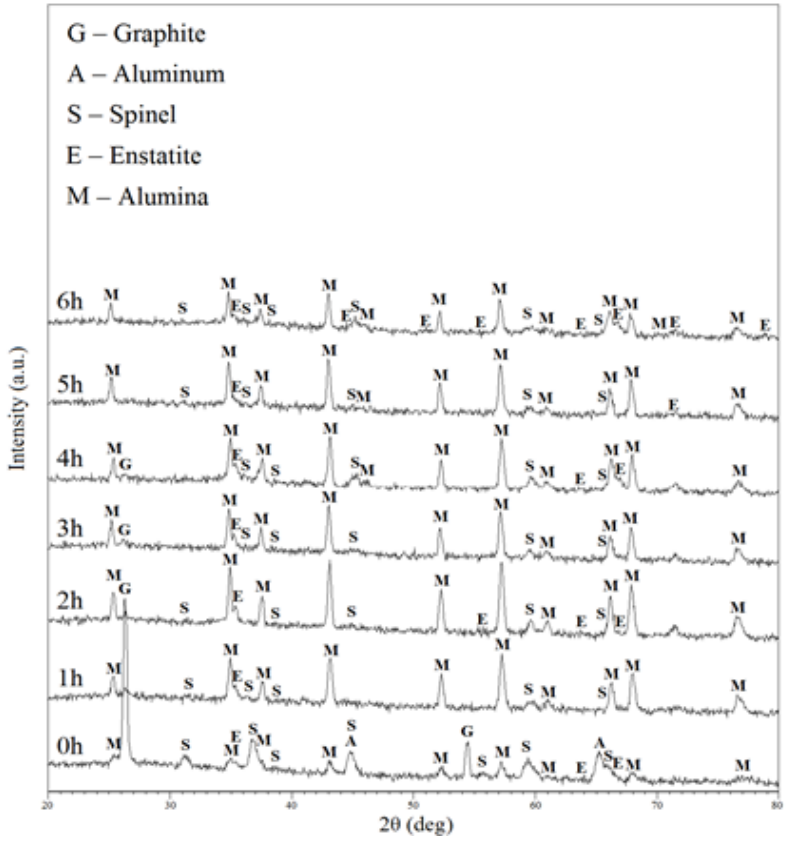

Figure 5.7. XRD patterns of obtained powders after mechanical activation for various periods of time and subsequent annealing at 1400 °C for 1 h in a vacuum.

Figure 5.8 shows the morphology and particle size of prepared SiC/spinel composites after 6 h ball milling time with subsequent annealing at 1200 for 1h in a vacuum. As can be seen, the prepared powder consist of agglomerates in the range of 2 to 35 µm (figure 5.8, see a and b). In higher magnifications it was revealed that each agglomerate consists of very small particles with the mean size of about 12 nm (figure 5.8, see c and d).

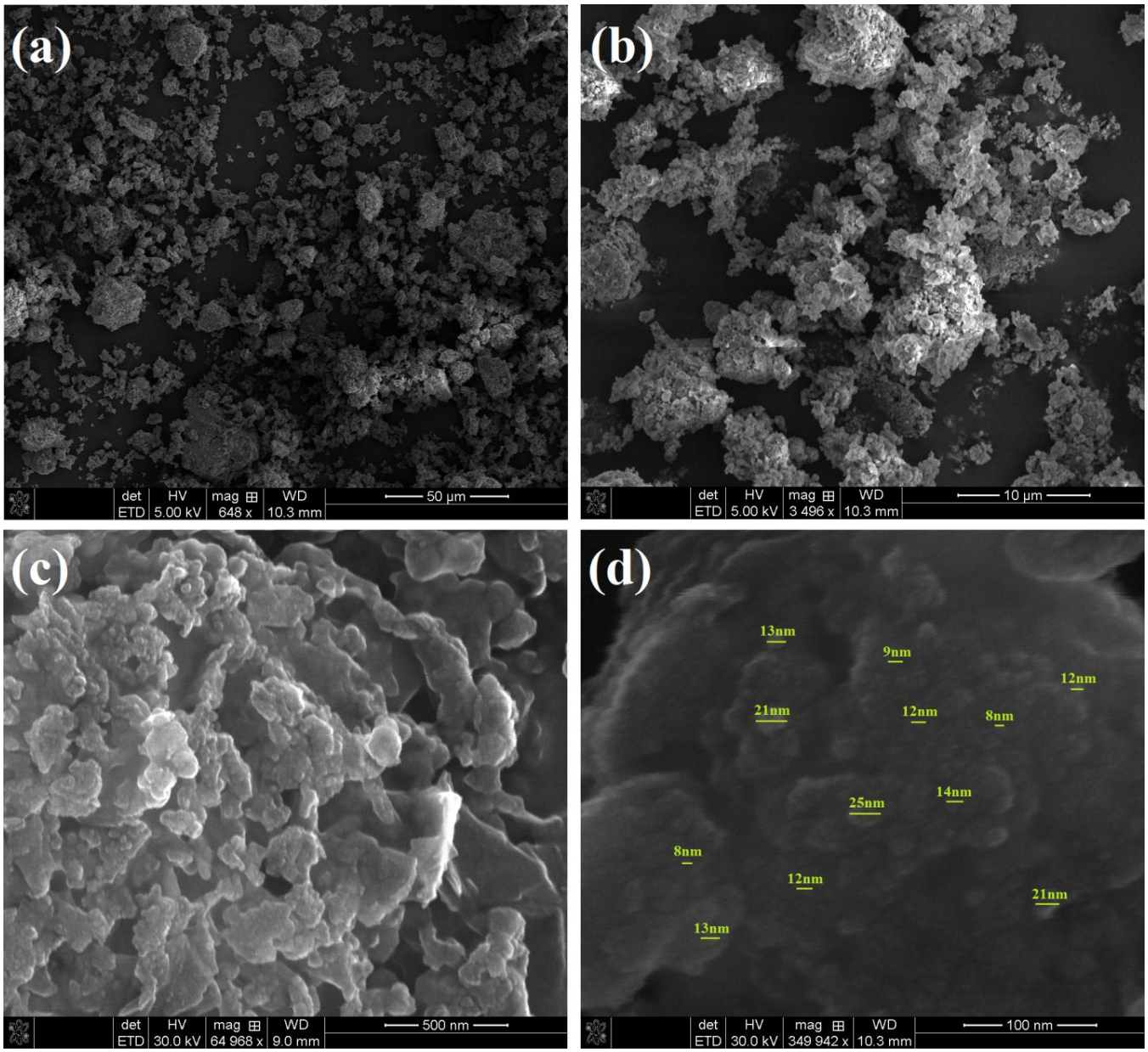

Figure 5.8. SEM micrographs of prepared SiC/spinel nanocomposite after 6h ball milling time with subsequent annealing at 1200 for 1h in a vacuum.

To investigate the morphology and crystallite size of the prepared nanocomposite powder after 6 h of mechanical activation with subsequent annealing at 1200 °C for 1 h in a vacuum, TEM analysis was performed. The results are shown in figure 5.9. As can be seen, the obtained nanocomposite had a particles size in the range of 1 to 15 nm with the mean of about 9 nm. Such a small particle size is crucially important to enhance the mechanical properties of the composite in structural applications.

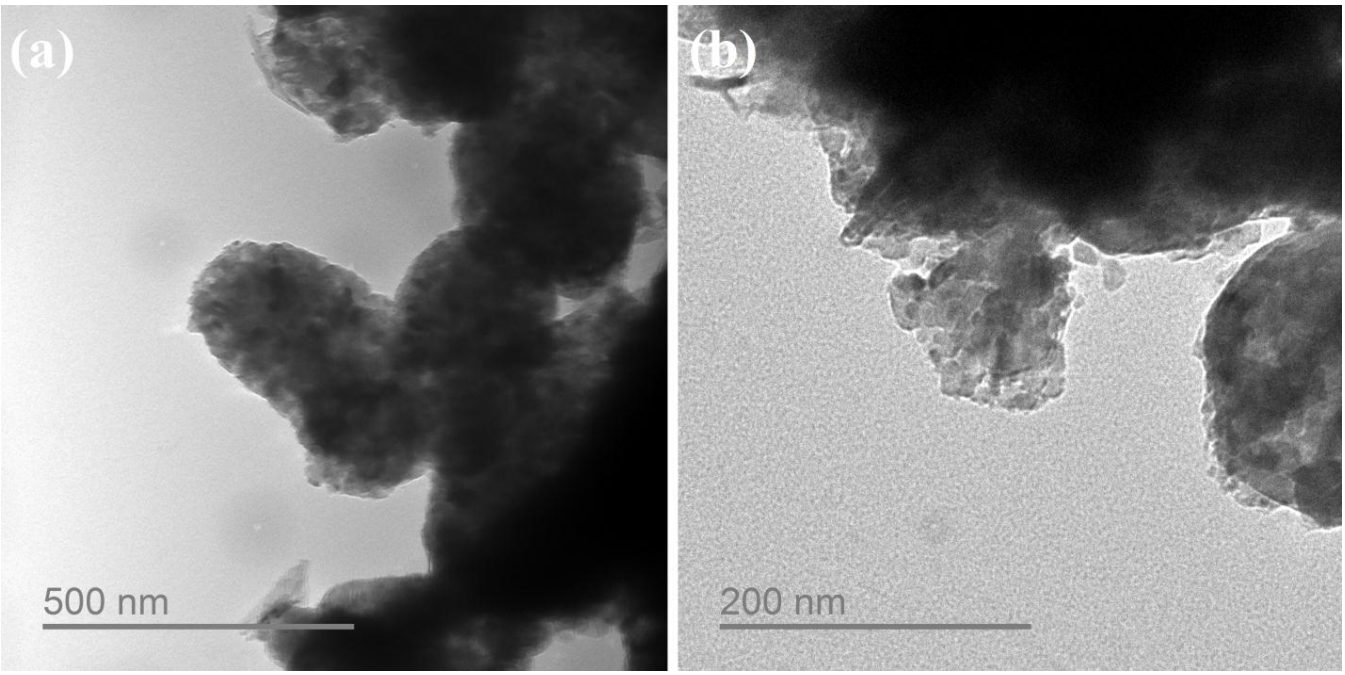

Figure 5.9. TEM micrographs of prepared SiC/spinel nanocomposite obtained from 6h ball milling of the initial powders with subsequent annealing at 1200 °C for 1h in a vacuum.

5.4 Conclusion

Pure SiC/spinel nanostructure powder was successfully produced by 6h of mechanical activation of talc, aluminum and graphite powders with subsequent annealing at 1200 °C for 1 h in a vacuum. Mechanical activation advanced the nanocomposite formation rate through increasing the contact surface area of reacting phases as a consequence of intense reduction of particles size, which is very important in the case of diffusion-controlled reactions. Detailed investigation showed that SiC/spinel was formed through a series of intermediate transition compounds. The mean particle size of the obtained nanocomposite structure was 9 nm according to TEM evaluation. It is believed that this nanocomposite would have self-healing capabilities due to the existence of SiC.

5.5 References

[1] Lange FF. Healing of surface cracks in SiC by oxidation. J Am Ceram Soc 1970;53:290.

[2] Petrovic JJ, Jacobson LA. Controlled surface flaws in hot-pressed SiC. J Am Ceram Soc 1976;59:34–7.

[3] Gulbransen EA, Jansson SA. High-temperature oxidation, reduction and volatilization reactions of silicon and silicon carbide. Oxid Metals 1972;4:181-201.

[4] McLean AF, Fisher EA, Bratton RJ. Brittle materials design, high temperature gas turbine. Tech Rept AMMRC CTR 1973;73:169-210.

[5] Korouš J, Chu MC, Nakatani M, Ando K. Crack healing behavior of silicon carbide ceramics. J Am Ceram Soc 2000;83:2788–92.

[6] Kim HW, Kim HE, Song H, Ha J. Effect of oxidation on the room-temperature flexural strength of reaction-bonded silicon carbides. J Am Ceram Soc 1999;82:1601–4.

[7] Mohapatra D, Sarkar D. Effect of in situ spinel seeding on synthesis of MgO-rich $MgAl_2O_4$ composite. J Mater Sci 2007;42:7286-93.

[8] Stubičar N, Tonejc A, Stubičar M. Microstructural evolution of some MgO–TiO_2 and MgO–Al_2O_3 powder mixtures during high-energy ball milling and post-annealing studied by X-ray diffraction. J Alloys Compd 2004;370:296-301.

[9] Gledhill AD, Li D, Mroz T, Goldman LM, Padture NP. Strengthening of transparent spinel/Si_3N_4 nanocomposites. Acta Mater 2012;60:1570-5.

[10] Tavangarian F, Emadi R. Synthesis and characterization of pure nanocrystalline magnesium aluminate spinel powder. J Alloys Compd 2010;489:600-4.

[11] Sarkar R, Das SK, Banerjee G. Effect of attritor milling on the densification of magnesium aluminate spinel. Ceram Int 1999;25:485-9.

[12] Ganesh I, Bhattacharjee S, Saha BP, Johnson R, Mahajan YR. A new sintering aid for magnesium aluminate spinel. Ceram Int 2001;27:773-9.

[13] Lee SK, Takahashi K, Yokouchi M, Suenaga H, Ando K. High temperature fatigue strength of crack-healed Al_2O_3 toughened by SiC whiskers. J Am Ceram Soc 2004;87:1259-64.

[14] Mohanty D, Sil A, Maiti K. Development of input output relationships for self-healing Al_2O_3/SiC ceramic composites with Y_2O_3 additive using design of experiments. Ceram Int 2011;37:1985-92.

[15] Ono M, Nakao W, Takahashi K, Nakatani M, Ando K. A new methodology to guarantee the structural integrity of Al_2O_3/SiC composite using crack healing and a proof test. Fatigue Fract Eng M 2007;30:599-607.

[16] Chlup Z, Flasar P, Ando K, Dlouhy I. Fracture behaviour of Al_2O_3/SiC nanocomposite ceramics after crack healing treatment. J Eur Ceram Soc 2008:28:1073-7.

[17] Nakao W, Ono M, Lee S, Takahashi K, K Ando. Critical crack-healing condition for SiC whisker reinforced alumina under stress. J Eur Ceram Soc 2005;25:3649-55.

[18] Zuo X, Zhang L, Liu Y, Cheng L, Xia Y. Oxidation behaviour of two-dimensional C/SiC modified with self-healing Si–B–C coating in static air. Corros Sci 2012;65:87-93.

[19] Lee S, Ono M, Nakao W, Takahashi K, Ando K. Crack-healing behaviour of mullite/SiC/Y_2O_3 composites and its application to the structural integrity of machined components. J Eur Ceram Soc 2005;25:3495-502.

[20] Tavangarian F, Emadi R. Mechanochemical synthesis of nanocrystalline forsterite powder. Int J Mod Phys B 2010;24:343-50.

[21] Tavangarian F, Emadi R. Effects of mechanical activation and chlorine ion on nanoparticle forsterite formation. Mater Lett 2011;65:126-9.

[22] Carter RE, Mechanism of Solid-state Reaction Between Magnesium Oxide and Aluminum Oxide and Between Magnesium Oxide and Ferric Oxide. J Am Ceram Soc 1961;44:116-20.

CHAPTER 6 SINTERING BEHAVIOR, MICROSTRUCTURE AND MECHANICAL PROPERTIES OF VACUUM SINTERED SIC/SPINEL NANOCOMPOSITE[1]

6.1 Introduction

Nanocrystalline materials with an average crystalline size of a few nanometers present unique properties including increased strength, high hardness, extremely high diffusion rates, and consequently reduced sintering times in comparison to the conventional coarse grain materials [1–6].

Magnesium aluminate spinel ($MgAl_2O_4$) is one of the most attractive materials in the field of ceramics engineering. Spinel shows good refractoriness, with a melting point of 2135 °C, low thermal expansion, high thermal shock resistance, high chemical stability and high strength even at high temperatures [7]. Its unique properties make it an ideal candidate for structural, refractory, optical, electrical and ceramic industries [8-10].

Nevertheless, there are some limitations from production and application point of views. The formation of spinel is accompanied with 5-8% volume expansion and therefore it is too difficult to produce dense spinel bodies through one step sintering [11,12]. Furthermore, the brittleness of spinel, which translates to easier microcracking, is another limiting factor in utilizing this material in industry [9,10].

In order to solve the first problem (volume expansion), spinel should be completely obtained from the calcination of the initial materials at high temperature to eliminate the volume expansion and then the obtained spinel should be formed to a desired shape and sintered at elevated temperature [13,14].

To overcome the second problem (microcracking), one way is to incorporate some self-healing agents in the base matrix (spinel). SiC is one of the most effective self-healing fillers which is used in various ceramics composites [15-20]. It is proved that in the presence of a crack, SiC can react with oxygen at high temperature to form SiO_2 and heal the crack [21-27]. Also it is reported that utilizing SiC in various ceramic composites such as SiC/Al_2O_3 [28] and SiC/ZrB_2 [29] can increase the strength of the composite even before sintering the prepared specimens in air and consequently before transformation of SiC to SiO_2. Hence it should be a good idea to evaluate the mechanical behavior of SiC/spinel nanocomposite in pristine condition without any healing in the structure.

In the present work, the sintering behavior, microstructure changes and mechanical and physical properties of SiC/spinel pellets were studied at various temperatures for different holding times. Furthermore, the phase transformation and mechanisms involved in the sintering process were investigated as well.

[1]This chapter previously appeared as Guoiqang Li, Fariborz Tavangarian, Sintering behavior, microstructure, and mechanical properties of vacuum sintered SiC/spinel nanocomposite, *Journal of Alloys and Compounds*, December, 2014. It is reprinted by permission of Elsevier (see the permission letter in Appendix A).

6.2 Experimental procedures

The preparation of SiC/spinel nanocomposite was carried out as described in chapter 5. Briefly, a proper amount of talc, aluminum and graphite were ball milled for 6 h in argon gas (to obtain stoichiometric $MgAl_2O_4$ containing 27.26 wt.% SiC) and then annealed at 1200 °C for 1h in a vacuum with the heating/cooling rate of 10 °C/min. The produced powder was uniaxially pressed into pellets in a hardened steel mold at a pressure of 200 MPa using 10 wt.% glycerol as a binder. The pellets were annealed from 1000 to 1500 °C for 1, 5, and 10h holding time in a vacuum. The phase transformation were investigated by X-ray diffractometry (MiniFlex XRD, Rigaku Corporation, Japan) with Cu Kα radiation (λ= 0.154178 nm). The XRD patterns were recorded in the 2θ range of 20–80° (step size of 0.05° and time per step of 1 s). The morphology of the prepared samples was studied by field emission scanning electron microscopy (Quanta3D FEG, FEI Company, USA) at an acceleration voltage of 30 kV. Energy-dispersive X-ray spectrometer (EDS) was used to study the surface chemistry of the obtained specimens. The transmission electron microscopy (TEM; JEM-1400) technique was utilized to characterize the morphology and the structure of the prepared samples. Nano-indentation tests were conducted using the Hysitron TI-900 Triboindenter (Minneapolis, USA) with a Berkovich tip to determine the hardness of the pellets. Cold crushing strength (CCS) was performed at room temperature using a Hydraulic Universal Testing Machine (Instron Model 5696, Canton, MA) at a rate of 0.5 mm/min. The bulk density (BD) of the sintered pellets was measured according to Archimedes principle [30]. For each experiment three samples were used.

6.3 Results and discussions

The XRD pattern and morphology of SiC/spinel nanocomposite powder are shown in figure 6.1 parts a and b.

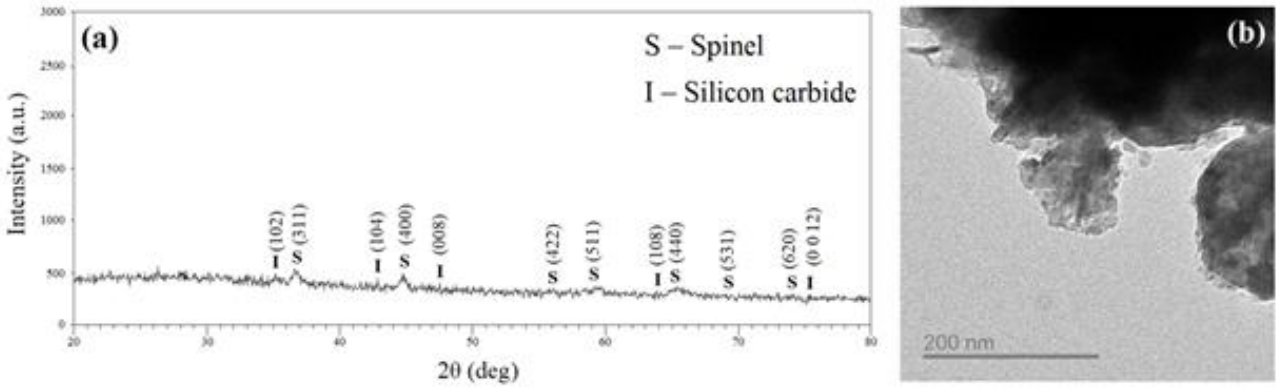

Figure 6.1. (a) XRD pattern and (b) TEM micrograph of obtained SiC/spinel nanocomposite powder after ball milling of talc, aluminum and graphite powders for 6h in argon gas with subsequent annealing at 1200 °C for 1h in a vacuum. Reprinted with the permission from [31].

All the XRD peaks correspond to the characteristic peaks of spinel and SiC structures. As can be seen in figure 6.1 part b, the obtained SiC/spinel powder had a crystallite size below 100nm [30]. Table 6.1 and figure 6.2 show the designation and the changes of the inside vacuum pressure of the tube furnace for various specimens as the temperature of the furnace increased with the heating rate of 10 °C/min. Also figure 6.2 shows the vacuum changes in the presence of 0.2 g glycerol. As soon as the inside pressure of the tube furnace reached 70 mTorr, the furnace was turned on and the vacuum pressure was monitored. Moreover, in order to make sure that the vacuum pressure changes are as a result of the specimens and not the tube, seals, vacuum flanges, valves and thermal blocks in the furnace, the same experiments was carried out exactly in the same condition in the absence of any sample (control experiment). As can be seen in the control experiment, there is a negligible increase in the vacuum pressure from 235 °C to 476 °C from 61 to 81 mTorr; however, for those temperatures higher than 1220 °C, the vacuum pressure increased rapidly. Hence air could penetrate into the tube furnace and react with specimens. In the presence of 0.2 g glycerol, with increasing the temperature, the vacuum pressure showed a quick increase and decrease due to the evaporation of glycerol up to 245 °C. On the other hand, in the pressed pellets without any glycerol, a gradual increase and decrease was observed. Finally, in the presence of 2 g pellets containing 10 wt.% glycerol, a continuous evaporation of volatile materials can be detected up to around 985 °C. This can be assigned to the gradual release of hydrated water and glycyrol from the structure [30]. In the pressed samples containing glycerol, glycerol is trapped inside the structure and needs to penetrate through open spaces and open channels to reach the free surfaces and hence it shows a continuous release of glycerol with increasing the temperature. Furthermore, there is a rapid increase in the vacuum pressure around 1300 °C. Considering the vacuum loss observed in control experiment, it can be concluded that some reactions may happen above 1300 °C and change the structure.

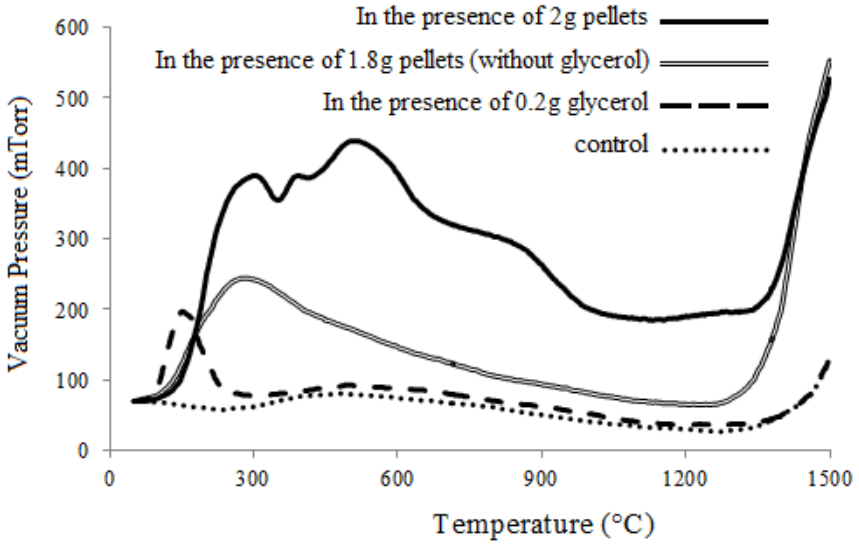

Figure 6.2. Vacuum pressure changes in the tube furnace with increasing the temperature for different samples.

Table 6.1. Designation, sintering temperature and holding time of SiC/spinel pellets.

Designation	Sintering temperature (°C)	Holding time (h)
A1	1000	1
A5	1000	5
A10	1000	10
B1	1100	1
B5	1100	5
B10	1100	10
C1	1200	1
C5	1200	5
C10	1200	10
D1	1300	1
D5	1300	5
D10	1300	10
E1	1400	1
E5	1400	5
E10	1400	10
F1	1500	1
F5	1500	5
F10	1500	10

Figure 6.3 shows the XRD patterns of sintered pellets at various times and temperatures. The XRD patterns of those samples sintered below 1300 °C (A1 to C10) correspond to spinel (XRD JCPDS data file No. 01-1154) and SiC (XRD JCPDS data file No. 03-1146) phases. No other phases were observed in those patterns. On the other hand, in those specimens sintered at temperatures higher than 1300 °C (D1 to F10) new phases were observed. As can be seen in figure 6.3, with increasing either the time or temperature of sintering, spinel dissociated into other phases. The first two secondary phases which can be observed in D1 are alumina (Al_2O_3) (XRD JCPDS data file No. 10-0173) and magnesia (MgO) (XRD JCPDS data file No. 43-1022). Therefore, the initial reaction that may occur during the decomposition of spinel may be expressed as follows:

$$MgAl_2O_4 \rightarrow Al_2O_3 + MgO \quad (6\text{-}1)$$

With increasing the holding time at 1300 °C to 5 h (D5), the intensity of peaks corresponding to spinel phase decreased while those correspond to alumina phase increased. In addition, new phases such as enstatite ($MgSiO_3$) (XRD JCPDS data file No. 03-0696) and forsterite (Mg_2SiO_4) (XRD JCPDS data file

No. 03-1117) were revealed in the XRD pattern. On the other hand, as it is shown in figure 6.2, at those temperatures above 1300 °C, due to the partial loss of vacuum and penetration of air into the system, SiC can react with oxygen and form SiO_2. Therefore, the next reaction may be expressed as the reaction between MgO and SiO_2. It is illustrated that MgO can initially react at the surface of SiO_2 to form enstatite, then the diffusion of MgO through the enstatite layer can start forming forsterite phase [32 - 35]. Hence, the following reactions may occur during the sintering of the samples at high temperature:

$$MgO + SiO_2 \rightarrow MgSiO_3 \quad (6\text{-}2)$$

$$MgSiO_3 + MgO \rightarrow Mg_2SiO_4 \quad (6\text{-}3)$$

On the other hand, alumina could react with SiO_2 to produce sillimanite (Al_2SiO_5) (XRD JCPDS data file No. 01-0626) according to the following reaction:

$$Al_2O_3 + SiO_2 \rightarrow Al_2SiO_5 \quad (6\text{-}4)$$

With increasing the holding time up to 10 hours (D10) amesite ($Al_2H_4Mg_2O_9Si$) (XRD JCPDS data file No. 02-0110) phase was also detected in the x-ray diffraction pattern. Hence the next reaction which may occur during the sintering of specimens can be expressed as the reaction of sillimanite with MgO as follows:

$$Al_2SiO_5 + 2MgO \rightarrow Al_2Mg_2SiO_7 \quad (6\text{-}5)$$

However it is more probable that firstly one mole sillimanite reacts with one mole MgO to form Al_2MgSiO_6 and then the product reacts with another mole MgO to form $Al_2Mg_2SiO_7$. The same reactions occurred for those samples sintered at higher temperatures for various holding times. Decomposition of spinel, release of carbon from silicon carbide, and the formation of new phases may have detrimental effect on the strength and hardness of the specimens.

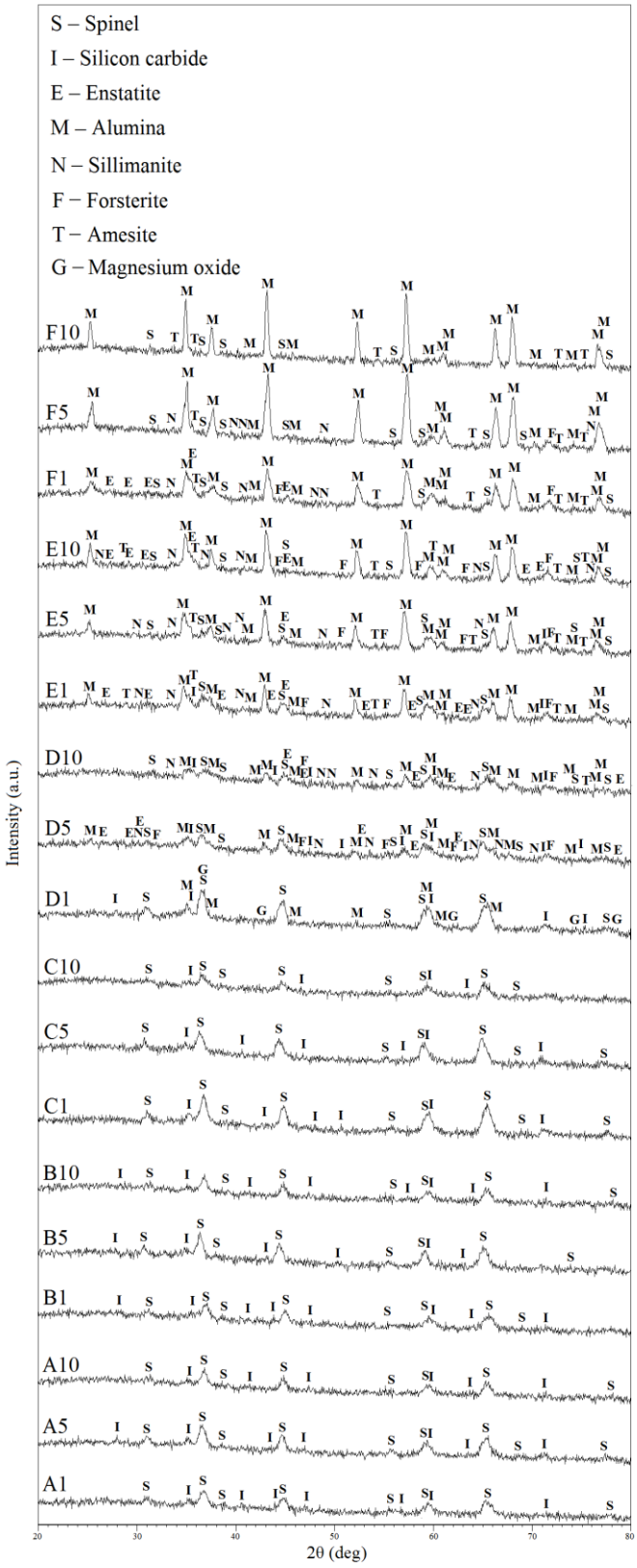

Figure 6.3. XRD patterns of SiC/spinel sintered pellets at various times and temperatures.

Figure 6.4 shows the hardness of the sintered pellets at various times and temperatures. As can be seen, the hardness of those samples sintered at temperatures higher than 1300 °C is very low. This can be ascribed to the release of carbon from the SiC/spinel nanocomposites, decomposition of spinel and formation of new phases such as sillimanite and amesite. The maximum hardness was obtained for C1 which is equal to 1.6 GPa. As can be seen in figure 6.4, at 1200 °C the hardness decreases with increasing the holding time, probably as a result of the grain growth and release of volatile materials. With increasing the holding time for those samples sintered at 1000°C, the hardness increased from 1h to 5h holding time and then decreased from 5h to 10 h holding time. The same trend was observed for samples at 1100 °C. The increase may be assigned to the release of residual stresses and sintering phenomenon while the decrease in the strength could be due to the partial release of carbon and volatile materials which is in agreement with the results obtained from figure 6.2. Also with increasing the annealing temperature for samples with 1h holding time the hardness increased from 77 to 1600 MPa, probably due to the relaxation of the residual stress and sintering phenomena. However with increasing the sintering temperature for those samples with holding time of 5 and 10 h, no significant changes was observed.

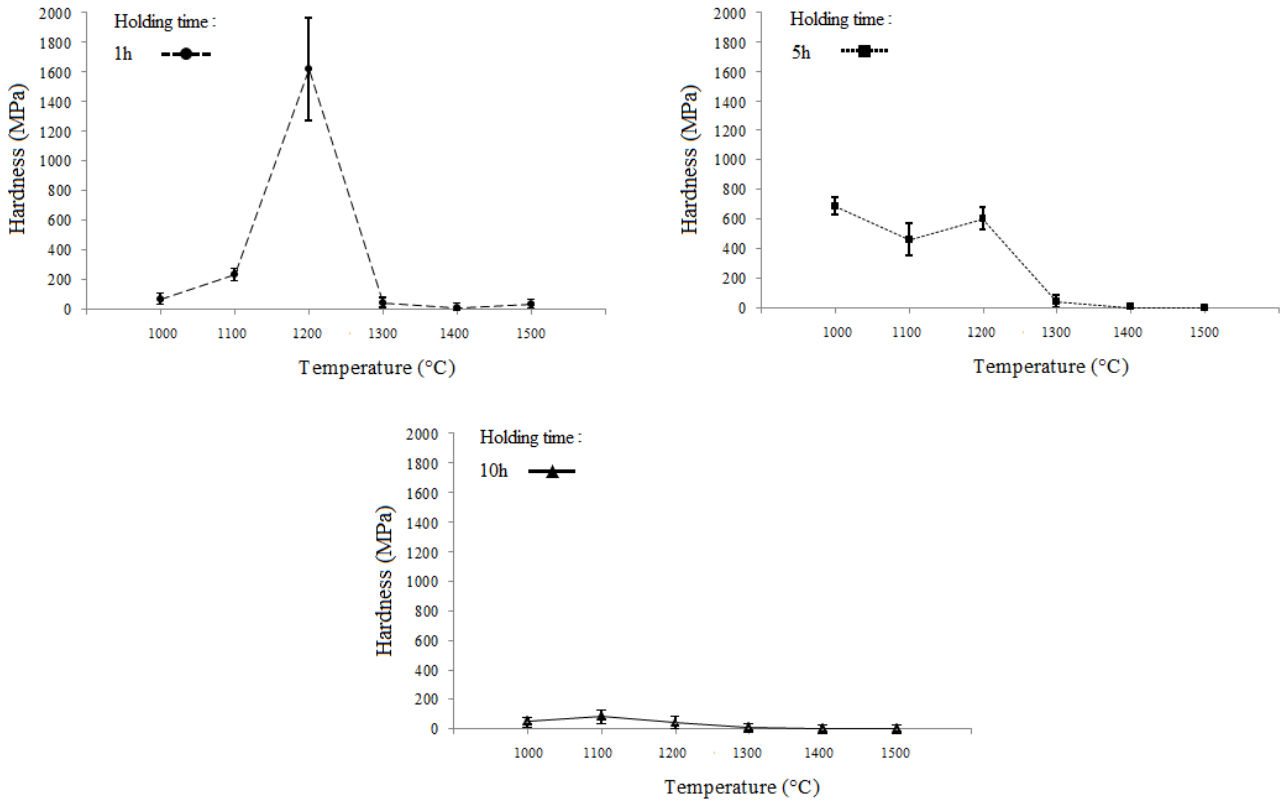

Figure 6.4. Hardness of SiC/spinel sintered pellets at various times and temperatures.

The BD of the prepared specimens is shown in figure 6.5. The highest BD was obtained for A10 which is due to the higher maintaining time at high temperature and subsequently better sintering of the pellets. Sintering is an agglomeration process in which the discrete particles coalescence at high temperature and produce a bulk mass. During the sintering process, the fraction of pores decreased and a more dense structure forms and subsequently increases the BD [36]. On the other hand, the lowest BD obtained for D10 may be due to the longer annealing time at high temperature and the release of more volatile materials which leave more pores in the specimens. The strength of some samples was so low that it was impossible to measure the BD by Archimedes principle. There are at least two parameters that may describe the BD behavior of various specimens. First, the sintering of small pores through the diffusional process which can increase BD and second, chemical reaction and evaporation of volatile materials that leave pores in the sintered samples and subsequently decrease the BD [37,38]. Therefore, the diagram does not show a uniform behavior for different samples due to the different percentage of incorporation of these two phenomena.

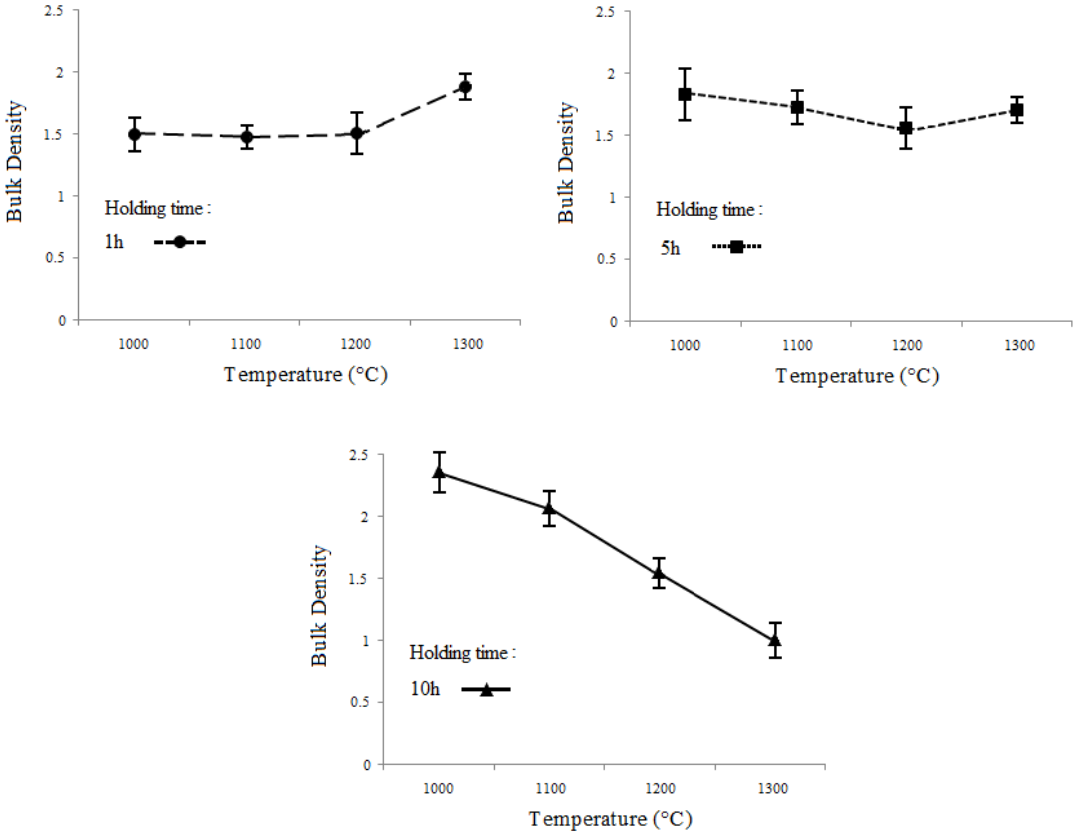

Figure 6.5. Bulk Density of SiC/spinel sintered pellets at various times and temperatures.

The results of cold crushing strength test are depicted in figure 6.6. D1 showed the maximum CCS equal to 129 MPa; However, due to the phase transformations occurred at those specimens sintered above 1300 °C, they cannot be considered as SiC/spinel nanocomposite. Among those samples with higher hardness (pellets sintered at temperatures lower than 1300 °C), the hardness of C1 was significantly higher than the other specimens. Also the CCS of C1 is 118 MPa which is almost comparable to the highest strength obtained for various pellets. Consequently, considering the results obtained from hardness, BD and CCS, C1 was selected as the best samples for further investigations.

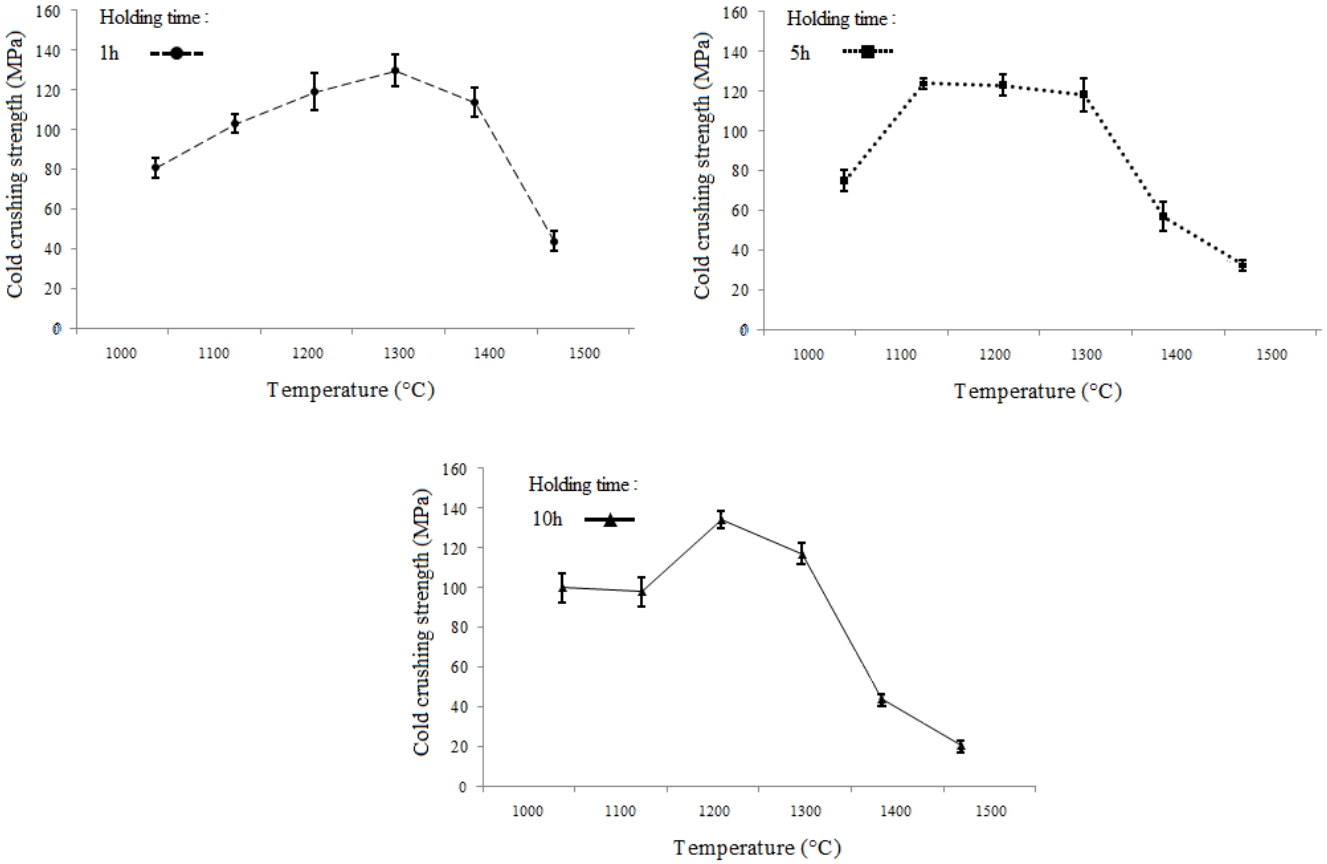

Figure 6.6. Cold crushing strength of sintered pelletes at various temperatures and times.

Figure 6.7 shows the SEM micrographs of the obtained samples after sintering at 1000 °C for various times in a vacuum. As can be seen in figure 6.7 parts a and b, for samples sintered at 1000 °C for 1h two different morphologies appeared. Some particles had a spherical shape (figure 6.7, see a) while some others had a flake shape and hence due to this non homogeneities the structure is more porous and it has many open spaces. With increasing the holding time to 5h at 1000 °C, the flake-shape particles decreased, the structure is more compact and low porosity can be seen due to the better reaction of

materials at longer holding time (figure 6.7, see c and d). After sintering of the bodies for 10h at 1000 °C, almost no flak-shape particles can be observed and the structure is well compacted. The SEM micrographs showed that the particles size of all samples is well below 100 nm.

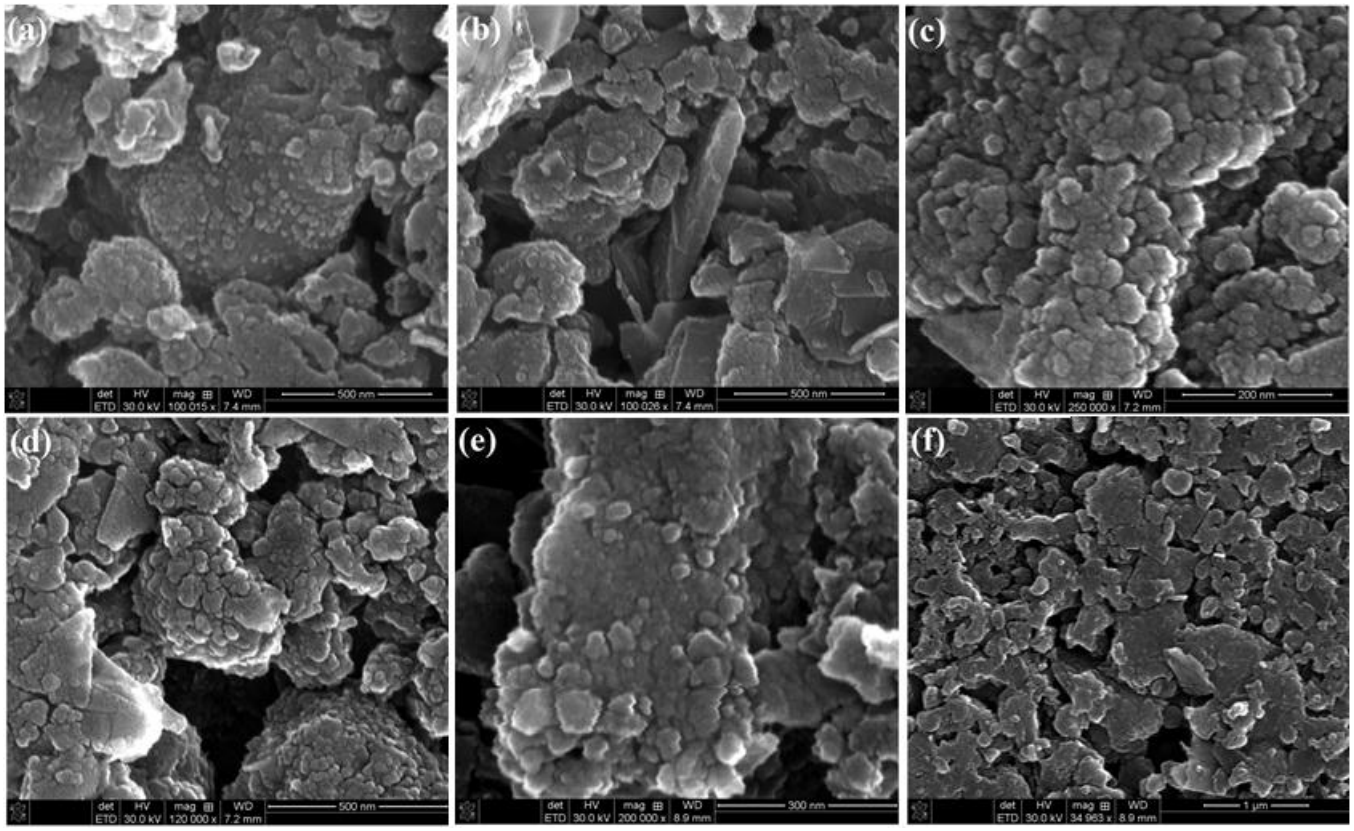

Figure 6.7. SEM micrographs of prepared SiC/spinel pellets sintered at 1000 °C for (a) and (b) 1h, (c) and (d) 5h, (e) and (f) 10 holding time in a vacuum.

Figures 6.8 and 6.9 show the SEM micrographs and EDS analyses of the obtained sample after sintering at 1200 °C for 1h in a vacuum, respectively. As can be seen, the surface of the pellets consists of two different morphologies: spherical and columnar structure. The EDS analysis confirmed that the weight percentage of different elements is almost near the stoichiometric value of SiC and spinel structures. Also due to the different morphology and higher sintering temperature, the obtained bodies are more compact as compared to those samples obtained at 1000 °C.

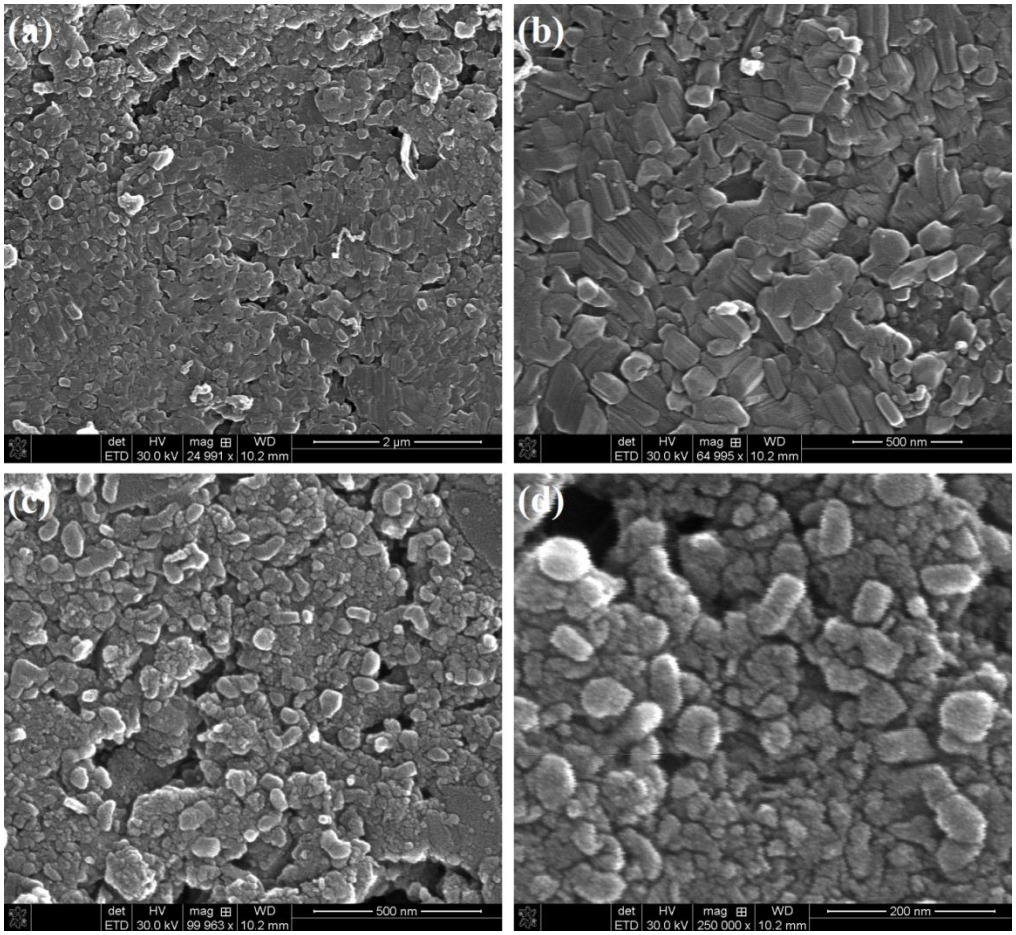

Figure 6.8. SEM micrographs of prepared SiC/spinel pellets sintered at 1200 °C for 1h in a vacuum.

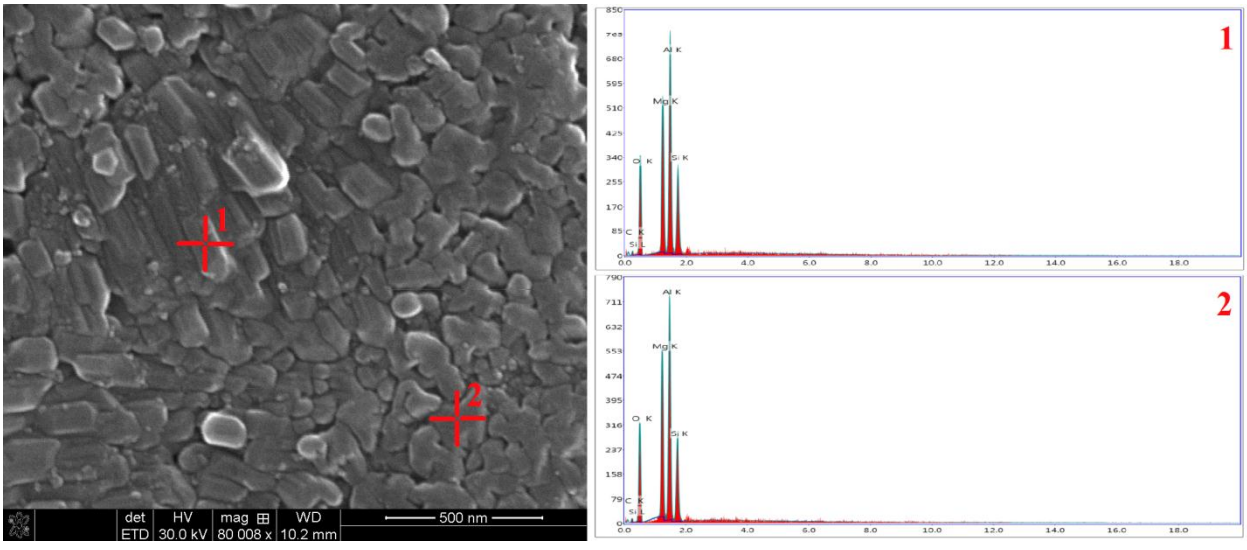

Figure 6.9. EDS analysis of prepared SiC/spinel pellets sintered at 1200 °C for 1h in a vacuum.

The particle size and morphology of some powders which was separated from C1 are shown in figure 6.10. Image analysis method was used to measure the particle size. The particle size of C1 was in the range of 14 and 70 nm with mean of 34 nm which proved the formation of nanocomposite structure.

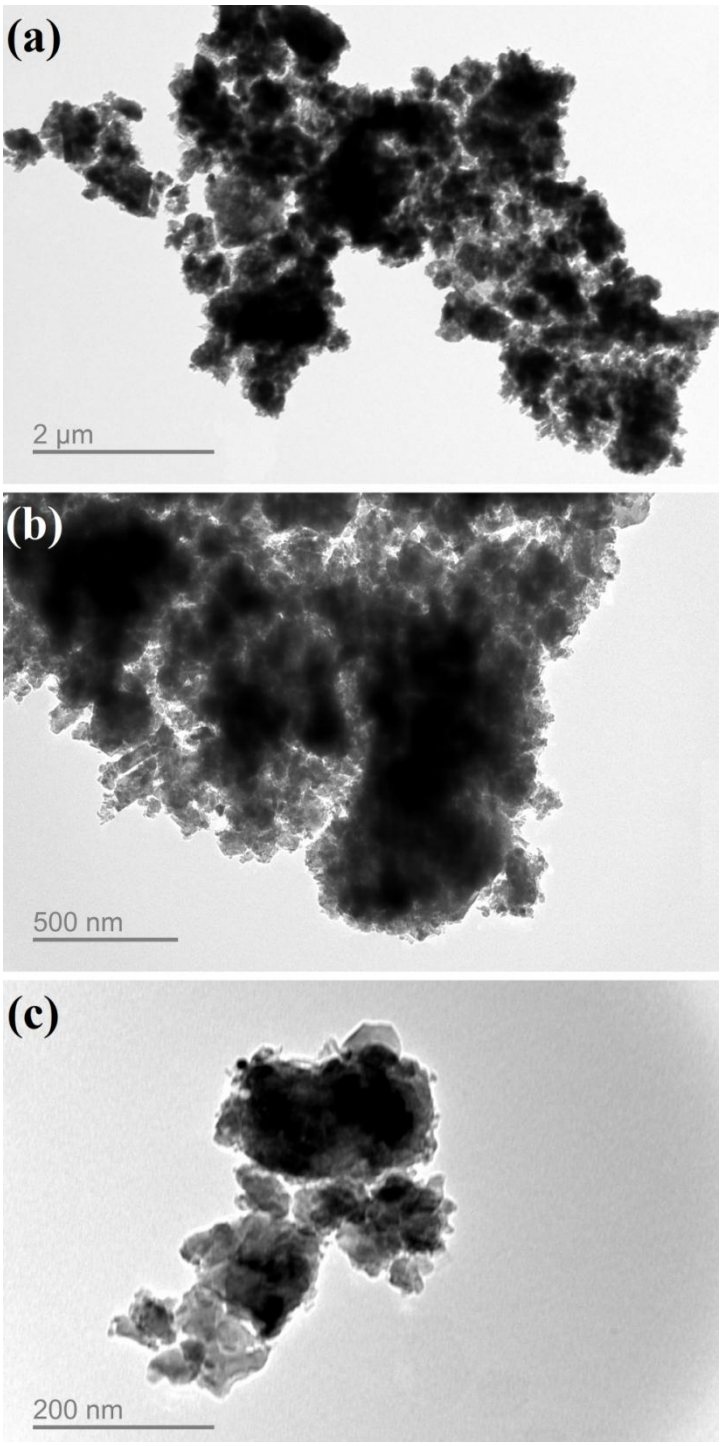

Figure 6.10. TEM micrograph of prepared SiC/spinel pellets sintered at 1200 °C for 1h in a vacuum.

6.4 Conclusion

This chapter reports the successful synthesis of bulk SiC/spinel nanocomposites from talc, aluminum and graphite powders. The influences of sintering times and temperature on the mechanical and physical properties and the microstructure characteristics of the SiC/spinel nanocomposites were studied. The mean grain size, hardness and cold crushing strength of the produced bulk SiC/spinel nanostructure, obtained after the sintering of green samples at 1200 °C for 1h, were 34 nm, 1.6 GPa and 118 MPa, respectively. Those samples that were sintered at temperatures higher than 1300 °C decomposed to different phases, with very low strength and hence were not suitable for further investigation.

6.5 References

[1] Tavangarian F, Emadi R. Synthesis and characterization of spinel-forsterite nanocomposites. Ceram Int 2011;37:2543-8.

[2] Emadi R, Tavangarian F, Esfahani SIR. Nanostructured Forsterite Coating Strengthens Porous Hydroxyapatite for Bone Tissue Engineering. J Am Ceram Soc 2010;93:2679-83.

[3] Tavangarian F, Li Y. Carbon nanostructures as nerve scaffolds for repairing large gaps in severed nerves. Ceram Int 2012;38:6075-90.

[4] Mirhadi SM, Tavangarian F, Emadi R. Synthesis, characterization and formation mechanism of single-phase nanostructure bredigite powder. Mater Sci Eng C 2012;32:133-9.

[5] Tavangarian F, Emadi R. Improving degradation rate and apatite formation ability of nanostructure forsterite. Ceram Int 2011;37:2275-80.

[6] Tavangarian F, Emadi R. Nanostructure effects on the bioactivity of forsterite bioceramic. Mater Lett 2011;65:740-3.

[7] Mohapatra D, Sarkar D. Effect of in situ spinel seeding on synthesis of MgO-rich MgAl2O4 composite. J Mater Sci 2007;42:7286-93.

[8] Stubičar N, Tonejc A, Stubičar M. Microstructural evolution of some MgO–TiO2 and MgO–Al_2O_3 powder mixtures during high-energy ball milling and post-annealing studied by X-ray diffraction. J Alloys Compd 2004;370:296-301.

[9] Gledhill AD, Li D, Mroz T, Goldman LM, Padture NP. Strengthening of transparent spinel/Si3N4 nanocomposites. Acta Mater 2012;60:1570-5.

[10] Tavangarian F, Emadi R. Synthesis and characterization of pure nanocrystalline magnesium aluminate spinel powder. J Alloys Compd 2010;489:600-4.

[11] Sarkar R, Das SK, Banerjee G. Effect of attritor milling on the densification of magnesium aluminate spinel. Ceram Int 1999;25:485-9.

[12] Ganesh I, Bhattacharjee S, Saha BP, Johnson R, Mahajan YR. A new sintering aid for magnesium aluminate spinel. Ceram Int 2001;27:773-9.

[13] Nakagawa ZE, Enomoto N, Yi IS, Asano K. Effect of corundum/ periclase sizes on the expansion behavior during synthesis of spinel. Proc Unitecer, 1995, Congress, Tokyo, 1995, 379–86.

[14] Baitley JT, Russel R. Sintered spinel ceramics. Presented at the 69th Annual Meeting of the American Ceramic Society, New York, 3 May 1967.

[15] Ando K, Furusawa K, Takahashi K, Sato S. Crack-healing ability of structural ceramics and a new methodology to guarantee the structural integrity using the ability and proof-test. J Eur Soc 2005;25:549–58.

[16] Ando K, Chu MC, Tsuji K, Hirasawa T, Kobayashi Y, Sato S. Crack healing behavior and high-temperature strength of mullite/SiC composite ceramics. J Eur Soc 2002;22:1313–9.

[17] Ando K, Kim BS, Chu MC, Saito S, Takahashi K. Crack-healing and mechanical behavior of Al_2O_3/SiC composites at elevated temperature. Fatigue Frac Eng M 2004;27:533–41.

[18] Lee SK, Ishida W, Lee SY, Nam KW, Ando K. Crack-healing behavior of mullite/SiC/Y_2O_3 composites and its application to the structural integrity of machined components. J Eur Soc 2005;25:3495–502.

[19] Houjou K, Ando K, Liu SP, Sato S. Crack-healing and oxidation behavior of silicon nitride ceramics. J Eur Ceram Soc 2004;24:2329–38.

[20] Takahashi K, Kim BS, Chu MC, Sato S, Ando K. Crack-healing behavior and static fatigue strength of Si_3N_4/SiC ceramics held under stress at temperature (800, 900 and 1000 ◦C). J Eur Ceram Soc 2003;23:1971–8.

[21] Petrovic JJ, Jacobson LA. Controlled surface flaws in hot-pressed SiC. J Am Ceram Soc. 1976;59:34–7.

[22] Gulbransen EA, Jansson SA. High-temperature oxidation, reduction and volatilization reactions of silicon and silicon carbide. Oxid Metals 1972;4:181-201.

[23] McLean AF, EA Fisher, Bratton RJ, Brittle materials design, high temperature gas turbine. Tech Rept AMMRC CTR 1973;73:169-210.

[24] Ando K, Sato S, Kobayashi Y, Chu MC. Crack healing behaviour of Si_3N_4 ceramics and its application to structural integrity– in Fracture from Defects, EFC-12. Edited by M. W. Brown, E. R de los Rios, and K. J. Miller. Engineering Materials Advisory Services, Sheffield, U.K., 1998, pp. 497.

[25] Korouš J, Chu MC, Nakatani M, Ando K. Crack healing behavior of silicon carbide ceramics. J Am Ceram Soc 2000;83:2788–92.

[26] Kim HW, Kim HE, Song H, Ha J. Effect of oxidation on the room-temperature flexural strength of reaction-bonded silicon carbides. J Am Ceram Soc 1999;82:1601–4.

[27] Kim YW, Ando K, Chu MC. Crack-healing behavior of liquid-phase-sintered silicon carbide ceramics. J Am Ceram Soc 2002;86:465–70 .

[28] Chou IA, Chan HM, Harmer MP. Effect of annealing environment on the crack healing and mechanical behavior of silicon carbide-reinforced alumina nanocomposites. J Am Ceram Soc 1998;81:203-8.

[29] Houjou K, Ando K, Liu SP, Sato S. Crack-healing and oxidation behavior of silicon nitride ceramics. J Eur Ceram Soc 2004;24:2329-38.

[30] Engin O, Tas AC. Manufacture of macroporous calcium hydroxyapatite bioceramics. J Eur Ceram Soc 1999;19:2569-72.

[31] Tavangarian F, Li G. Synthesis, characterization and formation mechanism of SiC/spinel nanocomposite. J Alloy Compd 2014;598:106–12.

[32] Brindley GW, Hayami R. Kinetics and mechanism of formation of. forsterite (Mg_2SiO_4) by Solid State Reaction of MgO and SiO_2. Philos Mag Lett 1965:12:505–14.

[33] Tavangarian F, Emadi R. Effects of mechanical activation and chlorine ion on nanoparticle forsterite formation. Mater Lett 2011;65:126–9.

[34] Tavangarian F, Emadi R. Effects of fluorine ion and mechanical activation on nanostructure forsterite formation mechanism. Powder Technol 2010;203:180–6.

[35] Tavangarian F, Emadi R. Mechanochemical synthesis of single phase nanocrystalline forsterite powder. Int J Mod Phys B 2010;24:343-350.

[36] Angappan S, Berchmans LJ, Augustin CO. Sintering behaviour of $MgAl_2O_4$-a prospective anode material. Mater Lett 2004;58:2283– 9.

[37] Bandyopadhyav G, Kennedy CR. Crack Healing and Strength Recovery in UO_2, J Am Ceram Soc 1976;59:415–9.

[38] Bandyopadhyav G, Kennedy CR. Isothermal crack healing and strength recovery in UO_2 subjected to varying degrees of thermal shock. J Am Ceram Soc 1977;60:48-50.

CHAPTER 7 CRACK SELF-HEALING OF SIC/SPINEL NANOCOMPOSITE[1]

7.1 Introduction

Spinel is one of the most attractive ceramics as a result of its outstanding properties. It has a high melting point (2135 °C) and high strength at both elevated and normal temperatures combined with high chemical inertness in acidic and basic environment make it an excellent refractory material [1]. It also shows good thermal shock resistant, high chemical stability and excellent dielectric properties and hence it has many applications in the metallurgical, electrochemical, and chemical industries [2-7].

One of the major limitations of ceramics is their brittleness. During the manufacturing process of various ceramics, many micro- and macro-cracks may develop in the structure. In order to overcome this problem, two major solutions are proposed by scientists: first to increase the strength and the fracture toughness of the ceramic by adding some fibres, whiskers, secondary particles or by phase transformation, microstructure control, etc [8-13]. The second solution is to produce advanced ceramics with the crack-healing ability. One of the best additives which can comply both aspects is SiC. It has been proved that the mechanical properties of single phase ceramics can be considerably improved with adding SiC particles. Niihara et al. [8-11] showed that adding 5 vol.% of SiC particles increased the strength of Al_2O_3 three times. Furthermore, Zhao et al. [12,13] illustrated a 42% increase in the strength of the alumina in the presence of SiC particles. On the other hand, numerous studies reported the effectiveness of SiC particles as a healing agent. Some of the common composites are SiC/Al_2O_3 [14-16], SiC/Si_3N_4 [17-19], SiC/ZrB_2 [20-22] and $SiC/Al_6Si_2O_{13}$ [23-25] to name a few. At high enough temperature, SiC reacts with oxygen and produce SiO_2 which is accompanied with almost 80% volume expansion. This volume expansion helps the closure of the crack and faster healing of the structure. Therefore, possibly SiC is one of the best healing agents that may be utilized in ceramic structures. There is currently a lack of study on the self-healing capability and behavior of SiC/spinel nanocomposite in the literature.

Here in this chapter we try to find out the self-healing potential of SiC/spinel nanocomposite. In the present chapter, the crack healing mechanism and the healing efficiency of the prepared SiC/spinel nanocomposite has been investigated by diametral tensile strength (DTS) test. The results obtained here can introduce SiC/spinel nanocomposite as a great ceramic composite with exceptional healing ability as the specimens can be completely healed and the strength of the pre-cracked specimens can be completely recovered after sintering the specimens at 1550 °C for 1min.

[1] This chapter has been accepted as Fariborz Tavangarian, Guoiqang Li, Bio-inspired crack self-healing of SiC/spinel nanocomposite, ELSEVIER, *Ceramics International*, in October 2014.

7.2 Experimental procedures

SiC/spinel nanocomposite containing 27.26 wt.% of SiC was prepared according to what is described in chapter 5. Briefly, appropriate amount of talc, aluminum and graphite powders were ball milled for 6 h in argon gas (to obtain stoichiometric $MgAl_2O_4$ containing 27.26 wt.% of SiC) and then annealed at 1200 °C for 1h in a vacuum with the heating/cooling rate of 10 °C/min. The obtained SiC/spinel nanocomposite powder was then uniaxially pressed into pellets with the height and diameter of 8 × 12 mm in a hardened steel mold at a pressure of 200 MPa using 10 wt.% glycerol as a binder and then sintered at 1200 °C for 1h in a vacuum with the heating/cooling rate of 10 °C/min. These samples are called VS. To study the crack self-healing behavior of the SiC/spinel nanocomposite, surface cracks were produced by the Vickers indenter in the middle of the pellets at a load of 9.8N (figure 7.1). Afterwards, the prepared specimens were annealed at elevated temperatures from 900 to 1700 ºC for various times in air. The experiments were performed in both air and vacuum to evaluate the influence of the atmosphere on the crack self-healing behavior. Diametral tensile strength (DTS) was performed on the prepared samples to determine the healing efficiency of the specimens as described in chapter 4.

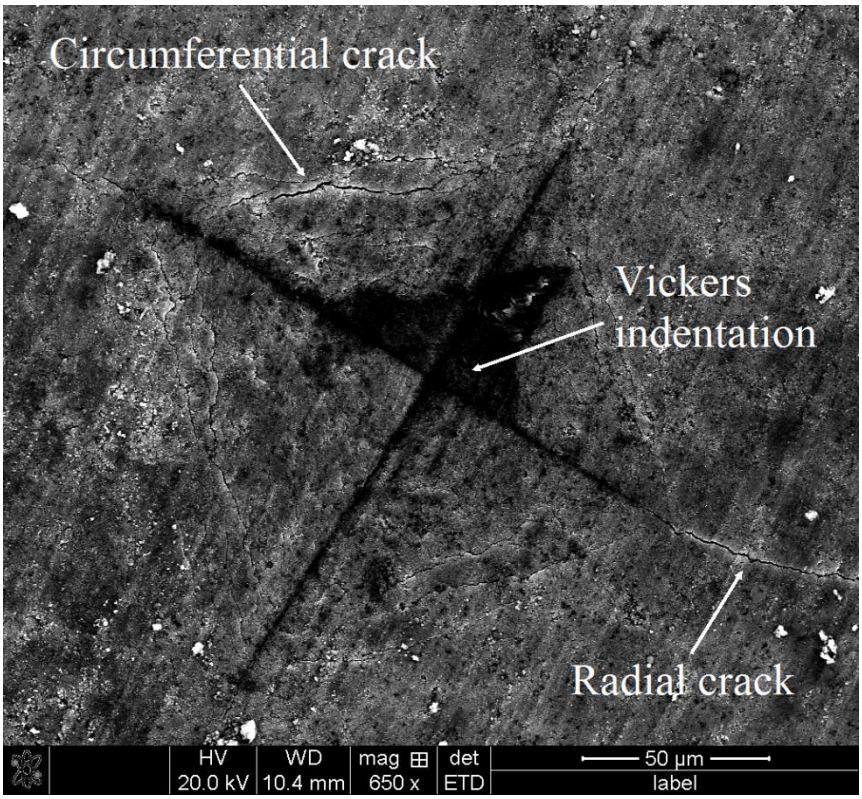

Figure 7.1. SEM micrograph of the surface cracks which was produced by the Vickers indenter in the middle of the bulk SiC/spinel nanocomposite.

However, in SiC/spinel specimens the starting point for indentation was 1 mm from the edge of the samples and 16 indentations were performed with the increments of 0.6 mm. These specimens were called VS-C. Both VS and VS-C samples were then sintered at various temperatures to investigate the DTS of the specimens. Table 7.1 shows the designation and sintering procedure of various specimens. The heating/cooling rate in all the experiments was 10 °C/min. The morphology of the specimens was studied by field emission scanning electron microscopy (Quanta3D FEG, FEI Company, USA) at acceleration voltages of 20 kV. The phase transformation of different specimens were investigated by X-ray diffractometry (MiniFlex XRD, Rigaku Corporation, Japan) with Cu Kα radiation (λ= 0.154178 nm). The XRD traces were recorded in the 2θ range of 20–80º (step size of 0.05º and time per step of 1 s). Diametral tensile strength (DTS) test was performed at room temperature using a Hydraulic Universal Testing Machine (Instron Model 5696, Canton, MA) at a rate of 5 mm/min.

Table 7.1. Designation and sintering procedures to prepare samples for DTS experiments.

Designation	Step 1	Step 2	Step 3
VS	Sintered at 1200 °C for 1h in a vacuum	Non-indented	-
VS-C	Sintered at 1200 °C for 1h in a vacuum	Indented	-
VS1500	Sintered at 1200 °C for 1h in a vacuum	Non-indented	Sintered at 1500 °C for 1 min in air
VS-C1500	Sintered at 1200 °C for 1h in a vacuum	Indented	Sintered at 1500 °C for 1 min in air
VS1540	Sintered at 1200 °C for 1h in a vacuum	Non-indented	Sintered at 1540 °C for 1 min in air
VS-C1540	Sintered at 1200 °C for 1h in a vacuum	Indented	Sintered at 1540 °C for 1 min in air
VS1545	Sintered at 1200 °C for 1h in a vacuum	Non-indented	Sintered at 1545 °C for 1 min in air
VS-C1545	Sintered at 1200 °C for 1h in a vacuum	Indented	Sintered at 1545 °C for 1 min in air
VS1550	Sintered at 1200 °C for 1h in a vacuum	Non-indented	Sintered at 1550 °C for 1 min in air
VS-C1550	Sintered at 1200 °C for 1h in a vacuum	Indented	Sintered at 1550 °C for 1 min in air

7.3 Results and discussions

In order to evaluate the crack self-healing behavior of pre-cracked SiC/spinel pellets, specimens were subjected to various heat treatment regimes discover out the healing temperature which is adequate to heal the cracks. First some samples were annealed for 1 min at 1000, 1200, 1400 and 1600 °C with heating/cooling rate of 10 °C/min. We found that the cracks are healed for those samples annealed at 1600 °C. So, to find out the minimum healing temperature we consecutively choose the middle temperatures between the healed and unhealed samples. For example, as at 1400 °C the samples were not healed but at 1600 °C they were; therefore, we chose 1500 °C to see whether they can be healed or not. Subsequently, we found that the minimum temperature which is required to heal the samples is 1545 °C. Also to study the influence of time on the healing behavior of pre-cracked samples, the

annealing time was also increased up to 100h for those samples sintered at 1200 °C but no healing could be observed.

Figure 7.2 shows the cracks before and after annealing at 1540 °C for 1 min with the heating/cooling rate of 10 °C/min. The indentation sign and the circumferential cracks before heat treatment are shown in figure 7.2 part a. Part b in figure 7.2 shows the same location of the sample after annealing at 1540 °C for 1 min. As can be seen, the cracks are still open and no healing was achieved in this sample. Parts c and d in figure 7.2 show the location of elliptical dotted line in figure 7.2 part a before and after healing at higher magnifications, respectively. It is clear that the grains are slightly sintered but the crack is still open.

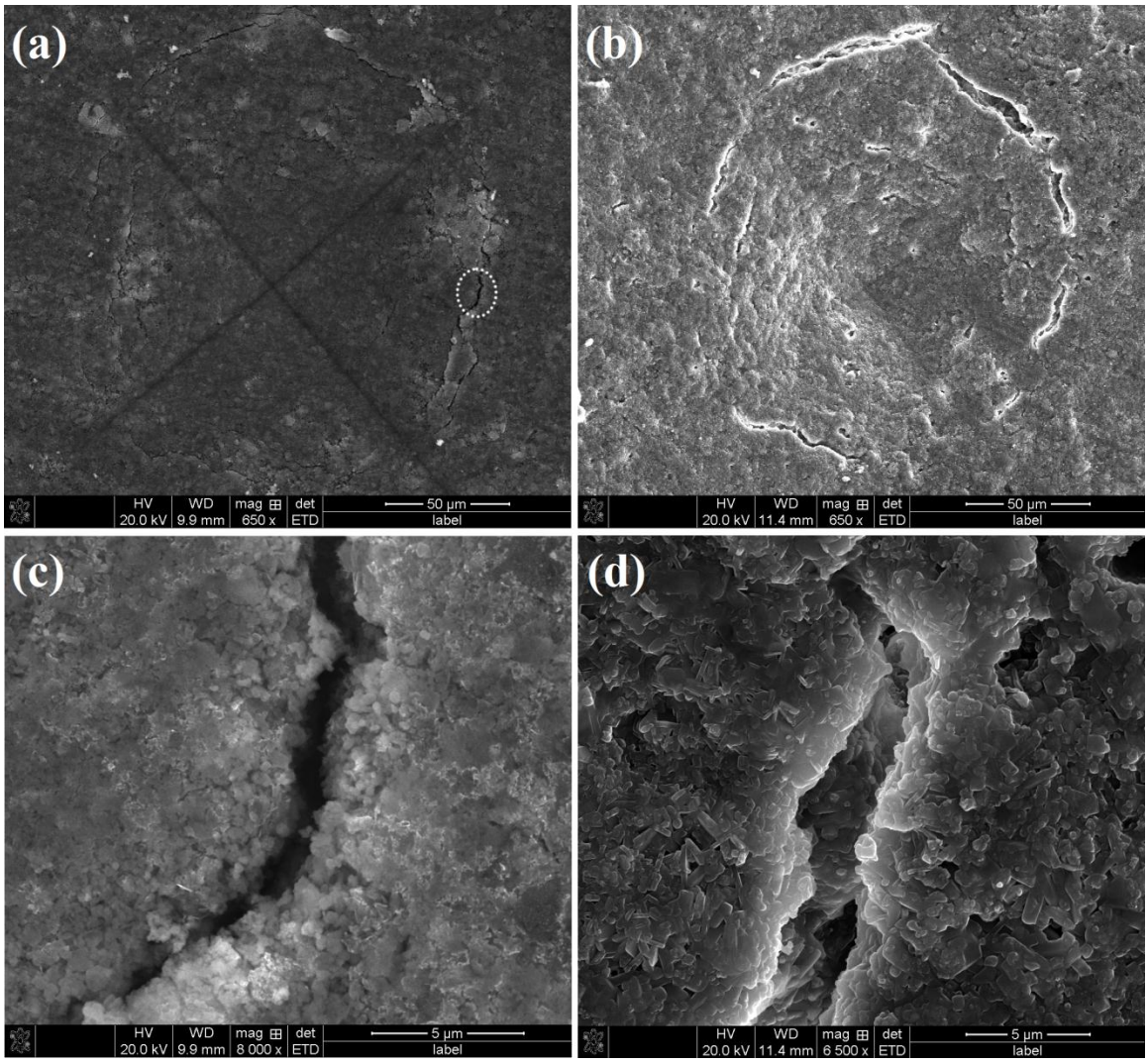

Figure 7.2. The location of a crack (a, c) before and (b, d) after sintering at 1540 °C for 1 min in air. (c) shows the location of the doted ring in (a).

Parts a and b in figure 7.3 show a pre-cracked specimen before and after heat treatment at 1545 °C for 1 min, respectively. As can be seen in this figure, all the cracks are healed and closed after heat treatment. With increasing the healing temperature for just 5 °C, the cracks can be healed completely. Figure 7.4 shows the location of the elliptical dotted line in figure 7.3 part a before and after heat treatment in higher magnifications. Also the SEM micrographs of the samples sintered at higher temperature are provided.

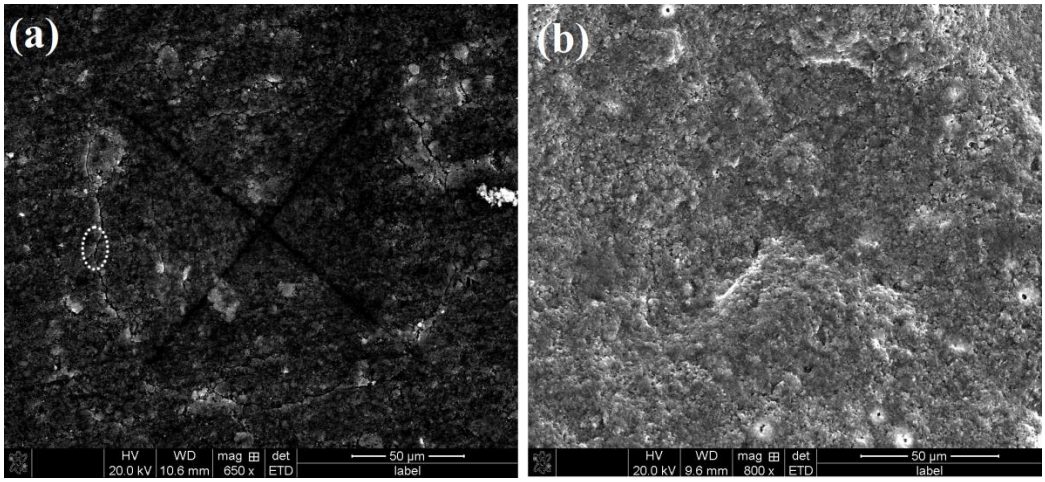

Figure 7.3. The location of a crack (a) before and (b) after sintering at 1545 °C for 1 min in air.

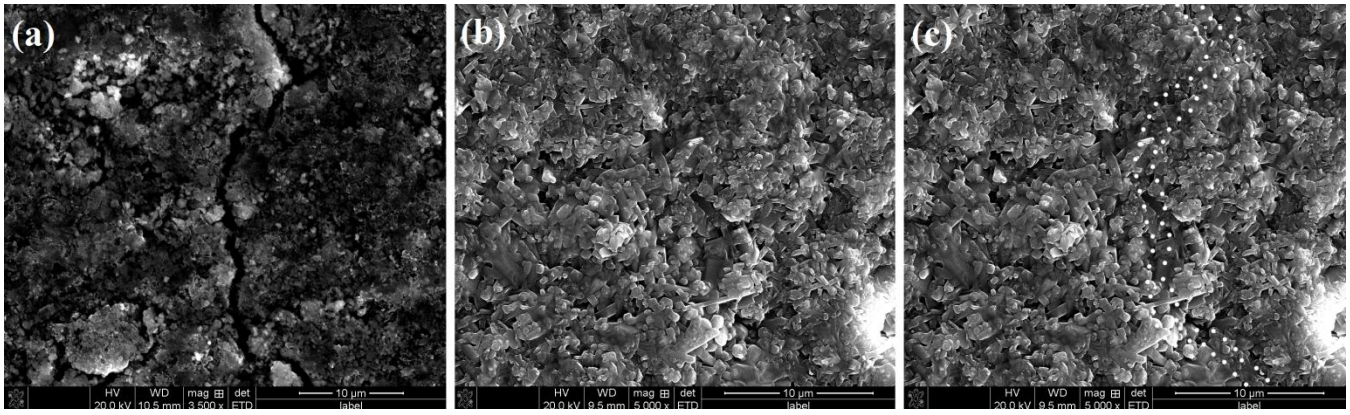

Figure 7.4. The location of a doted ring in figure 7.3 part a. (a) before and (b,c) after sintering at 1545 °C for 1 min in air.

Parts a and b in figure 7.5 show the location of cracks before and after sintering at 1550 °C for 1 min, respectively. As can be seen, all the cracks are closed and healed at this temperature. Figure 7.6 shows the location of the elliptical dotted line in figure 7.5 part a before and after heat treatment in higher magnifications. It can be seen that the crack is healed completely and a good connection between the crack walls is provided by the newly formed grains with columnar morphology.

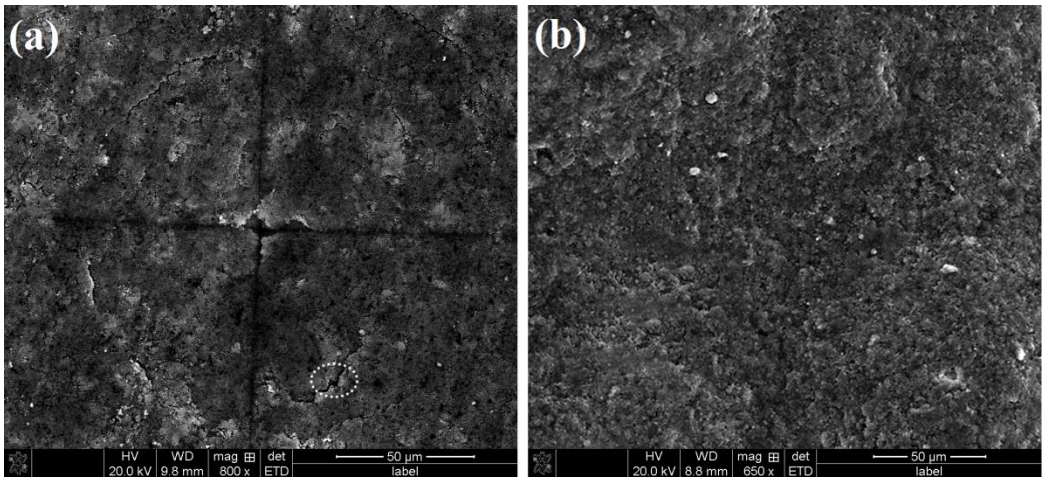

Figure 7.5. The location of a crack (a) before and (b) after sintering at 1550 °C for 1 min in air.

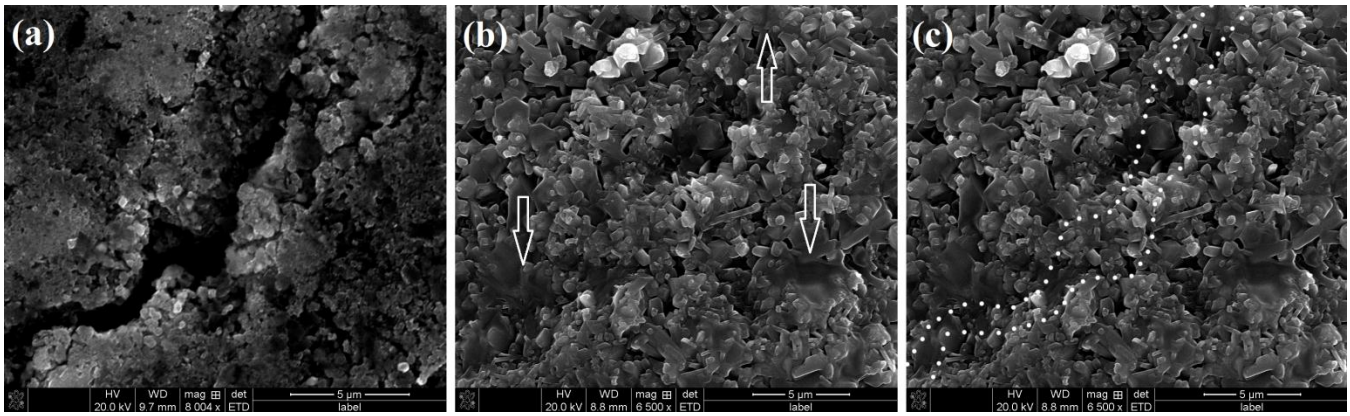

Figure 7.6. The location of a doted ring in figure 7.5 part a. (a) before and (b,c) after sintering at 1550 °C for 1 min in air.

In order to evaluate the influence of atmosphere on the healing behavior of the prepared samples, and to prove that oxygen is necessary to heal the cracks, a similar experiment was performed in a vacuum. The healing temperature was adjusted to 1545 °C with a holding time of 1 min and heating/cooling rate of

10 °C/min. The obtained SEM result is shown in figure 7.7. As can be seen, the cracks are not healed at all in a vacuum and the cracks are still open after the heat treatment. This observation also proves that the healing mechanism is not through the sintering of the grain and some chemical as well as structural changes are responsible for the healing process. As a result, oxygen should be available as one of the main ingredients for the healing process.

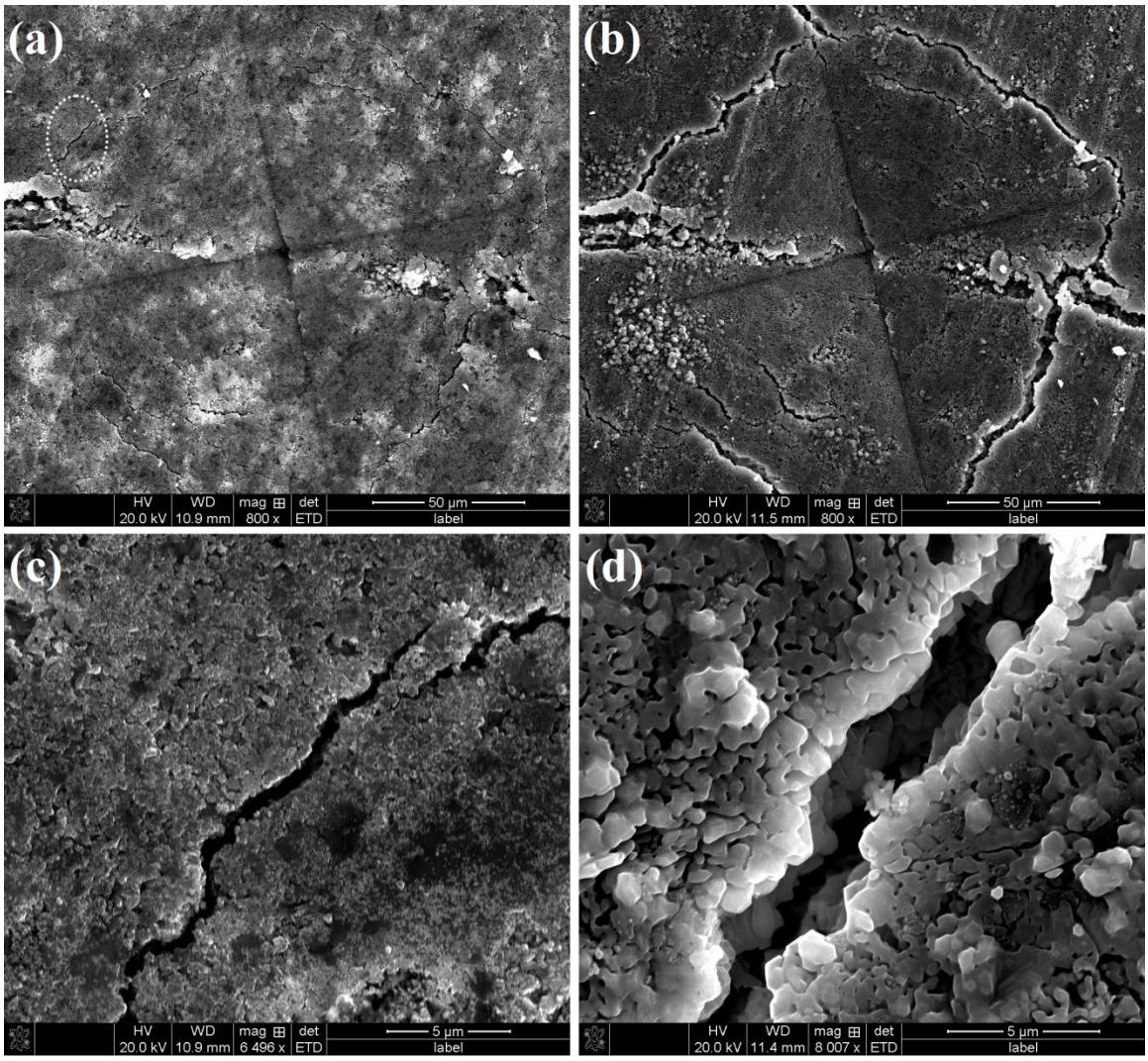

Figure 7.7. The location of a crack (a, c) before and (b, d) after sintering at 1545 °C for 1 min in a vacuum. (c) shows the location of the doted ring in (a).

To investigate the structural change happened during self-healing, XRD patterns of sampled healed at various temperatures were obtained. Figure 7.8 shows the XRD traces of sintered samples at different temperatures for 1 min. As can be seen, the XRD pattern of the sample at 25 °C corresponds to spinel

and SiC. After increasing the annealing temperature to 900 °C, some new peaks of cordierite ($Mg_2Al_4Si_5O_{18}$ or $2MgO.2Al_2O_3.5SiO_2$) (XRD JCPDS data file No. 01-082-1884) can be realized. Because cordierite consists of SiO_2, it seems that at the first stage some of SiC reacts with oxygen and formed SiO_2.

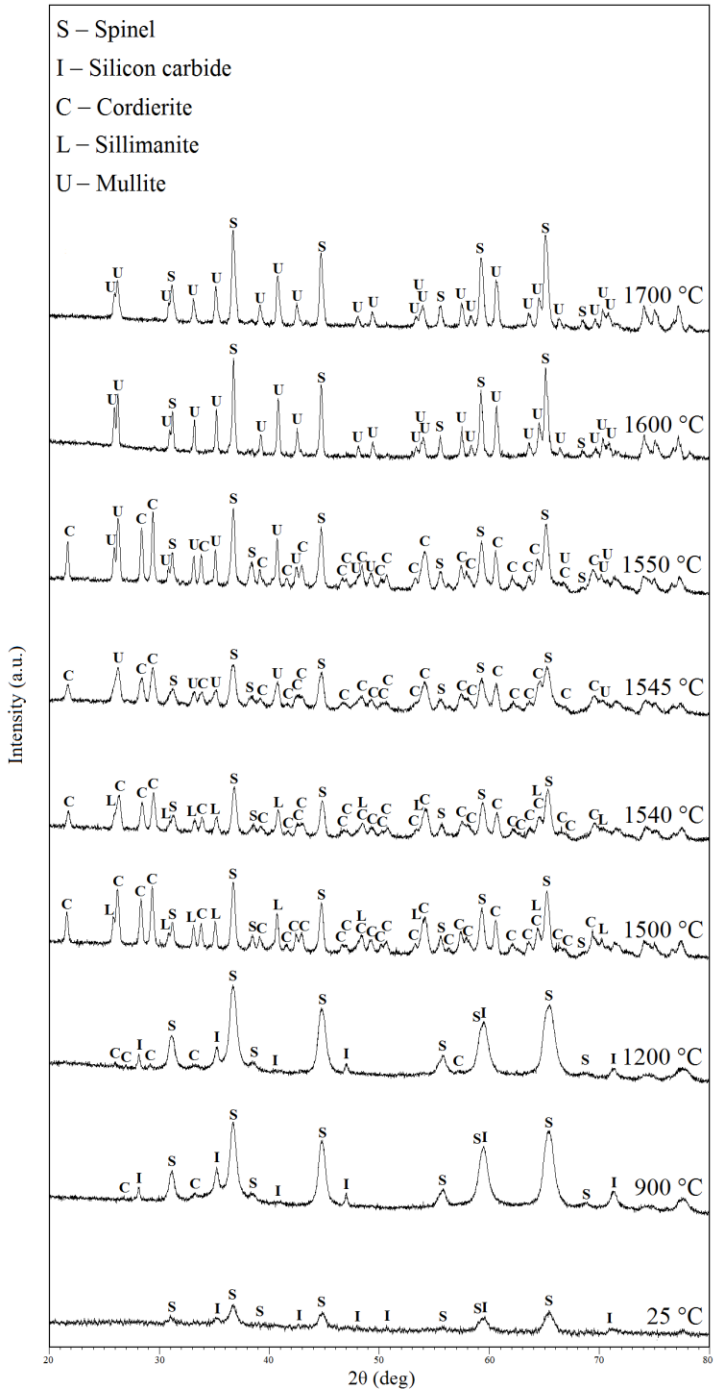

Figure 7.8. XRD patterns of sintered specimens in air at various temperatures for 1min holding time.

Then the produced SiO_2 reacts with spinel to produce cordierite, resulting in the following reactions:

$$SiC + 2O_2 \rightarrow SiO_2 + CO_2 \quad (7\text{-}1)$$

$$2MgAl_2O_4 + 5SiO_2 \rightarrow Mg_2Al_4Si_5O_{18} \quad (7\text{-}2)$$

After increasing the annealing temperature to 1500 °C, the intensity of cordierite peaks increased enormously due to the noticeable increase in the volume fraction of cordierite phase. On the other hand, the peaks of the sillimanite ($Al_2O_3.SiO_2$) (XRD JCPDS data file No. 02-0423) phase was also detected at this temperature. One possible reaction that may occur at this temperature could be expressed as the dissociation of cordierite phase into sillimanite and magnesium silicon oxide with the formula of ($Mg_2Si_3O_8$):

$$Mg_2Al_4Si_5O_{18} \rightarrow 2Al_2SiO_5 + Mg_2Si_3O_8 \quad (7\text{-}3)$$

No peaks of magnesium silicon oxide phase ($Mg_2Si_3O_8$) were detected in the XRD pattern, probably because to the fact that this phase is in the form of amorphous phase. Also no other changes were observed up to 1545 °C in which the position of sillimanite peaks at 2θ (33.15° and 35.16°, belong to the (220) and (112) crystal planes in sillimanite) starts to shift to higher angles (figure 7.9, see a), while the position of peaks at 2θ = 40.99° (belongs to the (131) crystal plane in sillimanite) remains unchanged (figure 7.9, see b). Raising the healing temperature to 1600 °C caused a complete vanishing of cordierite peaks and a complete shift of peaks from 2θ = 33.15° and 35.16° to 33.28° and 35.30° (belong to the (022) and (060) crystal planes of mullite phase with the formula $Al_6Si_2O_{13}$, XRD JCPDS data file No. 06-0258), respectively. The position of 2θ peaks at 40.99° did not change even at 1600 °C corresponding to the (242) crystal plane in mullite. Consequently, it can be concluded that with increasing the healing temperature the percentage of aluminum increased in the sillimanite structure and finally mullite phase can be formed. By analyzing all the above information, it seems that the next and the last stage in the healing process is the formation of mullite which causes the crack self-healing in the pre-cracked pellets.

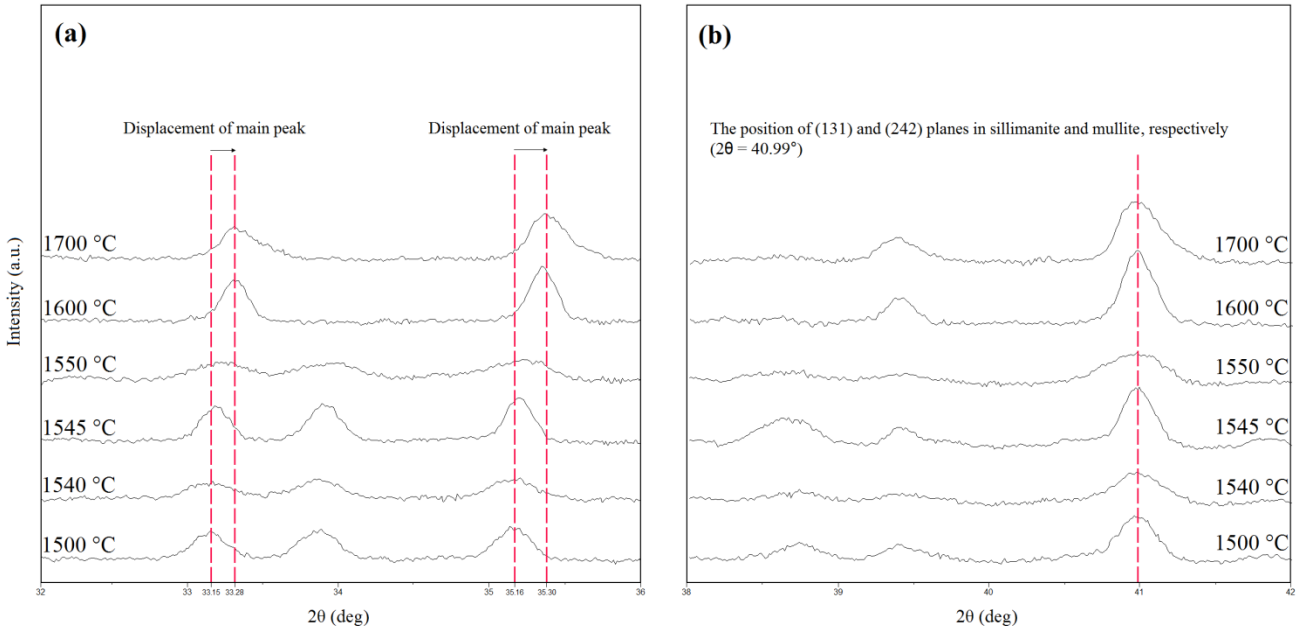

Figure 7.9. (a) Displacement of the main peaks of sillimanite to higher angles corresponding to the main peaks of mullite, (b) the position of (131) crystal plane of sillimanite and (242) crystal plane of mullite.

Therefore, one can show that one mole of spinel dissociated into MgO and Al_2O_3; MgO reacts with $Mg_2Si_3O_8$ to produce enstatite ($MgSiO_3$) while Al_2O_3 reacts with sillimanite to form mullite as follow:

$$2Al_2SiO_5 + Mg_2Si_3O_8 + MgAl_2O_4 \rightarrow Al_6Si_2O_{13} + 3MgSiO_3 \quad (7\text{-}4)$$

Another possible cause for the crack self-healing behavior may be explained by the presence of enstatite. Douy [26] showed that enstatite phase can be dissociated into forsterite and a SiO_2-rich liquid formed at 1557 °C. This temperature is substantially close to the minimum temperature that is required for our samples to be healed. Considering that in the XRD patterns no enstatite phase can be detected (figure 7.8), it can be concluded that at around 1545 °C enstatite dissociated into forsterite and SiO_2 and both these two phases are in the form of amorphous phase. No other changes were observed in those samples heat treated at 1700 °C.

The mean diametral tensile strength (DTS) of VS and VS-C were 2.63 (±0.33) and 1.59 (±0.53) MPa, respectively. According to equation (4-2), the amount of DTS reduction ($DTSR_{initial}$) in VS samples due to the presence of 32 indentations on both surfaces of VS-C specimens is equal to 39.54 %. Table 7.2 and figure 7.10 show the DTS of the indented and non-indented specimens and the amount of

strength recovery of the healed pellets after sintering at different temperatures, respectively. The maximum strength recovery (SR) of 99% was obtained for those samples heat treated at 1550 °C for 1 min as a result of complete healing of the structure. Although in the SEM specimens it was observed that the cracks were healed after sintering at 1545 °C for 1 min in air, the DTS test showed that the SR of those specimens are about 89%. It can be concluded that at 1545 °C the time and temperature of the sintering is not sufficient to make a strong bond between the walls of the cracks.

Table 7.2. Diametral tensile strength and DTSR of various specimens.

Sample	Mean diametral tensile strength (indented specimen)(MPa)(S.D.)	Sample	Mean diametral tensile strength (non-indented specimen)(MPa)(S.D.)	DTSR (%)
VS-C	1.59 (±0.53)	VS	2.63 (±0.33)	39.54
VS-C1500	6.45 (±0.63)	VS1500	7.49 (±0.51)	13.88
VS-C1540	6.48 (±0.58)	VS1540	7.28 (±0.33)	10.98
VS-C1545	6.83 (±0.31)	VS1545	7.13 (±0.51)	4.20
VS-C1550	7.16 (±0.41)	VS1550	7.19 (±0.38)	0.41

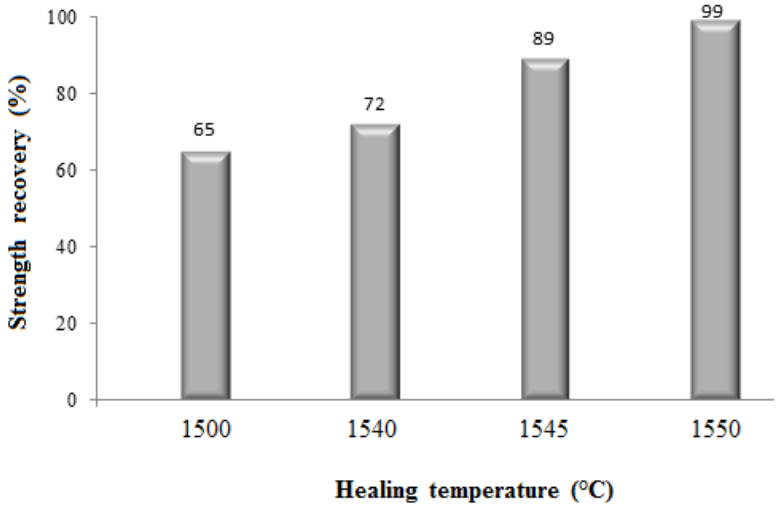

Figure 7.10. Strength recovery of different specimens.

Also these observations can be well explained by the obtained SEM micrographs. Arrows in figure 7.6 part b show the formation of a glassy phase after sintering the specimens at 1550 °C for 1 min while in those samples healed at 1545 °C for 1 min such a glassy phase was not observed. The formation of the

aluminosilicate glassy phase may be the major factor to heal the structure and increase the DTS of the indented specimens. Similar observations have been reported in previous studies [27-31]. Huang and Wen [27] reported that the formation of a glassy phase including Al_2O_3 and amorphous oxide of aluminosilicate glass is responsible for the bending strength recovery in Al_4SiC_4. Also, studies on SiC/Al_2O_3 composite showed that the formation of aluminosilicate glass and crystalline mullite (depends on the annealing temperature) is responsible for such a behavior [28-31]. In this study also, as it is proved by XRD patterns (figure 7.8), the formation of mullite and possibly some aluminosilicate glassy phase are responsible for complete crack healing and strength recovery in the specimens. The formation of mullite and/or the glassy phase established strong bonds between the crack walls and hence can recover the DTS of the indented specimens up to the level of the non-indented specimens.

7.4 Conclusion

In this chapter, we developed a new nanocomposite which has a potential to be used in a variety of applications and industries. The produced SiC/spinel nanocomposite can heal surface cracks after sintering at 1545 °C for only 1 min holding time in air. The produced mullite and/or dissociation of enstatite to forsterite and SiO_2 are the two possible mechanisms responsible for the crack self-healing behavior in SiC/spinel nanocomposite. However, it should be emphasized that complete strength recovery of the SiC/spinel nanocomposite occurred in those samples sintered at 1550 °C for 1 min. At 1545 °C the formation of mullite, dissociation of enstatite and formation of the glassy phase start however to produce a strong bond between the crack walls higher sintering temperature and time is required. Therefore it can be concluded that sintering the SiC/spinel nanocomposite for 1 min at 1550 °C can completely close the cracks and recover the lost strength due to the presence of Vickers indentations. This composite has the potential to be used as an integrated structure or in the form of healing agents in other ceramic matrixes.

7.5 References

[1] Mohapatra D, Sarkar D, Effect of in situ spinel seeding on synthesis of MgO-rich $MgAl_2O_4$ composite. J Mater Sci 2007;42:7286–7293.

[2] Baudin C, Martinaz R, Pena P. High-temperature mechanical behaviour of stoichiometric magnesium spinel. J Am Ceram Soc 1995;78:1857–1862.

[3] Ganesh I, Bhattacharjee S, Saha BP, Johnson R, Rajeshwari K, Sengupta R, Rao MV, Mahajan YR. An efficient $MgAl_2O_4$ spinel additive for improved slag erosion and penetration resistance of high-Al_2O_3 and MgO-C refractories. Ceram Int 2002;28:245–253.

[4] Ganesh I, Bhattacharjee S, Saha BP, Johnson R, Mahajan YR. A new sintering aid for magnesium aluminate spinel. Ceram Int 2001;27:773–779.

[5] Ganesh I, Johnson R, Rao GVN, Mahajan YR, Madavendra SS, Reddy BM. Microwave-assisted combustion synthesis of nanocrystalline $MgAl_2O_4$ spinel powder. Ceram Int 2005;31:67–74.

[6] Tavangarian F, Emadi R. Synthesis and characterization of pure nanocrystalline magnesium aluminate spinel powder. J Alloys Compd 2010;489:600–604.

[7] Tavangarian F, Emadi R. Enhancement mechanism of nanostructure forsterite formation rate by mechanical activation and ammonium chloride. Nano 2011;6:131-138.

[8] Niihara K, Nakahira A. strengthening of oxide ceramics by SiC and Si_3N_4 dispersions. in proceedings of third international symposium on ceramic materials and components for engines. Westerville, OH: The American ceramic society; 1988, p. 919-926.

[9] Niihara K, Nakahira A, Sasaki G, Hirabayashi M. Development of strong Al_2O_3 composites, in 124the proceedings of the international meeting on advanced materials, vol 4. Kawasaki, Japan: The Materials Research Society of Japan; 1989, p. 134.

[10] Niihara K, Nakahira A. Particulate strengthened oxide nanocomposites. in advanced structural inorganic composites. In: Vincenzini P, editor. Trieste, Italy, Elsevier, 1990, p. 637-64.

[11] Niihara K. New design concept of structural ceramic-ceramic nanocomposites, The centennial issue of the ceramic society of japan. J Ceram Soc Jpn 1991;99:974-82.

[12] Zhao J, Steams LC, Harmer MP, Chan HM, Miller GA, Cook RF. Mechanical behavior of alumina-silicon carbide 'Nanocomposites'. J Ceram Soc Jpn 1993;76:503-10.

[13] Steams LC, Zhao J, Harmer MP. Processing and microstructure development in $A1_2O_3$-SiC 'Nanocomposites'. J Eur Ceram Soc 1992;10:473-7.

[14] Ando K, Kim BS, Chu MC, Saito S, Takahashi K. Crack-healing and mechanical behaviour of Al_2O_3/SiC composites at elevated temperature. Fatigue Fract Eng Mater Struct 2004;27:533-41.

[15] Osada T, Nakao W, Takahashi K, Ando K. Kinetics of Self-Crack-Healing of Alumina/Silicon Carbide Composite Including Oxygen Partial Pressure Effect. J Am Ceram Soc 2009;92:864-9.

[16] Mohanty D, Sil A, Maiti K. Development of input output relationships for self-healing Al_2O_3/SiC, ceramic composites with Y_2O_3 additive using design of experiments. Ceram Int 2011;37:1985-92.

[17] Ando K, Chu MC, Yao F, Sato S. Fatigue strength of crack-healed Si_3N_4/SiC composite ceramics. Fatigue Fract Eng Mater Struct 1999;22:897-903.

[18] Takahashi K, Ando K, Murase H, Nakayama S, Saito S. Threshold stress for crack-healing of Si_3N_4/SiC and resultant cyclic fatigue strength at the healing temperature. J Am Ceram Soc 2005;88:645-51.

[19] Jung YS, Nakao W, Takahashi K, Ando K, Saito S. Crack healing of machining cracks introduced by wheel grinding and resultant high-temperature mechanical properties in a Si_3N_4/SiC composite. J Am Ceram Soc 2009;92:167-73.

[20] Monteverde F, Bellosi A, Oxidation of ZrB_2-based ceramics in dry air. J Electrochem Soc 2003;150:552-9.

[21] Zhang X, Xu L, Du S, Han W, Han J. Preoxidation and crack-healing behavior of ZrB_2-SiC ceramic composite. J Am Ceram Soc 2008;91:4068-73.

[22] Liang J, Wang Y, Fang G, Wang G. Influence of oxidation healing for cracks on the strength of hot-pressed ZrB_2–SiC–AlN ceramics. Int J Appl Ceram Technol 2012;9:441-6.

[23] Lee SK, Ono M, Nakao W, Takahashi K, Ando K. Crack-healing behaviour of mullite/SiC/Y_2O_3 composites and its application to the structural integrity of machined components. J Eur Ceram Soc 2005;25:3495-502.

[24] Nakao W, Mori S, Nakamura J, Takahashi K, Ando K. Self-crack-healing behavior of mullite/SiC particle/SiC whisker multi-composites and potential use for ceramic springs. J Am Ceram Soc 2006;89:1352-7.

[25] Takahashi K, Uchiide K, Kimura Y, Nakao W, Ando K, Yokouchi M. Threshold stress for crack-healing of mullite reinforced by SiC whiskers and SiC particles and resultant fatigue strength at the healing temperature. J Am Ceram Soc 2007;90:2159-64.

[26] Douy A. Aqueous synthesis of forsterite (Mg_2SiO_4) and enstatite ($MgSiO_3$). J Sol–Gel Sci Technol 2002;24:221–228.

[27] Huang XX, Wen GW. Mechanical properties of Al_4SiC_4 bulk ceramics produced by solid state reaction. Ceram Int 2007;33:453-8.

[28] Chiu CC. Influence of surface oxidation on thermal shock resistance and flexural strength of SiC/Al_2O_3 composites. J Mater Sci 1994;29:2078-82.

[29] Kim HE. Oxidation behavior and effects of Oxidation on the strength of SiC-wisker reinforced alumina. J Mater Sci 1994;29:1656-61.

[30] Luthra KL, Park HD. Oxidation of silicon carbide-reinforced oxide-matrix composites at 1375° to 1575°C. J Am Ceram Soc 1990;73:1014-23.

[31] Wu HZ, Lawrence CW, Roberts SG, Derby B. The strength of Al_2O_3/SiC nanocomposites after girding and annealing. Acta Mater 1998;46:3839-48.

CHAPTER 8 SUMMARY AND FUTURE WORKS

8.1 Summary

In this dissertation, the crack self-healing behavior of nanostructure spinel and SiC/spinel nanocomposite were investigated. The results showed that the produced cracks in spinel can be healed after sintering the specimens at 1600 °C for 100h. On the other hand, SiC/spinel nanocomposite are able to heal the surface cracks after sintering at 1550 °C for 1 min. 91 and 99% strength recovery were obtained in spinel and SiC/spinel nanocomposite, respectively. The crack healing mechanism in spinel is sintering while the crack-healing mechanism of SiC/spinel nanocomposite is through the formation of mullite, aluminosilicate glassy phase and dissociation of enstatite to forsterite and SiO_2. In the case of SiC/spinel nanocomposite, oxygen is one of the main ingredients in the healing process. .

8.2 Recommendations for future works

This is the first report on the crack-healing behavior of spinel and SiC/spinel nanocomposite. Much more investigations are essential to advance our knowledge regarding the crack healing mechanisms of spinel and SiC/spinel nanocomposite. The following recommendations can advance our insight into their crack-healing behavior and their potential applications in industries in the near future:

- According to the experiment results in this dissertation, spinel has the crack healing ability. However, a long time period is required to heal the surface cracks in spinel. Utilizing some additives such as TiC, Y_2O_3 and ZrO_2 may decrease the sintering time and temperature to achieve complete healing.

- The influence of SiC whiskers on the crack healing behavior of spinel needs to be investigated. Also by applying different loads and producing cracks with various widths, the maximum crack width that can be healed needs to be investigated. On the other hand, multiple crack healing behavior of spinel ceramic needs to be investigated by utilizing bending test, healing the specimens and repeating these steps to see the influence of repeated cracking-healing cycles and the number of times that cracks can be healed.

- The crack-healing behavior of MgO-$MgAl_2O_4$ and $MgAl_2O_4$-Al_2O_3 can be examined to study the influence of MgO and Al_2O_3 phases on the crack healing behavior of Spinel.

- The cross section of the cracks can be investigated in the case of SiC/spinel nanocomposite to investigate any possible phase change inside the crack opening and find out the crack healing mechanism inside the crack opening. Furthermore, the crack healing behavior of spinel and SiC/spinel nanocomposite can be investigated under constant and cyclic stresses at elevated temperature.

APPENDIX A: LETTERS OF PERMISSION TO USE PUBLISHED MATERIALS

The Permissions from Elsevier publishing company are presented as follow:

Copyright Clearance Center RightsLink®

Home | Account Info | Help | Live Chat

Title: Mechanical activation assisted synthesis of nanostructure MgAl2O4 from gibbsite and lansfordite

Author: Fariborz Tavangarian,Guoqiang Li

Publication: Powder Technology

Publisher: Elsevier

Date: November 2014

Copyright © 2014 Elsevier B.V. All rights reserved.

Logged in as:
Fariborz Tavangarian
Account #:
3000495331

LOGOUT

Order Completed

Thank you very much for your order.

This is a License Agreement between Fariborz Tavangarian ("You") and Elsevier ("Elsevier"). The license consists of your order details, the terms and conditions provided by Elsevier, and the payment terms and conditions.

Get the printable license.

License Number	3496050677885
License date	Oct 25, 2014
Licensed content publisher	Elsevier
Licensed content publication	Powder Technology
Licensed content title	Mechanical activation assisted synthesis of nanostructure MgAl2O4 from gibbsite and lansfordite
Licensed content author	Fariborz Tavangarian,Guoqiang Li
Licensed content date	November 2014
Licensed content volume number	267
Licensed content issue number	n/a
Number of pages	6
Type of Use	reuse in a thesis/dissertation
Portion	full article
Format	both print and electronic
Are you the author of this Elsevier article?	Yes
Will you be translating?	No
Title of your thesis/dissertation	CRACK SELF-HEALING IN SIC/SPINEL NANOCOMPOSITE
Expected completion date	Dec 2014
Estimated size (number of pages)	130
Elsevier VAT number	GB 494 6272 12
Permissions price	0.00 USD
VAT/Local Sales Tax	0.00 USD / 0.00 GBP
Total	0.00 USD

ORDER MORE... CLOSE WINDOW

Title: Synthesis, characterization and formation mechanism of SiC/spinel nanocomposite

Author: Fariborz Tavangarian,Guoqiang Li

Publication: Journal of Alloys and Compounds

Publisher: Elsevier

Date: 15 June 2014

Order Completed

Thank you very much for your order.

This is a License Agreement between Fariborz Tavangarian ("You") and Elsevier ("Elsevier"). The license consists of your order details, the terms and conditions provided by Elsevier, and the payment terms and conditions.

Get the printable license.

License Number	3496050597080
License date	Oct 25, 2014
Licensed content publisher	Elsevier
Licensed content publication	Journal of Alloys and Compounds
Licensed content title	Synthesis, characterization and formation mechanism of SiC/spinel nanocomposite
Licensed content author	Fariborz Tavangarian,Guoqiang Li
Licensed content date	15 June 2014
Licensed content volume number	598
Licensed content issue number	n/a
Number of pages	7
Type of Use	reuse in a thesis/dissertation
Portion	full article
Format	both print and electronic
Are you the author of this Elsevier article?	Yes
Will you be translating?	No
Title of your thesis/dissertation	CRACK SELF-HEALING IN SIC/SPINEL NANOCOMPOSITE
Expected completion date	Dec 2014
Estimated size (number of pages)	130
Elsevier VAT number	GB 494 6272 12
Permissions price	0.00 USD
VAT/Local Sales Tax	0.00 USD / 0.00 GBP
Total	0.00 USD

ORDER MORE... CLOSE WINDOW

Title:	Sintering behavior, microstructure and mechanical properties of vacuum sintered SiC/spinel nanocomposite
Author:	Guoqiang Li,Fariborz Tavangarian
Publication:	Journal of Alloys and Compounds
Publisher:	Elsevier
Date:	5 December 2014

Order Completed

Thank you very much for your order.

This is a License Agreement between Fariborz Tavangarian ("You") and Elsevier ("Elsevier"). The license consists of your order details, the terms and conditions provided by Elsevier, and the payment terms and conditions.

Get the printable license.

License Number	3496050804454
License date	Oct 25, 2014
Licensed content publisher	Elsevier
Licensed content publication	Journal of Alloys and Compounds
Licensed content title	Sintering behavior, microstructure and mechanical properties of vacuum sintered SiC/spinel nanocomposite
Licensed content author	Guoqiang Li,Fariborz Tavangarian
Licensed content date	5 December 2014
Licensed content volume number	615
Licensed content issue number	n/a
Number of pages	7
Type of Use	reuse in a thesis/dissertation
Portion	full article
Format	both print and electronic
Are you the author of this Elsevier article?	Yes
Will you be translating?	No
Title of your thesis/dissertation	CRACK SELF-HEALING IN SIC/SPINEL NANOCOMPOSITE
Expected completion date	Dec 2014
Estimated size (number of pages)	130
Elsevier VAT number	GB 494 6272 12
Permissions price	0.00 USD
VAT/Local Sales Tax	0.00 USD / 0.00 GBP
Total	0.00 USD

ORDER MORE... CLOSE WINDOW

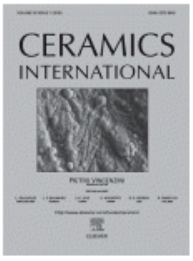

Title:	Bio-inspired crack self-healing of SiC/spinel nanocomposite
Author:	Fariborz Tavangarian,Guoqiang Li
Publication:	Ceramics International
Publisher:	Elsevier
Date:	Dec 31, 1969

Order Completed

Thank you very much for your order.

This is a License Agreement between Fariborz Tavangarian ("You") and Elsevier ("Elsevier") The license consists of your order details, the terms and conditions provided by Elsevier, and the payment terms and conditions.

License number	Reference confirmation email for license number
License date	Oct 25, 2014
Licensed content publisher	Elsevier
Licensed content publication	Ceramics International
Licensed content title	Bio-inspired crack self-healing of SiC/spinel nanocomposite
Licensed content author	Fariborz Tavangarian,Guoqiang Li
Licensed content date	Available online 24 October 2014
Licensed content volume number	n/a
Licensed content issue number	n/a
Number of pages	1
Type of Use	reuse in a thesis/dissertation
Portion	full article
Format	both print and electronic
Are you the author of this Elsevier article?	Yes
Title of your thesis/dissertation	CRACK SELF-HEALING IN SIC/SPINEL NANOCOMPOSITE
Expected completion date	Dec 2014
Elsevier VAT number	GB 494 6272 12
Billing Type	Invoice
Billing address	4020 Gourrier Ave. APT 1 Baton Rouge, LA 70808 United States
Permissions price	0.00 USD
VAT/Local Sales Tax	0.00 USD / 0.00 GBP
Total	0.00 USD

CLOSE WINDOW

VITA

Fariborz Tavangarian was born in Esfahan, Iran. He received his BS and MS in Materials Engineering from Isfahan University of Technology (Esfahan) in 2007 and 2010, respectively. He was selected as national genius by Iran's National Elite Foundation in 2011. Also he was awarded as the 7th Best Young Specialists of Nanotechnology and 44th Scholars of Nanotechnology in the 6th Nano Award Festival in Iran determined by Iran Nanotechnology Initiative Council. He joined the Department of Mechanical Engineering at Louisiana State University as a research assistant and started his Ph.D under the supervision of Prof. Guoiqang Li. in 2011. Fariborz Tavangarian has made technical contributions in several areas, including biomaterials, nanomaterials, tissue engineering, nanocomposite and ceramic materials. He has authored 27 scientific articles in internationally peer-reviewed journals and has been widely-recognized by his fellow scientists for his numerous research contributions, as evidenced by the more than 300 citations from scientists all around the world. The *h-index* of his publications is 13 which shows the quality of his publications. Fariborz Tavangarian is expected to receive his Doctor of Philosophy degree at the 2014 Fall Commencement.